Tampere University

THOMAS KERST

Optical Stand-Off Detection of Alpha Radiation in Nuclear Facilities

Tampere University Dissertations 129

Tampere University Dissertations 129

THOMAS KERST

Optical Stand-Off Detection of Alpha Radiation in Nuclear Facilities

ACADEMIC DISSERTATION
To be presented, with the permission of
the Faculty of Engineering and Natural Sciences
of Tampere University,
for public discussion in the auditorium RG202
of the Rakennustalo building, Korkeakoulunkatu 5, 33720 Tampere,
on 4th of October 2019, at 12 o'clock.

ACADEMIC DISSERTATION
Tampere University, Faculty of Engineering and Natural Sciences
Finland

Responsible supervisor and Custos
Professor Juha Toivonen
Tampere University
Finland

Pre-examiners
Professor Michael Famiano
Western Michigan University
The United States of America

Docent Toni Laurila
Aalto University
Finland

Opponent
Doctor Lars René Lindvold
Technical University of Denmark
Denmark

Cover design: Roihu Inc.

ISBN 978-952-03-1246-6 (print)
ISBN 978-952-03-1247-3 (pdf)
ISSN 2489-9860 (print)
ISSN 2490-0028 (pdf)
http://urn.fi/URN:ISBN:978-952-03-1247-3

PunaMusta Oy – Yliopistopaino
Tampere 2019

PREFACE

This work was carried out in the Applied Optics group in the Photonics Laboratory at Tampere University (TUNI). My doctoral studies were supported by the NINS3 project and partly by the MetroDecom II project, both of which are funded through Business Finland and the European Union. It was their support that allowed me to fully concentrate on my work.

I would like to take the opportunity to thank my supervisor Prof. Dr. Juha Toivonen for providing the possibility to work on this Thesis, for allowing me to use his expensive equipment and for insisting on high standards in thinking and writing clearly. I am also grateful to Dr. Rikard Malmbeck for the valuable discussions and for providing radioactive material to my heart's content. I would also like to extend my gratitude to Prof. Dr. Peter Dendooven and my collaborators at TUNI, Helsinki Institute of Physics and JRC Karlsruhe, BfS and PTB.

I would like to acknowledge a few people in the laboratory who made the stay worthwhile. Sofia Suomala introduced me to Finnish academic live. Kim Patokoski thankfully makes for a quiet and concentrated office mate. He and Jan Viljanen took the time to introduce me to some fundamentals of martial arts. Mikko Huttunen helped out on short notice in a measurement campaign with some of his own group's equipment. Mahsa Ghezelbash makes for pleasant and uncomplicated company.

I am grateful to my former teacher Christine Lehr for her valuable advice she administered 15 years ago. For their constant support for me and my projects I wish to thank my family. My dear mother Ivette Wienck in particular is deserving of much of this reverence. My final and perhaps most heartfelt expression of gratitude is devoted to my partner Jaakko Muikku.

> "Everybody does have a book in them, but in most cases that's where it should stay."
>
> — Christopher Hitchens

ABSTRACT

Numerous nuclear power plants will soon reach the end of their lifetime and must be decommissioned. The number of upcoming decommissioning projects is unprecedented and new technologies are needed to rapidly and reliably identify radioactive contamination. Remote detection of alpha radiation by optical means is one of those new technologies. It collects the ultraviolet (UV) scintillation of nitrogen molecules (N_2) in air, the radioluminescence, to reveal the presence of alpha emitters.

This Thesis summarises the advances of the technology since its first conception and demonstrates its efficacy by remotely detecting alpha contamination in a nuclear research facility. It shows that alpha imaging requires the absence of daylight and that this limitation, together with lower-than-required sensitivity levels, make the technology mostly untenable for use in decommissioning tasks. Radioluminescence of nitric oxide (NO) is presented as a means to improve the sensitivity levels. It is shown that replacing the air around an alpha emitter with a mixture of 50 ppm of NO in N_2 amplifies the production of ultraviolet light by more than two orders of magnitude. The technique is shown to render the detection resistant to influences of daylight.

A theory is developed that provides an explanation for the production of NO radioluminescence. The theory hypothesises that a specific form of fluorescence quenching and unique access to a reservoir of energy account for much of the light production. It is shown to correctly predict the conditions under which a N_2 purge can create NO radioluminescence in otherwise ambient air.

A fully resolved spectrum of the radioluminescence in water is presented. The origins of the radioluminescence are discussed and its utility for the remote detection of alpha radiation in liquids is highlighted.

The Thesis outlines techniques that enable optical alpha detection to overcome both the daylight and the sensitivity problem. Limitations that keep the technology from finding widespread use in decommissioning tasks are directly addressed. The theory can be used to further enhance radioluminescence intensity.

CONTENTS

ORIGINAL PUBLICATIONS

Publication I T. Kerst, J. Sand, S. Ihantola, K. Peräjärvi, A. Nicholl, E. Hrnecek, H. Toivonen and J. Toivonen. Standoff Alpha Radiation Detection for Hot Cell Imaging and Crime Scene Investigation. *Optical Review* 25 (2018), 429–436.

Publication II T. Kerst and J. Toivonen. Intense Radioluminescence of NO/N_2-mixture in Solar Blind Spectral Region. *Optics express* 26 (2018), 33764–33771.

Publication III T. Kerst, R. Malmbeck, N. l. Banik and J. Toivonen. Alpha Radiation-Induced Luminescence by Am-241 in Aqueous Nitric Acid Solution. *Sensors* 19 (2019), 1602.

Publication IV T. Kerst and J. Toivonen. Dynamic Enhancement of Nitric Oxide Radioluminescence with Nitrogen Purge. *accepted for publication in 'Scientific Reports'* (2019).

AUTHOR'S CONTRIBUTION

This thesis summarises four peer-reviewed scientific publications. Their contents, key results and the author's contribution to each of them are:

Publication I This work presents the remote detection of alpha contamination in a nuclear research facility. An EMCCD camera had been used to image radioluminescence in air, thereby revealing alpha contamination in difficult-to-access areas like hot cells. Johan Sand conceived the experiment and conducted the imaging. The author measured and analysed the spectrum of radioluminescence in air and inferred from it the limits of the technique. The author wrote the manuscript.

Publication II This work presents the creation of intense radioluminescence of NO in the solar blind spectral region. This had been achived by supplanting the air around an alpha emitter with a gas mixture of 50 ppm of NO in N_2. It provides an explanation of the phenomenon by arguing that a form of N_2 radioluminescence quenching, excitation transfer, leads to the production of intense NO radioluminescence. Both Juha Toivonen and the author conceived the experiments and built the theory. The author carried out the experiments and analysed the data. The author wrote the manuscript.

Publication III This work presents the spectrum of radioluminescence in water. It shows that this type of radioluminescence is very weak in comparison to this in air and that it is produced homogeneously in the liquid. It argues that this radioluminescence is unlikely a form of Cerenkov radiation and speculates that it is a form of luminescence of one of the radiolysis intermediaries. Juha Toivonen, Rikard Malmbeck and the author conceived the experiments. Rikard Malmbeck and Nidhu lal Banik prepared the radioactive samples. Rikard Malmbeck, Nidhu lal Banik and the author carried out the experiments. The author prepared the optics, analysed the data and wrote the

manuscript.

Publication IV This work presents the creation of nitric oxide radioluminescence in ambient air by using a nitrogen purge. It presents arguments under which conditions NO radioluminescence can be used in ambient air without the need to have a tightly controlled atmosphere around alpha emitters. It supplements its claim with experiments that build on the theory that has been laid down in Publication II. Both Juha Toivonen and the author conceived of the experiments. The author carried them out, analysed the data, built the theory and wrote the manuscript.

SYMBOLS AND ABBREVIATIONS

CCD	charge-coupled device
EMCCD	electron-multiplying charge-coupled device
ICCD	intensified charge-coupled device
PMT	photomultiplier tube
IR	infrared, 700 nm - 1 mm
UVA	ultraviolet A, 315 nm - 400 nm
UVB	ultraviolet B, 280 nm - 315 nm
UVC	ultraviolet C, 100 nm - 280 nm, the solar blind spectral region
UV	ultraviolet, 10 nm - 400 nm
VIS	visible, 400 nm - 700 nm
Am-241	americium-241 isotope
Bi-213	bismuth-213 isotope
Co-60	cobalt-60 isotope
Pb-206	lead-206 isotope
Po-210	polonium-210 isotope
Po-213	polonium-213 isotope
Pu-239	plutonium-239 isotope
U-235	uranium-235 isotope
U-238	uranium-238 isotope
ppb	parts per billion, per billion (10^9) units
%	per cent, per hundred (10^2) units

ppm	parts per million, per million (10^6) units
α	alpha decay
β^-	beta minus decay
β^+	beta plus decay
a_0	bohr radius
$\eta_{\alpha,\mathrm{UV}}$	conversion efficiency of an alpha particle's kinetic energy into UV light
$\bar{\nu}_e$	electronic antineutrino
E_e	electronic energy
ν_e	electronic neutrino
α_f	fine structure constant
γ	gamma decay
H	hamiltonian
$n(\lambda)$	index of refraction at wavelength λ
QE	quantum efficiency
Q_X^S	quenching of state S by species X
μ	reduced mass
E_r	rotational energy
J	rotational quantum number
$\downarrow$	spin $-\hbar/2$
$\uparrow$	spin $+\hbar/2$
$\omega_e\chi_e$	vibrational anharmonicity
E_v	vibrational energy
ω_e	vibrational frequency
v	vibrational quantum number
ψ	wavefunction

1 INTRODUCTION

Nuclear power plants, like any industrial facility, have finite lifetimes. After cessation of operation they need to be decommissioned. This includes the removal of fuel, dismantling of the plant, decontamination of components, demolition of the buildings and repatriation of the land to "greenfield" status for unrestricted re-use.

In the years to come more than 200 nuclear power plants will be decommissioned [1]. The lifetime of many power plants that have been built in the 1970s and 1980s will come to an end [2]. As of 2019, the average power plant that has a licence to operate for 40 years has already done so for 34 years [1, 3]. Licence extensions beyond this period are rarely granted. In addition, the disaster of Fukushima in 2011 caused many countries to gradually reduce their reliance on nuclear power and close down their plants [4]. Belgium, Germany, Spain and Switzerland gradually phase out of nuclear power [5, 6] with Germany having pledged to shut down its last nuclear power plant by the end of 2022 [7]. The large amount of upcoming decommissioning projects will consume plenty of resources and require the attention of many skilled professionals. Their number is unprecedented. The expected market size in Europe alone is expected to be more than 80 billion dollars [8, 9].

The costs for decommissioning a nuclear power plant are substantially higher than the decommissioning cost for other types of plants. A typical coal power plant, for instance, is about ten times cheaper to decommission [10]. The precise numbers vary from case to case, but the order of magnitude can be assumed to be in this range. Also, the duration over which they are decommissioned spans many tens of years. This is almost exclusively a consequence of the presence of radioactive material [11]. It has to be removed with processes that are occupationally hazardous, expensive, time-intensive and at the same time present environmental risks [12]. The precise decommissioning cost for each power plant is different and typically changes when radiation limits and prices for final deposit change [3]. However, the expenses for the safe removal of radioactive substances, the decontamination, reliably makes

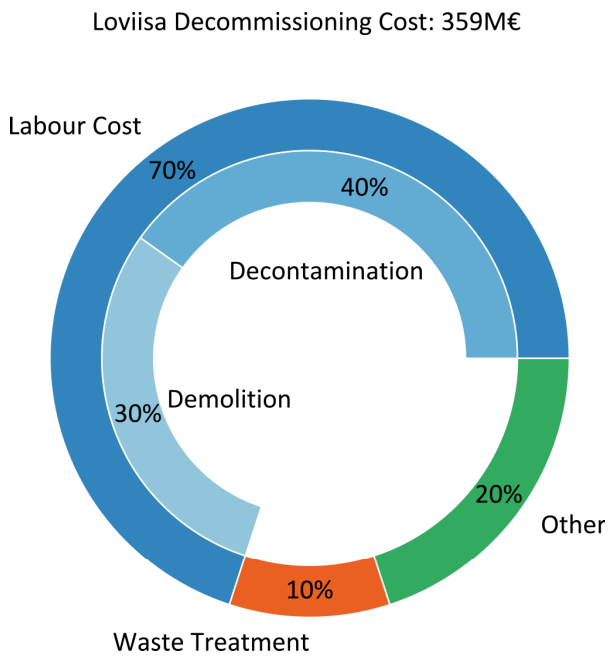

Figure 1.1 Loviisa decommissioning cost estimate as of 2012. Over half of all labour costs are assigned to activities related to decontamination. Only a small fraction of the total costs is allocated to actual waste treatment. The distribution of the costs has been estimated using data from [3]. The total cost of 359 M€ is an estimate made by the plant operator.

for the bulk of the total costs in any given scenario. Fig. 1.1 shows the estimated decommissioning cost as of 2012 for one of the oldest Finnish Nuclear power plants "Loviisa" [13]. It is considered a well managed power plant and its cost estimates have formed a reliable basis for decommissioning cost estimates in general. It is one of the few plants whose licence has been extended to 50 years [3]. In the estimated costs it becomes clear that they are driven by salaries for extensive amounts of manual labour. Over half of all this labour is related to decontamination.

During decontamination, radioactive material is removed from all components of the plant. For the most part, this concerns the reactor and connected pieces but it also applies to the plant at large. Decontaminated components are committed to normal recycling, and those which are beyond cleaning become, much like spent fuel, part of radioactive waste [14, 15]. In the case of the Loviisa nuclear power plant, the government regulations mandate that all components with an activity larger than $0.1\,\mathrm{kBq\,kg^{-1}}$ are to be considered radioactive waste and transported to Olkiluoto for

final storage [16].

Alpha contamination is among the most difficult types of contamination to detect and to clean. With its short range of only about 4 cm in air [17] an alpha particle is notoriously difficult to detect and requires that every single cavity and every single crack in each component be manually examined for potential contamination. Worse still, alpha contamination that ends up enclosed in metal components remains undetected. Melting alpha contaminated metal components causes the entire processing facility to become contaminated [18]. The common way to detect alpha radiation is to take a swipe sample and then analyse it with a Geiger-Müller counter [19] or a liquid scintillation counter [20]. It is easy to see how this hugely inefficient process makes up much of the labour that goes into decontamination. However, even massive amounts of manual labour do not reliably detect all alpha radiation, as the occasional report of the melting of Am-241 in steel reprocessing plants attest [21].

Alpha particles stopped in air create light that travels further than the particles themselves. Like all other forms of ionising radiation, alpha particles cause the production of light (radioluminescence) when they are stopped in air [22]. Unlike most other forms of ionising radiation, however, alpha particles have a high stopping power [23] and thus loose all their kinetic energy over a very short travel distance, of which a fraction of 10^{-5} is converted into ultraviolet light [24, 25, 26]. Thus an alpha particle with an energy of 5 MeV [17] creates roughly 100 UV photons in air [27], commonly referred to as 'radioluminescence'. Those small amounts of light are very difficult to detect. Even if detected, they are often indistinguishable from instrumental background. From this perspective it is unsurprising that the detection of radioluminescence has commonly not been thought of as a means of detecting the alpha particles themselves.

Recent developments of scientific grade cameras and photomultiplier tubes have made the detection of radioluminescence possible. The demand for those technologies originally comes from other fields, however, since the works of Lamadie [28] and Baschenko [24] it is clear that they can be successfully employed to detect alpha radiation. Following these first demonstrations, a whole field of research opened up with the declared aim to detecting alpha radiation by optical means alone [26, 29, 30, 31, 32]. If anything, the technique promises to be a less laborious and dangerous method than swiping over possibly contaminated pieces of disassembled nuclear reactors. In a 2016 article [33] a preliminary high point of this technology was presented when a

surface activity of $300\,\mathrm{Bq\,cm^{-2}}$ (that is 300 alpha decay events per second per square centimetre) at 1 m distance could be measured. Even though this is still far from the requirements set by governments, it makes it clear that radioluminescence detection has the potential to take the place of swipe tests in nuclear decommissioning.

The main limitations of air radioluminescence imaging are insensitivity to small emitters and a too large sensitivity to background lighting [34]. Successful techniques to tackle the latter problem generally resulted in worsening the former [29, 33, 35]. For all the success the collection of radioluminescence in air has shown, it is unlikely to dramatically increase its sensitivity without adding another component to the detection scheme that provides this increase.

1.1 Aim and Scope of this Work

The aim of this Thesis is to show that there are chemical species which emit radioluminescence with more advantageous properties compared to those of N_2 radioluminescence. Some species are better than others and in the past many different atoms, molecules and compounds have been proposed to take the place of N_2 as a means to improve the performance of alpha imaging [34]. However, the gains of replacing N_2 rarely outweigh the cost. When decommissioning a nuclear power plant, it is generally not worth investing even more time and money to control the gas atmosphere if it does not make the optical detection achieve the levels of sensitivity that are needed to comply with regulations and legislation. In an industrial setting, incremental improvement is not enough. Thus, the scope of this thesis is limited to those species that likely satisfy the cost-benefit calculus.

The process of finding a suitable species is slowed down by the scarcity of studies on the subject. The literature on the default species N_2 is vast not because it has been recognised for its ability to enable alpha imaging but because its luminescence properties are advantageous in other fields of research and technology. One of its industrial uses is this of an optical indicator to reveal small defects in railway overhead wires [36]. In astroparticle physics, it serves as an indicator for the presence of cosmic rays [37]. In fact, many of the most comprehensive studies done on the mechanisms that create N_2 (radio)luminescence come from this field [22]. It has to be stated as it is: the detailed knowledge of how useful N_2 luminescence can be to remotely detect alpha radiation had been provided by wholly unrelated fields. It had

not been gained in a deliberate line of research that aimed to study the radioluminescence of various chemical species. To this day, the number of comprehensive studies that do feature radioluminescence spectra of various species is small. This is critical for the purposes of this Thesis since it aims to find species with advantageous radioluminescence properties. And the meaning of 'advantageous' is narrowly defined by the use case of a decommissioning task. Thus, a central aim of this Thesis must be to consult the few available works on the radioluminescence of various species and discern suitable candidates. Thankfully, though, some of the older works stand out in the level of detail and comprehensiveness.

The advantageous properties require the radioluminescence of a suitable species to be created with vastly higher intensities than this in air and it must be usable even when daylight is present. In the Thesis, it is argued that the radioluminescence of NO fulfils both requirements simultaneously. Thus, the central aim is to demonstrate it and thus provide the proof that the limitations of daylight and low radioluminescence yield can be overcome. Another aim is to study the conditions under which the radioluminescence production is optimised. Within the scope of this Thesis, this means that the aim is to discern the precise concentrations of gases that need to be present around an alpha emitter such that a maximum amount of NO radioluminescence is created. Such a study necessarily includes the formulation of a theory, which can reasonably well explain the behaviour and predict conditions under which it can be recreated. A proof of principle for this theory is the detection of a weak alpha emitter in broad daylight by using NO radioluminescence.

Another aim of the Thesis is to study forms of radioluminescence that emerge in water. Many nuclear waste products are processed in liquid form [38] and the need to detect contamination by spill or leakage is obvious. The status of the literature around the topic of radioluminescence in liquids is even more precarious than this around gases. To the best of the author's knowledge, only 1 study before the year 2000 had been done and it reports the emission of blue light from an alpha active Po-210 source that had been immersed in water [25]. It is quite possible that more studies and reports exist, however, it is difficult to not notice the absence of schemes to optically detect radioluminescence in liquids, given the knowledge that it is feasible to do so with alpha contamination that is located in ambient air. Thus, another aim of the thesis is to study the radioluminescence in water and provide data that is potentially useful for alpha contamination detection in nuclear facilities.

In all those studies, the focus lies explicitly on application-relevant forms of radioluminescence. Many species, whose radioluminescence has properties that fulfil one requirement but not the other, are simply not discussed. Also, the theoretical treatment is limited to the extent to which it brings value to the application. Many details and adjacent phenomena do not find entrance into the treatment. They are mentioned, described and discussed as future improvements of the theory.

2 RADIOACTIVE CONTAMINATION

The primary reason to maintain high security standards around nuclear reactors is to prevent the spread and proliferation of its contents. The reactor contains isotopes which are immensely detrimental to physical health [39]. As an example, Am-241 is an isotope of americium that is produced in nuclear reactors burning Pu-239 [40]. Ingested amounts as small as 9 ng [41, 42] are likely to cause cancer and at elevated levels more immediate health problems [43]. Americium and its oxides are airborne [44] and readily disperse into the environment when released. Thus, measures are taken to hold it inside the reactor and keep it from spreading. Am-241 is only one of the isotopes contained in the reactor and most other isotope exhibit properties that are similarly detrimental to physical health. Any material that leaves the confines of the reactor, intentionally or not, is contamination and any place that contains it is contaminated.

Table 2.1 Types of nuclear decay, their emission and typical energy ranges. Compiled with data from [42, 45].

Decay Type	Emission	Typical Released Energy
α	${}^{4}_{2}\mathrm{He}^{2+}$ (alpha particle)	narrowly around 5 MeV [17]
β^-	e^-, $\bar{\nu}_\mathrm{e}$ (beta particle)	keV — MeV
β^+	e^+, ν_e	keV — MeV
Electron Capture	ν_e	keV — MeV
γ	λ (gamma ray)	keV — MeV
Internal Conversion	λ (X-ray)	keV — MeV
Neutron Emission	n	MeV

Am-241 and most other isotopes produced in a nuclear reactor are radioactive. Radioactive isotopes have unstable nuclei with excess amounts of energy which they eventually release in a process of nuclear decay [46]. While it is impossible to predict

when exactly a specific nucleus will decay [47], it is possible to estimate over which period of time half the number of a collection of identical nuclei will do so. With the exceptions of gamma decay and internal conversion, nuclear decay causes an isotope to transmutate into another one. Transmutated isotopes are often radioactive themselves. U-238 has to complete 13 nuclear transmutations before it eventually turns into stable Pb-206 [42].

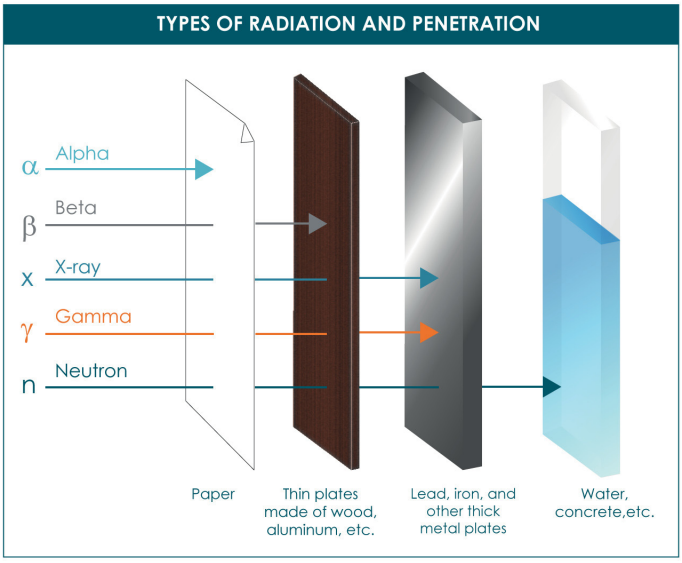

Figure 2.1 Types of nuclear radiation, their penetration and shielding against. This figure has first been presented in [48].

Energy emitted during nuclear decay takes the form of ionising radiation. Ionising radiation is radiation with energy sufficient to detach electrons from atoms or molecules. The element with the lowest ionisation energy is caesium with about 3.9 eV [49] and by this definition any radiation with more energy than 3.9 eV[1] is ionising. Removing the same electron from an atom that is part of a molecule typically requires more energy since the electron rests in the potential well that keeps the atoms in a molecular bond. In general, the ionisation energy of an electron in a molecule is higher. However, this need not be necessarily true as the example of F_2 shows, where ionising the molecule requires less energy than ionising a single F atom [51]. However, the energy range tends to be roughly the same and is typically

[1] This value marks the separation point of the UVA and the UVB spectral regions at 315 nm [50]

in the range of eV. In radiation protection and legislation the threshold is usually put higher at about 10 eV, however, the precise value differs from legislator to legislator [52]. By detaching electrons, ionising radiation changes the chemical composition of the material it comes in contact with and thus is damaging to biological tissue [53]. For the most part, it is ionising radiation that makes radioactive material dangerous. The fact that ingesting heavy metals is not healthy either is an additional risk factor [54]. A list of different types of nuclear decay, their emissions and energy ranges is presented in Tab. 2.1.

Radiation emitted during nuclear decay can consists of both particles and electromagnetic waves. X-rays and gamma rays are essentially electromagnetic waves with wavelengths of a few nanometers or shorter. As such they penetrate all material but those containing elements with heavy nuclei such as lead [55]. Alpha particles and electrons are charged particles and interact with the environment much more strongly than electromagnetic waves do [56]. In air, alpha particles travel for about 4 cm before being stopped, whereas beta particles travel about 1 m [24]. Neutrons penetrate more deeply into matter than electrically charged particles and interact mostly with the nuclei of light atoms like hydrogen through scattering events [57, 58]. To effectively shield against radiation, their interaction with the environment has to be known. In Fig. 2.1 qualitative shielding for the most hazardous types of nuclear radiation is shown.

Radioactive contamination makes its presence known by the characteristic way it interacts with matter. For example, electrons emitted in a β^--decay can carry energies of many MeV. With an electron rest mass of only 511 keV those highly-energetic electrons are necessarily ultrarelativistic and are ejected with speeds close to the speed of light in vacuum. In optically dense media those electrons exceed the phase-velocity of light in the medium and cause the emission of a characteristic blue light known as Cerenkov radiation [60, 61]. For the fastest electrons, even water with a refractive index around $n \approx 1.3$ [62] is optically dense enough. The presence of Cerenkov radiation reveals the presence of highly energetic charged particles and indicates that the area in which it arises might be contaminated. Fig. 2.2 shows Cerenkov radiation emanating from water that surrounds a nuclear reactor. Its presence indicates that ionising radiation in and around the reactor might be found.

Decontamination is the process of detecting and removing radioactive material from places where it should not be. For types of radiation where detection is straight-

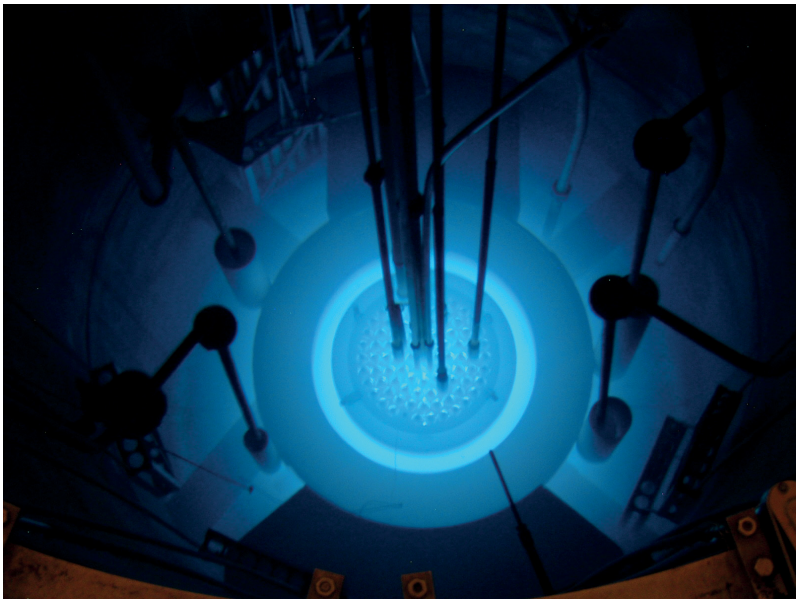

Figure 2.2 Cerenkov radiation around the TRIGA II reactor. The TRIGA II reactor is a test nuclear reactor at Kansas state university. This image is a single frame taken from a video featuring the reactor [59].

forward like it is for beta particles, the detection poses few difficulties. Beta radiation both readily interacts with the environment and travels, depending on the energy, a few metres in ambient air. This enables to use either classical Geiger-Müller-based ionisation chambers. However, the most economical and efficient solution is beta radiation detection using a scintillation counter [23]. Noteworthy is also the use of silicon strip detectors, a semiconductor-based approach which can be used to accurately determine the energy of the beta particle impacting it [20]. Those devices are typically more costly than scintillation counters, however. Neutron radiation detection requires a more subtle approach since neutrons do not readily interact via the electromagnetic force with their environment as beta particles do. In the most common approach to detecting them, the kinetic energy of neutrons is used via a variety of absorption reactions (radiation capture, nuclear fission and others) to release charged particles, which are then detected. The design of a neutron detector is usually highly optimised for a specific range of energies that the neutrons to be detected are believed to have. However, all of the approaches have in common that they must first make the neutron interact with some material to release charges that

then can be used as an indicator for the presence of neutron radiation. The list of possible detectors is comprehensive, and it might be best to consult the handbook on radiation security of Knoll [23], or related works, to gain more information on the matter. The book also covers more specific designs like U-235 fission chambers.

The Thesis foucses mainly on detection of alpha radiation. Though beta and neutron radiation are undoubtatly relevant in decommissioning nuclear power plants, too, it is alpha radiation detection that typically presents difficulties.

2.1 Alpha Contamination

Alpha radiation is different from other nuclear radiation in that it is very localised. An alpha particle consists of two protons and two neutrons which nets to two elementary charges. In contrast to beta particles, an alpha particle has double the charge and interacts via the Coulomb force with matter much more intensely. Hence, after being ejected from the nucleus, an alpha particle typically comes to a halt more quickly than a beta particle of comparable energy does. A particle's energy loss per unit length is typically represented as a function of the distance it has already traveled, which is commonly referred to as a particle's Bragg curve. A Bragg curve depends on the particle's charge, its initial kinetic energy and the electromagnetic properties of the medium. Fig. 2.3 shows a Bragg curve drawn for a 5.5 MeV alpha particle that is being stopped in air. After having traversed a distance of about 4 cm the forces that slow down the particle become much stronger and bring the particle to a final and sudden halt. It is the position of maximum loss that marks the range of an alpha particle in air. The distinct and sudden increase in stopping power is called the Bragg peak. The Bragg peak occurs because the charged particle's interaction cross section with the environment increases as the particle is slowed down. The rate by which the particle loses energy is inversely proportional to the square of their velocity, which explains the peak occurs just before the particle comes to a complete halt [63]. The position of the Bragg curve shifts depending on a particle's initial energy. The Bragg Peak of more energetic particles is found at larger distances. Alpha particles mostly interact with the electron clouds around atoms and rarely with the nuclei themselves [64, 65]. They are much heavier than electrons and upon collision only change their travel direction by a minuscule amount. Hence, their trajectories tend to be straight lines.

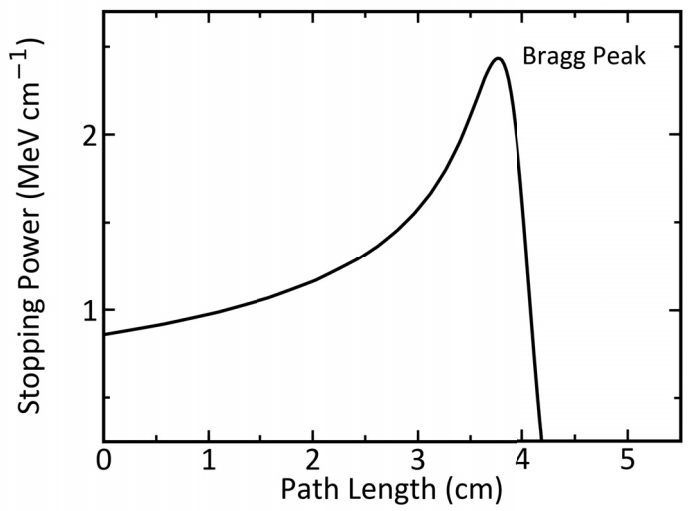

Figure 2.3 Bragg curve of $5.5\,\mathrm{MeV}$ alpha particle in air. Shortly before coming to a halt, the alpha particle is slowed down the most. This sudden increase in stopping power before a total halt is the Bragg peak. The curve has been compiled using data from [66].

The short range of an alpha particle makes it easy to shield it but at the same time a serious health risk. The stopping power of solids is generally vastly greater than that of air, which allows to use a sheet of paper to serve as effective protection layer against alpha radiation. Even human skin provides adequate protection, which makes for a common misconception that alpha radiation is small threat to health [56]. However, if an alpha active substance enters the body, then the quick stopping of alpha particles becomes the very mechanisms that efficiently disintegrates biomolecules [67]. For example, radon is a noble gas created in the uranium decay chain and it commonly accumulates indoors and in places with insufficient ventilation [42]. As a noble gas it is colorless, odorless and tasteless [68]. All of its 37 isotopes are radioactive and most of them decay be emitting an alpha particle [42]. Radon easily enters the body through the respiratory track where it causes all sorts of maladies, including lung cancer [69]. Alpha activity and its virtual undetectability make radon a leading environmental cause of cancer mortality [70].

An alpha particle deposits its kinetic energy into the air and thereby ionises atoms and molecules. In an elastic scattering event an alpha particle can only transfer a small amount of kinetic energy to a newly released electron. Conservation of momentum sets an upper limit of a fraction of about $1/1800$ of the alpha particle's kinetic

energy at the time of ionisation [23], which means that electrons generated by alpha particle ionisiation typically do not have more than 3 keV of kinetic energy. Generally it is much lower. As a result, thousands of ionisations have to happen before an alpha particle comes to rest. The numerous electrons freed this way further interact with the medium. They either ionise even more molecules or they lose their energy in scattering events [71]. The air is said to be exposed to an electron bombardment.

Bombardment by electrons causes the air to fluoresce. It converts the electron's energy into light of wavelengths between 300 and 430 nm with a conversion efficiency between 17.6 photons MeV^{-1} and 20.8 photons MeV^{-1} of electron energy [72]. It takes thousands of low-energy electron created during alpha-particle stopping in ambient air to create a few photons of light. In contrast, a single low-energetic beta-particle with energies in the order MeV can produce the same air luminescence. The conversion efficiency changes with changes in ambient pressure and temperature [73], however, the mechanisms that produces the glow is the same: Electrons with kinetic energies of less than 1 keV electronically excite nitrogen molecules which then relax by emitting ultraviolet light [22]. Electrons with energies GeV or higher also produce air radioluminescence, but they do so at a much reduced conversion efficiency [74]. Thus beta particles that are emitted with high kinetic energy, do not produce air radioluminescence in the same capacity as electron bombardment does.

Air fluorescence can serve as an indicator of the presence of alpha radiation. Though the presence of air fluorescence only indicates electron bombardment, it can also indicate the mechanism that gave rise to it. In the field of astroparticle physics for instance, the detection of air fluorescence is tantamount to the detection of cosmic rays [37]. In the absence of cosmic rays, electric arcs [75] or other sources of free electrons, air fluorescence indicates the presence of alpha contamination. Thus, the fluorescence is a form of alpha-induced radioluminescence. It is still fluorescence in the sense that light is emitted through decay of an excitation via a dipole-transition. The name "radioluminescence" highlights the fact that the presence of ionising radiation was necessary to produces this excitation in the first place. The kind of radioluminescence discussed in this Thesis is limited to alpha-induced radioluminescence. From now on it is simply addressed by the shorthand "radioluminescence" and any connection to alpha radiation is implied.

The detection of radioluminescence is the principle basis on which optical detection of alpha radiation rests [76]. For practical reasons optical detection of alpha

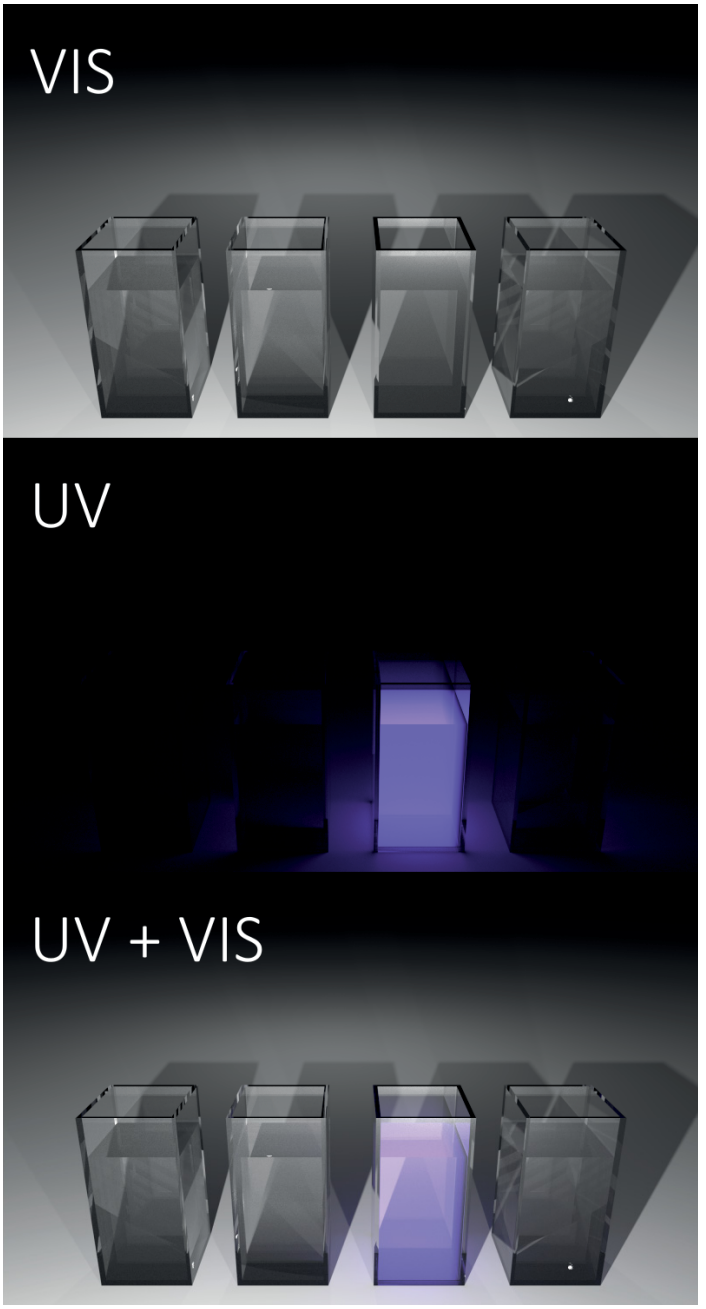

Figure 2.4 Principle of radioluminescence detection. **Top**: Four filled cuvettes are lined up and imaged in visible light. One of the cuvettes is known to contain a contaminated liquid. **Centre**: The same scene imaged by collecting only UV light. The liquid in one of the cuvettes is glowing. **Bottom**: An overlay image shows that the liquid in the 3^{rd} cuvette is alpha contaminated.

radiation works with radioluminescence of N_2 and to some extent with N_2^+. However, it is noteworthy to point out that a number of different atoms and molecules have been shown to emit radioluminescence when exposed to alpha radiation [77, 78]. The technique itself remains agnostic as to which particular molecule produced the radioluminescence, it simply collects light. And if there is reason to believe that this light is indicative of the presence of alpha radiation, then the detection of this light is as good as the detection of the radiation itself. Then the practical implementation goes like this: An area that is suspected to be alpha contaminated is imaged by only collecting ultraviolet light. An overlay of this image with an image in daylight then reveals the position of the alpha contamination. In Fig. 2.4 an example of this method, carried out in a hypothetical scenario, illustrates the principle.

Optical detection of alpha radiation detection works by collecting ultraviolet light to the exclusion of all other wavelengths. The benefits are two-fold. First, the amount of natural background light in the UV is substantially lower than this in regimes of longer wavelengths [79]. Second, detection of UV photons allows for much increased sensitivity, when compared to the detection of photons of longer wavelengths. The reason for that comes with the technology that is being used. Photomultipler tubes (PMT) are devices capable of detecting single photons and they are an excellent choice in detecting low light levels. As such, they have found widespread use in the field of optical alpha detection [33]. PMTs work by multiplying electrons that have been released from a photocathode which had been struck by a photon. If an appropriate cathode material is chosen, then only the strike of a photon that falls within a certain wavelength range releases such an electron. This makes a PMT insensitive to background lighting of undesired wavelengths. In the case of UV-sensitive photocathodes, it also makes it robust against thermal noise [80]. A photocathode sensitive to photons of shorter wavelength is exponentially less likely to have a electron released by thermal effects than a photocathode that is sensitive to photons of longer wavelengths. This particular advantage accounts for much of the reason why typically only UV light is being collected.

The most well understood and widely used type or UV radioluminescence is this of N_2. It is sensible to introduce and discuss this particular type of radioluminescence first.

3 RADIOLUMINESCENCE IN AIR

Radioluminescence in air typically refers to the fluorescence emitted by N_2 exclusively. That is not to say that there aren't other chemical species found in air that produce radioluminescence. Atmospheric dry air consists of 4 parts of N_2 (78 %), 1 part of O_2 (21 %), small amounts of Ar (1 %) and a few other trace gases [81]. All of these molecules and some of their ions are known to produce radioluminescence [77]. However, it is N_2 that is typically sufficiently abundant to produce detectable amounts of light in the UV. It is for that reason that radioluminescence in air and radioluminescence of N_2 are sometimes used somewhat interchangeably. A more nuanced description of radioluminescence in air can also include the contributions of the molecular nitrogen ion N_2^+ [22, 82]. For the intents and purposes of this Thesis, a reduction of radioluminescence in air to radioluminescence of N_2 provides a sufficient level of detail.

3.1 The Nitrogen Spectrum

N_2 is a diatomic molecule. It consists of two nitrogen atoms with each of them having their 7 electrons form the ground state configuration

$$\mathrm{N}(^4S_{3/2}) : 1s^2 2s^2 2p^3. \tag{3.1}$$

The electrons of both atoms combine to fill the molecular orbitals of N_2 in accordance with Tab. 3.1 to produce the molecular ground state configuration

$$\mathrm{N}_2(X\,^1\Sigma_g^+) : (\sigma_g 1s)^2(\sigma_u^* 1s)^2(\sigma_g 2s)^2(\sigma_u^* 2s)^2\underbrace{(\pi_g 2p)^4(\sigma_g 2p)^2}_{\text{triple bond}}, \tag{3.2}$$

where a subscript g indicates an orbital's inverse symmetry with respect to the molecule's centre (g stands for *gerade*, German: even) and u an orbital's inverse anti-

symmetry with respect to the molecule's centre (u stands for *ungerade*, German: uneven). σ orbitals are cylindrically symmetric and π orbitals anti-symmetric with respect to the intermolecular axis. An asterisk as a superscript denotes that the orbital is antibonding whereas an orbital without an asterisk is bonding. An bonding orbital contributes to the bond strength by approximately the same amount an antibonding one reduces it [51]. Thus, from the electron configuration in Eq. (3.2) it becomes apparent that the nitrogen atoms are very tightly held together by a triple bond made up of three bonding orbitals. The bond has a dissociation energy of $945.41\,\mathrm{kJ\,mol^{-1}}$ [40], which makes it necessary to use relatively large amounts of energy to break the bond or have the molecule chemically react. N_2 is chemically inert.

Table 3.1 Ground state electron configuration of N_2. The atomic orbitals of two nitrogen atoms with 7 electrons each combine to form a stable triple bond. With all electrons paired, the ground state's total spin is zero and the term symbol is ${}^1\Sigma_g^+$.

N	N	$N_2:\sigma$	$N_2:\sigma^*$	$N_2:\pi$	$N_2:\pi^*$
$1s^2$	$1s^2$	$(\sigma_g 1s)^2$	$(\sigma_u^* 1s)^2$		
$2s^2$	$2s^2$	$(\sigma_g 2s)^2$	$(\sigma_u^* 2s)^2$		
$2p^3$	$2p^3$	$(\sigma_g 2p)^2$		$(\pi_g 2p)^4$	

The molecular energy is the sum of the total kinetic energy T and total potential energy V the system of nuclei and electrons contains. The Hamiltonian which accounts for all of the energy contributions is

$$H = T_e + T_n + V_{en} + V_{ee} + V_{en}, \tag{3.3}$$

where $T_{e/n}$ is the kinetic energy of the electrons/nuclei, $V_{ee/nn}$ the Coulombic repulsion between electrons/nuclei and V_{en} the attractive potential between electrons and nuclei. The Hamiltonian is the operator whose eigenvalue E is the energy contained in the system, which is described by the Schrödinger equation with

$$H\psi = E\psi, \tag{3.4}$$

where ψ is the wavefunction of the system. In the Born-Oppenheimer approximation this equation is elegantly solved by recognising that a nucleon is about 2000

times more massive than an electron [51]. Thus, any movement by the massive inert nuclei is thought to be met with an almost instantaneous rearrangement of the much lighter electrons. In this approximation, Eq. (3.4) separates into two distinct Schrödinger equations, where one describes the electronic and the other one the nucleonic contribution. They act independently of one another and treat the position variables of the other system as mere constants, rather than as variables [83]. In the Born-Oppenheimer approximation the total energy E simplifies to a sum of three distinct contributions

$$E = E_e + E_v + E_r, \tag{3.5}$$

where E_e describes the energy contained in the electron configuration, E_v the energy contained in the quantised vibration of the nuclei around their equilibrium points and E_r the energy contained in the quantised rotation of the nuclei around their centre of mass. Typically the electronic contribution accounts for most of the total energy, where the vibrational contribution is orders of magnitudes smaller than the electronic one and the rotational contribution is orders of magnitudes smaller than the vibrational one. As a rule of thumb, $E_e \gg E_v \gg E_r$ applies.

The potential energy contained in a molecule changes with the distance between the nuclei. A contracted molecule has a high potential energy with Coulombic repulsion being strong. A molecule with very large distances between the nuclei is essentially dissociated and does not have any potential energy, the Coulombic repulsion is weak. In the case of a bonding electron configuration, there exists a energetic minimum between these two extremes that marks the point where the bond length is at equilibrium. In 1929 Morse suggested to approximate this potential curve for the special case of a diatomic molecule with an anharmonic oscillator of the form [85]

$$V(r) = D_e \left(1 - e^{-a(r-r_e)}\right)^2, \qquad r \geq 0, \tag{3.6}$$

where r is the internuclear distance, $D_e = V(\infty) - V(r_e)$ the dissociation energy, r_e the equilibrium bond length and $a = 2\pi\omega_e c\sqrt{\mu/2D_e}$ the steepness of the potential. μ is the molecule's reduced mass and ω_e the fundamental frequency of vibration in units of wavenumbers. Though making several approximations and being of generally limited quantitative use [86], the ease by which the equation of the Morse

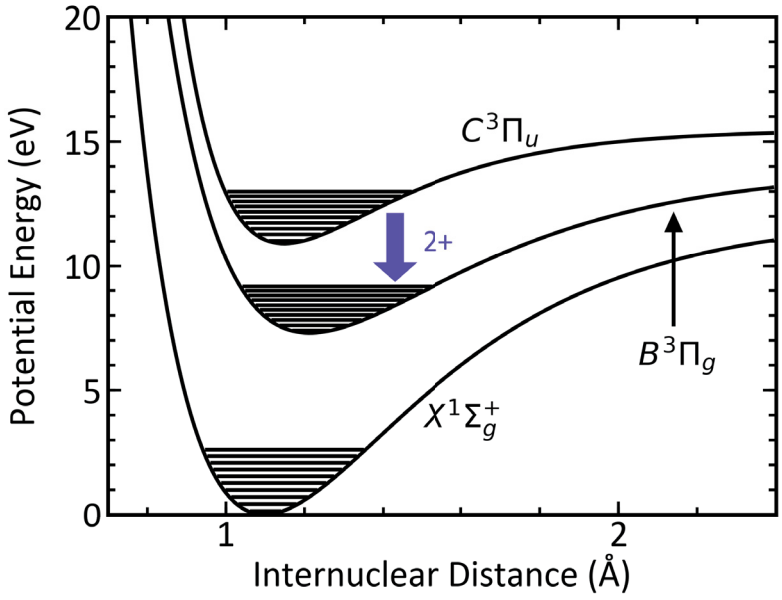

Figure 3.1 Morse potentials for N_2. Potentials including the first 10 vibrational levels are drawn for selected electron configurations. Radiative decay from the $C^3\Pi_u$ state to the $B^3\Pi_g$ state creates ultraviolet emissions that form the 2+ systems. The potentials have been drawn using the extensive compilation of molecular constants of Lofthus and Krupenie [84].

potential can be manipulated and graphically displayed justifies its continuing popularity.

Adding vibrational and rotational energies to the electronic energy completes the picture and yields a molecule's entire energy. Within the scope of this Thesis rotational energies are not considered. Their contribution to the energies of the photons that make up radioluminescence in air is not significant enough to justify an extensive treatment. A work that does treat them in much greater detail is this of Waldenmaier [82], it is his work that might be consulted for further study. Vibrational energies, however, do play a central part in explaining the N_2 radioluminescence spectrum. The algebraic form of the vibrational energies including the first correction term is [51]

$$E_v = hc\omega_e\left(v+\frac{1}{2}\right) - hc\omega_e\chi_e\left(v+\frac{1}{2}\right)^2, \qquad v \in \mathbb{N}_0, \tag{3.7}$$

where v is the vibrational quantum number, ω_e the fundamental frequency in units

of wavenumbers and $\omega_e\chi_e$ the first order vibrational anharmonicity. In Fig. 3.1 Morse potentials for different electron configurations of N_2 show the deep potential wells of the N_2 molecule. Each electronic potential shows its first 10 vibrational levels.

Electron bombardment causes ground state N_2 to become excited. The ground state has a total spin of 0 while those of the next three excited states, *A*, *B* and *C*, have a total spin of 1 [84]. Hence an excitation from the ground state to either one of the excited states by mere energy deposit alone is forbidden, since the angular momentum in such a reaction would not be conserved [87]. An exchange of one of the molecule's valence electron with an electron from the bombardment, however, does allow for the excitation. Electrons carry a spin of $S = \hbar/2$ and exchanging one of the electrons in either the $(\sigma_g 1s)$ or the $(\pi_g 1s)$ orbitals with an electron of opposite spin provides the needed angular momentum. The excitation of the upper state involved in producing N_2 radioluminescence, the *C* state, happens via the electron exchange [82, 88]

$$e^-(\uparrow) + N_2(X^1\Sigma_g^+) \rightarrow N_2(C^3\Pi_u) + e^-_{\text{exchanged}}(\downarrow), \tag{3.8}$$

which is considered to be the primary path for the excitation of the *C* from the ground state [89]. This process is most efficient with incident electrons of 14 — 15 eV energy at an excitation cross section of about $1.6\,a_0^2$ [74, 90, 91, 92, 93], where $a_0 = 5.2917721093(80) \cdot 10^{11}$ m is the Bohr radius [94]. For higher electron energies the cross section rapidly drops [95]. The only other mechanism that might be relevant is the recombination of ionised molecules [82]

$$e^- + N_2^+(X^2\Sigma_g^+) \rightarrow N_2(C^3\Pi_u). \tag{3.9}$$

Other excitation paths like decay from higher electronic states are considered insignificant [89].

Radiative decay from the *C* to the *B* state produces ultraviolet emissions between 300 and 420 nm. All emissions combined form a characteristics spectral pattern, which is commonly referred to as the 2nd positive system or 2+ in shorthand [82, 84]. In Fig. 3.2 the radioluminescence in air between 250 and 450 nm is presented. It was obtained by placing a 32 MBq Am-241 source in front of a scanning monochromator (Horiba Scientific, Product Code: iHR 550) and counting the radiolumines-

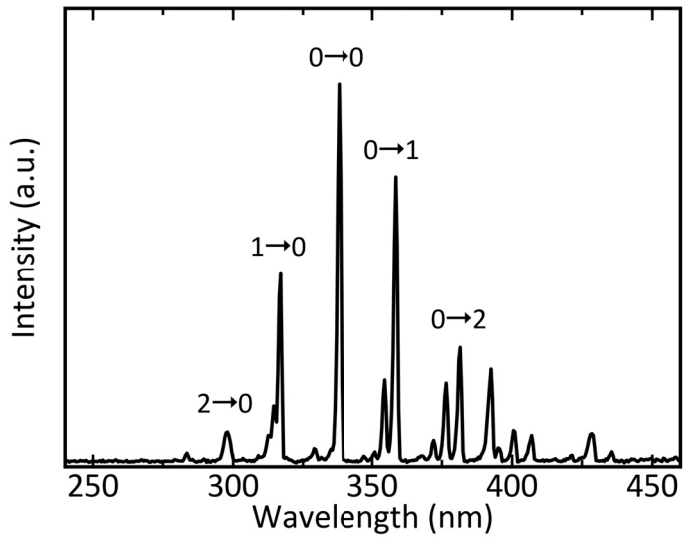

Figure 3.2 Spectrum of radioluminescence in air. Compiled using spectroscopic data from Publication I. Labels of the form $v' \rightarrow v''$ have been added to the most significant peaks and indicate the corresponding vibrational transitions.

cence photons that passed the monochromator at a given wavelength with a UV sensitive low-noise PMT (Perkin Elmer, Product Code: MD-1982P). The throughput was optimised by collecting the radioluminescence light with a Keplerian telescope (Thorlabs, Product Code: LA4052-UV, $f = 35\,\mathrm{mm}$ and Thorlabs, Product Code: LA4924-UV, $f = 175\,\mathrm{mm}$) before guiding it into the monochromator. The grating that had been used had a groove density of $1\,800\,\mathrm{gr\,mm^{-1}}$ (Horiba Scientific, Product Code: 53020) and the monochromator was operated with a slight width of 1 mm. Both combined to a spectral resolution of 1 nm. The efficiencies of all involved optical elements are displayed in Fig. 3.3.

The subdivision of the electronic states into vibrational levels causes the 2+ spectrum to appear as a sequence of distinct spectral lines. A radiative decay $C^3\Pi_u(v' = 0) \rightarrow B^3\Pi_g(v'' = 0)$ produces a photon of the wavelength 337.13 nm that is emitted into a random direction. A more energetic photon of the wavelength 315.93 nm is created when the same decay occurs from the upper vibrational level $v' = 1$. The limited number of ways the excited state can radiatively decay makes the spectrum appear in spectral lines, rather than as a continuum. A summary of the most relevant of the lines is given in Tab. 3.2.

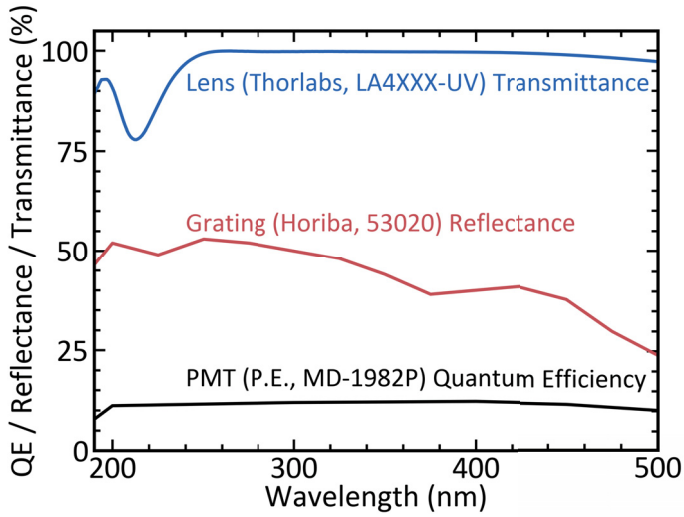

Figure 3.3 Efficiencies of the devices used to record the spectrum of the light emitted by radioactively excited N_2. The PMT (Perkin Elmer, Product Code: MD-1982P, black, [96]) quantum efficiency was small but flat throughout the measurement range. The reflectance of the grating (Horiba Scientific, Product Code: 53020, red, [97]) varied strongly with the wavelength. The transmittance of the UV coated lenses (Thorlabs, Product Code: LA4XXX-UV, blue, [98]) was mostly flat. The recorded spectrum displayed in Fig. 3.2 has been corrected for the displayed efficiencies.

Table 3.2 Relative intensities of selected spectral lines of the 2+ system. Lines that are located in the UVC are marked with an asterisk. The table has been compiled from data presented in [84, 99] and Publication I.

λ(nm)	v'	v''	I_{rel}(%)	λ(nm)	v'	v''	I_{rel}(%)
268.7*	4	0	< 1	337.13	0	0	100
281.98	3	0	5	357.69	0	1	67
297.68	2	0	12	380.49	0	2	22
315.93	1	0	67	405.94	0	3	7

The majority of the excitations does not radiatively decay. They are lost to collisional quenching with the surrounding molecules instead. All molecules in air, including N_2, quench the C state. Some are worse than others and O_2 and H_2O are particularly noteworthy examples of quenchers that drastically reduce the radioluminescence yield. Even though water typically is only present as a trace gas, its generally large quenching coefficients make even small amounts of water quickly noticeable. Quenching affects different upper state vibrational quantum numbers v' differently. A short list of the most important quenchers and their respective quenching rates are presented in Tab. 3.3.

Table 3.3 Quenching rates of the $N_2\,C^3\Pi_u(v'=0,1)$ states by molecules found in air. The list is an abridged version of Tab. 3 in [82].

Quenching Species X	$Q_X^{N_2(C,v'=0)}\,(10^{-10}\,\mathrm{cm^3\,s^{-1}})$	$Q_X^{N_2(C,v'=1)}\,(10^{-10}\,\mathrm{cm^3\,s^{-1}})$
N_2	0.11 ± 0.00	0.29 ± 0.00
O_2	2.76 ± 0.01	2.70 ± 0.03
H_2O	5.43 ± 0.12	5.78 ± 0.17

Radioluminescence in air is weak compared to most other light sources. In ambient air, the stopping of a single alpha particle in air creates the production of about 100 UV photons [27]. Those photons are mainly emitted by N_2 with small contributions from N_2^+. The number of photons increases by about 7 % when the alpha particle is stopped in dry air and by about 500 % when being stopped in an atmosphere which is made up entirely of N_2. As a result, even a large contamination of 100 kBq produces of an amount of light that is about one million times smaller than this of a typical 100 W light bulb. The only sensible way to optically detect such a source is by either spectrally separating its emission from this of other light sources or by not having other light sources to begin with.

3.2 Imaging Alpha Contamination

The original idea to image alpha radiation was conceived by Imbard and Pineau in 2001 [100]. In their patent titled "Remote α Source Location Device and Method" they describe the use of optics and a suitable detector to collect radioluminescence as a means to detect alpha radiation. It took 3 more years for the first actual demon-

stration to come to fruition when Baschenko presented in 2004 a UV-sensitive film with which he photographed a 37 MBq Pu-239 alpha active source from 30 m distance [24]. The photograph was made in total darkness. In his paper, Baschenko also elaborated on the possible obfuscation of a radioluminescence photograph by gamma radiation. By placing a gamma active 18.5 MBq Co-60 source next to the plutonium and still being able to take a photo, he proved that UV imaging is a viable method to remotely detect alpha radiation.

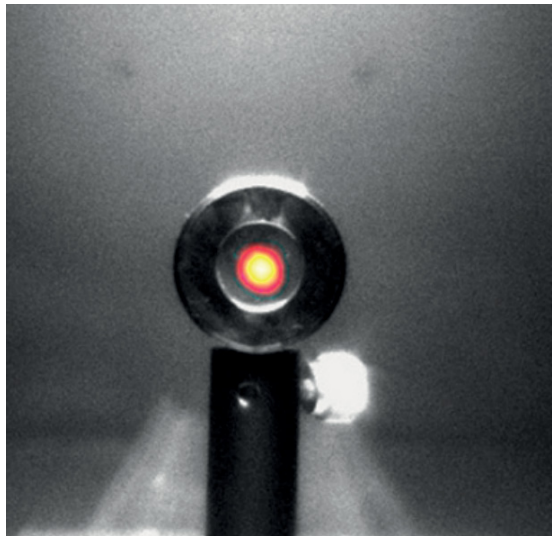

Figure 3.4 World's first CCD image of an alpha source. The grayscale image shows a typical post and sample holder taken in visible light. The red overlay has been created by imaging the very same scene by only collecting UV light. The red spot in the centre of the sample holder shows an increased production of UV light and thus betrays the presence of alpha contamination. This image is a crop from Fig. 2(b) of the original work published by Lamadie and colleagues [28].

Yet the pioneering results that would show the technique's capabilities in actual nuclear installations were published by Lamadie and colleagues in 2005 [28]. Motivated by practical concerns, they pointed to the fact that the primarily alpha active actinides are typically weak gamma emitters, which makes detecting them with the more well-known method of gamma imaging rather difficult. They resorted to the back then already-known technique of alpha imaging. However, instead of relying on UV-sensitive film they used a scientific grade charge-coupled device (CCD) to image the actinides. With this substantial improvement in hardware, they detected

alpha contaminations with activities as low as a few hundred $\mathrm{Bq\,cm^{-2}}$ with a total of 5 h integration time. The first image of an alpha source taken with a CCD is reprinted in Fig. 3.4.

It was Mahé from the very same group who later used the same technique to image alpha contamination inside a glovebox through as much as 10 mm thick plexiglass without breaching the confinement [31]. From this point onwards, the technique quickly evolved with the first use of intensified charge-coupled device (ICCD) and more sophisticated methods of image acquisition [101, 102]. Much like Baschenko before them, Lamadie and Mahé noticed how sensitive the successful implementation of alpha imaging is to the levels of background lighting. The detector technology itself, on which much of the current technology that underpins alpha imaging rests, has been developed by Cousins and Ingrid and their respective groups [103, 104].

One of the primary interests in alpha imaging comes from nuclear safeguard. Chichester and colleagues suggested that it might be beneficial in sampling plutonium work [105]. He elaborates that it might help to verify plutonium works which have been declared and possibly help to identify those which are not. Similarly, Jessice Feener suggested that alpha imaging might be a viable method to verify nuclear warheads [106]. She asks the question whether a nuclear warhead, which exposes its fissile material directly to the air, reveals sensitive details about the warhead designs via UV emissions. Though she concludes that enriched uranium is too weak an alpha emitter to produce sufficient UV light, she cannot draw similar conclusions for plutonium powered warheads [30]. More investigation into the subject would be necessary.

To this date the most promising technology is still based on CCD technology. In a study in 2015 Sand and colleagues from Tampere University and the JRC in Karlsruhe designed an experiment where CCD, ICCD and electron-multiplying CCD (EMCCD) cameras where compared side-by-side [32]. Though all three technologies had been employed to one degree or another before this work [28, 102, 107], a direct comparison had not been conducted. All three technologies make use of CCD image sensors, however, ICCD and EMCCD are generally more capable to detect faint light sources. An EMCCD employs on-chip electron multiplication before readout to reduce the impact of the otherwise constant readout-noise. This greatly reduces the noise floor and helps to detect weak light sources. An ICCD uses the photoelec-

tric effect for the initial conversion of the photon to an electron. In this manner it was very similar to a PMT. It is different from a PMT, however, in that it then amplifies the signal with a pixelated microchannel plate which is read out by conversion of the electron burst into light via a phosphor screen connected to the CCD element. The central conclusion of the work was, that low readout noise is essential for the rapid optical detection of alpha sources. Both ICCD and EMCCD achieve this in different ways, where the ICCD has been found to perform slightly better. Overall, both types of cameras were found to be beneficial upgrades over a mere CCD sensor in that they effectively reduce the time in which alpha sources can be imaged.

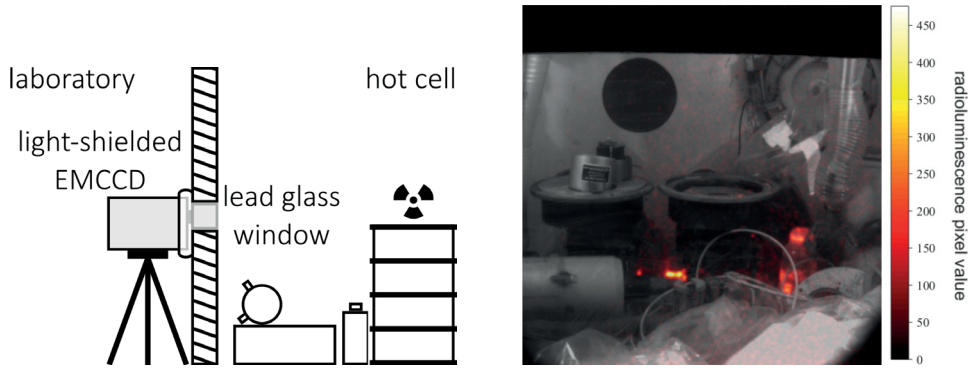

Figure 3.5 An EMCCD finding alpha contamination in a hot cell. **Left**: An EMCCD placed next to the lead window of a darkened hot cell formed an image of light of wavelengths longer than 400 nm. The light was produced inside the hot cell and reached the camera through a lead window. The image has first been shown in Fig. 3 in Publication I. **Right**: The overlay image of visible image (greyscale) and UV image (red) reveals places of intense alpha contamination. This image has first been shown in Fig. 6 in Publication I.

The results presented in Publication I of this Thesis build on this work. There an EMCCD camera (Andor, Product Code: iXon3 897) has been used to image alpha radiation in contaminated areas from a safe distance. The imaging procedure followed the imaging best practices derived by Sand and colleagues [32] and localised the contamination with an overlay image as first employed by Lamadie et al. [28]. The focus of this work was to demonstrate that the technology had matured enough such that it could be reliably used in scenarios where a contamination was known to be present but not precisely localised. The contamination was assumed to be strong enough that approaching it physically and using a classical swipe test would have been connected with large security risks.

The scenarios that had been chosen were a (staged) nuclear crime scene and an actual hot cell. In both scenarios radioluminescence in air had been collected. In the case of the crime scene the camera was equipped with an interference filter that only allowed light with wavelengths 314 and 354 nm (Semrock, Product Code: FF01-334/40-25) to reach the camera sensor. Though this meant that only the $1 \rightarrow 0$ and $0 \rightarrow 0$ peaks of the entire radioluminescence spectrum were captured, it was necessary to use the filters to diminish the effects of background lighting. The overlay images shown in Fig. 3.5 clearly show that both sources with an activity of tens of MBq had been resolved and successfully localised. More importantly, this had been done from a safe distance and exposure of neither equipment nor personnel to the radiation source was necessary.

The same procedure was applied to image the insides of a hot cell. Hot cells, or more formally 'shielded nuclear radiation containment chambers', are containments that are required to protect individuals from ionising radiation of highly active sources. They are suitable to contain material such as nuclear waste and they are the only type of confinement where nuclear fuel can be purified in a process called plutonium-uranium redox extraction [38]. The windows that allow to look inside a hot cell are necessarily made of lead glass to protect the viewer from gamma radiation [108]. Lead glass absorbs light of wavelengths shorter than 400 nm ([109], for a collection of transmission spectra of lead glasses used in radiation shielding, the work of Limkitjaroenporn and colleagues [110] might be consulted) which leaves very little of the radioluminescence in air to escape the hot cell and therefore usable for alpha imaging. The most intense transmission of N_2 radioluminescence is the $0 \rightarrow 3$ transition which is about 7 % as intense as the emission at 337.13 nm (c.f. Tab. 3.2). Nevertheless, upon placing the EMCCD next to the lead glass window and have it form an image, alpha sources had clearly been identified. The overlay images are shown in Fig. 3.5. This was mainly possible because hot cells store the strongest of sources emitting ionising radiation and thus even small fractions of the radioluminescence reaching the camera is sufficient to form an image.

3.3 Operation in Illuminated Environments

Radioluminescence in air consists of few photons which makes its detection in even completely dark environment a challenging task. If, however, light from sources

other than alpha particles is present, then the measurement becomes more challenging still. If measurement in a completely dark environment cannot be guaranteed, then the intensity and character of the background illumination impose strict limitations on the extent to which alpha radiation can imaged.

In the absence of background lighting, the detection of any UV light is tantamount to the detection of radioluminescence. If background lighting cannot be avoided, then the only viable way to reliably detect radioluminescence is preventing the background illumination to reach the detector. This is achieved by spectrally separating the light that strikes the optics. The central idea is that if the wavelength of the incoming light falls within a predefined permissible spectral range, then it gets transmitted and reaches the detector. If it does not, then it gets either reflected or absorbed. Depending on the spectrum of the background lighting, designing such optics can either be a manageable or an insurmountable task.

The difficulty of designing the optics is coincidental with the spectral range the background illumination covers. If it does not cover UV wavelengths at all, then equipping the detection optics with a short pass filter with a transmission cut-off at about 400 nm or a bandpass filtering around selected spectral lines effectively hinders background lighting from reaching the detector. This is what has been done in Publication I, where interference filters were employed to reject background lighting from door signs. This technique has also proven successful for Sand and colleagues [33], where they equipped a PMT with a stack of three interference filters. There they imaged alpha radiation by mounting a PMT on a pan-tilt system to create a low-resolution yet high-sensitivity image of radioluminescence in air. The filters were instrumental in enabling the team to operate in an environment illuminated by visible light.

Cases where background lighting does not cover UV wavelengths are relatively easy to handle. This is in part because the spectral discrimination is straight forward and indiscriminately considers any form of UV light 'desired' while considering all other forms of light emitted in different wavelength regimes 'undesired'. It is also partly due to the circumstance that the relevant filters are nowadays readily available off-the-shelf. For example, interference filters are often a solid choice for shielding against background lighting. A number of those filters can easily be combined to achieve the desired background rejection while at the same time maintain good transmission of desired light. Their transmission properties do not so much depend

on characteristics inherent to the material they are made of. Instead, thickness and arrangement of the thin layers of different dielectric material determine its optical properties [111]. This enables to construct filters with nearly limitless customisable transmittance properties. In most cases relevant for alpha imaging, however, a custom solution is not necessary. A generally large demand for interference filters has made it that the selection of readily available interference filters is constantly growing while at the same time their prices are constantly falling. Among this selection, there are typically filters that fit the specific need at hand.

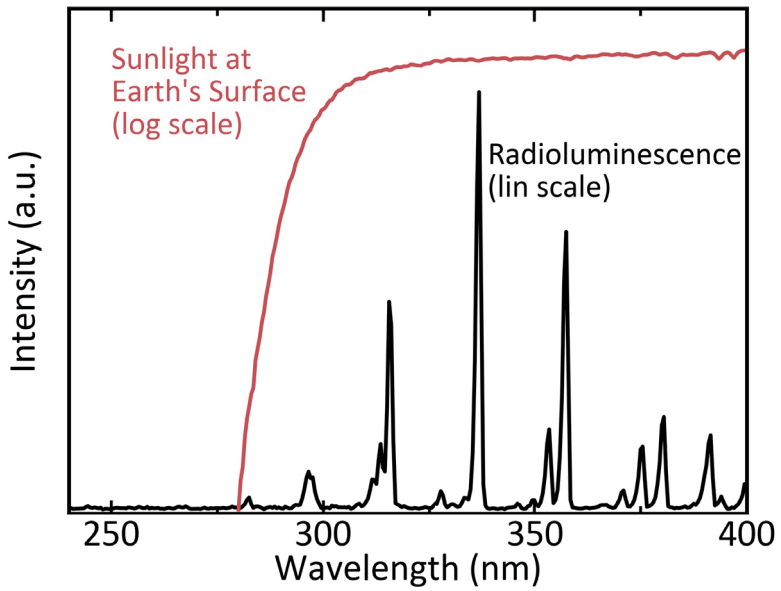

Figure 3.6 Spectral overlap of daylight and radioluminescence in air. Most of the radioluminescence in air (black, linear scale) is found at wavelengths longer than 280 nm with only a small fractions being found at shorter wavelengths. It is this small fraction that does not spectrally overlap with the sunlight reaching the earth's surface (red, logarithmic scale) and is thus useable for alpha imaging in daylight. This figure uses spectral data that has been reported in [79] and Publication I.

The presence of UV components in background lighting makes designing an appropriate filtering system much more challenging. A mere rejection of non-UV light is no longer sufficient and the mere collection of UV light leaves the question open whether the detected light originated from alpha radiation or from the background. An appropriate optical design must allow some parts of the UV radioluminescence to reach the detector while at the same time reliably prevent UV background light

from doing the same. As a consequence, the design is very much dependent on the precise spectrum of the background lighting. And as long as the radioluminescence spectrum is not wholly included in the spectral coverage of the background, then a discrimination is in principle possible and alpha imaging viable. As a hypothetical example, if the background consisted of an LED that emits light at 290 nm, then employing bandpass filters centred around the 337.13 nm spectral line would be sufficient to prevent it from reaching the detector.

A very common scenario where a UV background is present and its discrimination highly desirable is alpha imaging in daylight. Sunlight reaching the earth's surface is present with a continuous spectrum from 280 nm on to higher wavelengths. Its spectrum is shown in Fig. 3.6 where it becomes clear that towards the short wavelengths the intensity of daylight is rapidly dropping. Sunlight of wavelengths 100 to 280 nm is absorbed by ozone in the upper atmosphere and prevented from reaching the earth's surface [79, 112]. This part of the UV spectrum is being referred to as the UVC or 'the solar blind spectral region' and its defining characteristic is the absence of sunlight at earth's surface. The other two UV regions where sunlight is present are the UVB with a spectral range 280 - 315 nm and the UVA with a spectral range 315 - 400 nm, which contains as much as 95 % of all UV background [50]. Making the detection optics unresponsive to photons of wavelengths longer than 280 nm, that is to make it solar blind, while at the same time leaving it responsive to the UVC adequately discriminates between radioluminescence and background and enables alpha imaging in daylight.

Little of the radioluminescence in air is located in the UVC. From Tab. 3.2 it can be seen that the most intense spectral line is the $4 \rightarrow 0$ line at 268.7 nm which is less than 1 % as intense as the main line at 337.13 nm. It is easy to see how an implementation of alpha imaging in daylight will suffer from a much reduced sensitivity. However, it is possible and Ivanov and colleagues first proposed such a solar blind alpha imaging scheme at a conference in 2009 [35] and finally implemented it in 2011 [29]. They used a camera commonly employed to detect electric arcs in the train overhead wires and thus the camera Ivanov chose was by its very design only sensitive to UVC light.

Another successful demonstration of alpha imaging in broad daylight was delivered by Sand and colleagues [33] in 2016. The authors used an inherently solar blind PMT based on a design around a ceasium-telluride photocathode and equipped it

with bandpass filters to only detect the 268.7 nm spectral and adjacent lines. The sensitivity to weaker alpha sources was much reduced compared to a PMT that imaged the radioluminescence in the UVA. It leaves to conclude that by using solar blind optics, a detection system gains the ability to image alpha radiation in daylight but at the same time looses its ability to resolve weaker sources. This is an inherent limitation of the method imposed by the spectral overlap of sunlight and radioluminescence in air.

Table 3.4 Spectral discrimination required for different types of background illumination. This list is an extended version of Tab. 1 in Publication I.

Background Spectrum	Spectral Discrimination
Darkness	None required
VIS, IR or longer (400 nm -)	Short pass and/or bandpass filtering
Daylight (280 - 800 nm)	Solar blind filtering
Partial UV coverage (100 nm -)	Spectrum dependent
Full UV coverage (100 nm -)	Impossible

It might be argued that daylight is one of the major challenges that keeps an otherwise much matured technology from finding widespread use in alpha contamination detection. The concepts and methods laid out in the following chapter have been developed in an attempt to overcome this particular challenge. However, before discussing the daylight problem in greater detail it is sensible to summarise the measures that enable alpha imaging in illuminated environments: In a background lighting free environment imaging is possible without further adjustment of the optics. In a UV-free background, employing appropriate optical filters are essential tools to enable alpha imaging. Imaging in an environment containing UV background light is more difficult and generally requires a case-by-case treatment. Sunlight is a common form of UV background and overcoming it comes at the cost of a much reduced sensitivity. Those cases and their measures also also tabulated in Tab. 3.4.

4 RADIOLUMINESCENCE OF NITRIC OXIDE

A major challenge in radioluminescence detection is differentiating between signal photons and background. With as little as 100 isotropically emitted UV photons [27] per stopped alpha particle, it is not surprising that even in complete darkness it is difficult to distinguish radioluminescent light from a single decay event from instrumental background. In practice, this meant that conventional photography could only image the strongest of alpha sources, even then requiring very long exposure times [24]. The introduction of CCD technology [28] to the field saw vast improvements in alpha imaging, which is mostly owed to the technology's much reduced noise and dynamic range. Especially the reduction of readout noise turned out to be of critical importance, which was demonstrated with the comparison of CCD, ICCD and EMCCD [32]. However, the fundamental principle that makes all three variants of CCD a better fit for alpha imaging over film is the same: by dropping the camera's noise floor, faint light emissions are revealed and small alpha sources detected.

The presence of daylight renders most of the radioluminescence in air unusable for alpha imaging. The spectral overlap of daylight with radioluminescence in air forces the spectral response of any imaging system to be sensitive to UVC light alone. If the imaging system does not fulfill this criterion and is sensitive to parts of the electromagnetic spectrum other than the UVC, then daylight will invariably supersede the faint radioluminescence. This limits the usable part of radioluminescence to the less than 1 % [22] of radioluminescence in air that is located in the UVC. This is a hard limit imposed on the alpha imaging technique which is not easily overcome and leads to a much reduced sensitivity.

The major advances in the field of alpha imaging have been technology driven. It were not fundamentally new concepts or fundamentally new techniques that brought back alpha imaging into active research, but a vastly improved imaging technology. As a consequence, work on alpha imaging typically largely consists of optimising

the employed light detection system and tailoring the spectral response of the optics. And yet, for all the advances the new technology has brought about, it is not immediately obvious how it can help to overcome the spectral limitations daylight imposes on any alpha imaging scheme. If it is not for yet another revolution in imaging technology that drops the noise floor by yet another few orders of magnitude, then perhaps the solution has to be found in other methods.

Those other methods typically fall in one of two categories. The methods in the first category are characterised by the replacment of passive radioluminescence detection with an active detection scheme. A good example is the work of Yao and colleagues in 2013 [113], where they used a pulsed nitrogen laser to excite N_2 from the *B* to the *C* state. N_2 can only be in the *B* state when it had previously been excited, for instance by alpha radiation. Thus, when firing the laser through the air above an alpha source, then photons are removed in the process of reexiciting the N_2 molecule in the *B*-state. The measured reduction in laser pulse power then serves as an indicator for the presence of alpha radiation. An active technique like this can work in daylight, since the measurement of laser power reduction is not limited by background illumination. Using laser absorption, Yao and colleagues were able to detect a 1.48 GBq alpha-active Po-210 source from 10 m distance. Studies on achievable sensitivities have been left for future publications.

The second category comprises methods based around the idea that relying on radioluminescence from species other than N_2 might lead to better detection. The idea is compelling, as many chemical species emit light in one form or another when exposed to alpha radiation. The list of studied species is long and radioluminescence of OH, CN, NH, CO_2, N_2^+, He, O^- has been observed [114, 115, 116]. Often more accidental than intentional. In most cases the radioluminescence of species other than N_2 is of little relevance, since the detection of alpha radiation is typically carried out in scenarios where those type of radioluminescence is simply not present. Most relevant cases involve alpha contamination being surrounded by air, which limits the chemical species that are present to mostly N_2, N_2^+, NO, Ar and a few minor others [77, 117]. Among those, only N_2 and N_2^+ are relevant, since they are the only species that both are sufficiently abundant and at the same time produce sufficiently high levels of radioluminescence that even quenching by O_2 and H_2O leaves some light to be detected [82, 118, 119, 120]. From this point of view it is little surprising that alpha imaging is traditionally centred around N_2 and to some extent

N_2^+ radioluminescence.

If, however, the gas atmosphere around an alpha emitter can be altered, then conditions can be created that enable any desired species to produce radioluminescence. It might be argued that such an approach misses the point of detecting alpha contamination altogether, since a typical scenario involves contamination of unknown magnitude to be located in place over which little or no control can be exercised. At best the illumination might be alterd by turning off the lights or waiting for night time, but a complete control over the gas atmosphere is rarely possible. However, this Thesis considers mostly the scenario of nuclear power plant decommissioning and in this scenario, radiation security regulations mandate that potentially contaminated parts and material be stored and processed inside shielded environments like gloveboxes and hot cells [121]. In those conditions, control over the atmosphere must be exercised.

Controlling the gas atmosphere around an alpha source enables to choose a luminescent species whose spectrum is especially well suited for alpha imaging in daylight. At minimum, it requires luminescence from a species that emits radioluminescence in the UVC. Further, it requires it to do so efficiently. N_2 emits in the UVC, but with a conversion efficiency of $\sim 10^{-7}$ [122] of the alpha particle's kinetic energy to UVC photons it lacks the required efficiency. The scientific literature reports on radioluminescence of numerous atoms and molecules and it is beyond the scope of this Thesis to list all of them. However, the listing of a few recent results on suitable species appears to be in order.

Argon is a well-known UVC radioluminescent species. Argon finds use in various stages of the decommissioning process [121] and its mostly UVC covering radioluminescence spectrum is well documented [117]. There is still some debate over the precise mechanisms by which Ar is excited [116, 123], but it might not be too bold a statement to make that flooding a glovebox with Ar gas is a safe choice when aiming to generate UVC radioluminescence. Other notable species that are commonly discussed are Kr, Xe [123] and CH_4 [124]. In a study in 2018, Anita Crompton and colleagues [78] studied the radioluminescence of various gases in the UVC and found that Xe as a radioluminescent species might produce as much as a 6 times more UVC radioluminescence compared to the amount of UVC radioluminescence that is produced in a pure N_2 atmosphere.

Another molecule that has been observed to emit in the UVC is NO. NO pro-

duces radioluminescence in the so-called γ- and β-bands which are primarily located in the UVC [125]. It is one of those species whose radioluminescence is observed more by accident rather than by deliberation. Its radioluminescence tends to appear in the spectra of gas mixtures where NO is thought to be either absent or only present in miniscule amounts. In 1966, at the peak of the atomic age [126], Dondes and colleagues measured the radioluminescence spectra of a variety of different gas mixtures that had been exposed to alpha particles emitted by a Po-210 source [77]. One of the gases was purified N_2, which had been determined to have a total volume concentration of impurities of less than 100 ppm. Whenever the purified N_2 was added in evan small amounts to any other gas mixture that at the same time did not contain O_2, then the γ-band and sometimes the β-band would appear. Fig. 4.1 shows such a spectrum that the researchers found in their work. The authors explain this appearance with NO impurities being present in the N_2 and speculate, based on the quenching of the NO γ-band in various different gas mixtures, that its emissions in an otherwise pure N_2 gas would be maximised at a concentration of less than 500 ppm. More importantly, however, they noticed that NO radioluminescence exhibits a "fairly high intensity" and that O_2 appears to inhibit the mechanisms that produces it.

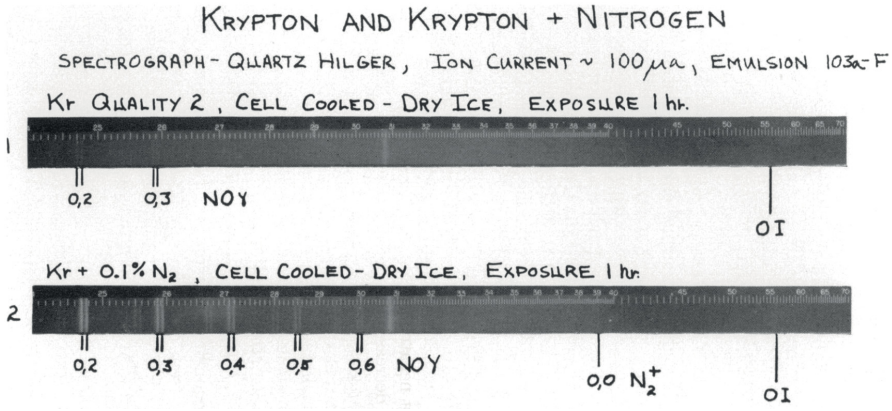

Figure 4.1 The NO γ-band appearing in a radioluminescence spectrum of Kr. In the upper spectrum the Kr continuum between 220 and 450 nm is seen. Upon adding 0.1 % N_2, strong NO γ-band emissions appear. The numbers of the format v', v'' indicate a spectral line's corresponding vibrational quantum numbers. This figure is a crop from Fig. 4A first presented in [77].

NO radioluminescence has been noticed by many other authors since then. In

a 2017 study by Brett and colleagues [116], the NO γ-band was found in a radioluminescence spectrum of purified N_2 gas. Again, more by accident rather than by deliberation. The authors do not specify the purity of the gas, but it is to be argued that it might not have been pure enough to remove any trace amounts of NO. All of their spectra that have been measured in purified N_2 show the NO γ-band. This is well in line with the observations which have been made more than 50 years prior. Noteworthy about the reported spectra is that the intensity of the NO γ-band is larger than the intensity of the N_2 radioluminescence. Purified nitrogen in scientific use comes in 2019 typically with purity levels of about 99.999 % or greater [127]. Thus, it has to be concluded that the NO impurities produce radioluminescence that is more intense than the radioluminescence of N_2 which is a million times more abundant. Many more experiments have demonstrated the existence and intensity of NO radioluminescence [76, 107, 128], but perhaps it is fair to say that the early report of Dondes et al. contains one of the most comprehensive descriptions of the phenomenon so far. They are also one of the first to remark on its unusual high intensity, and propose mechanisms by which this comes about in this and their related publication [77].

Given these reports it is likely that NO is uniquely well suited to produce the large amounts of UVC radioluminescence which are required to overcome the daylight problem. In this chapter of the Thesis, a theory is laid down that attempts to explain the creation of NO radioluminescence. The conditions necessary to create NO radioluminescence in both a controlled gas environment and ambient air are inferred from this theory. Experimental data is presented to provide evidence for the correct representation of the physics by the theory and to validate the implementation that show the deliberate generation of NO radioluminescence.

4.1 The Nitric Oxide Spectrum

Like N_2, NO is a diatomic molecule, and it can be spectroscopically described in a concise form that does not need to invoke a full quantum mechanical description. Unlike N_2, NO is a hetereonuclear molecule which, in this particular case, causes its ground state and first electronic excited state to have identical spin multiplicity. This will become a relevant ingredient in explaining the intensity of the γ-band emissions. NO is made up of atomic nitrogen which carries 7 electrons and atomic oxygen

which carries 8 electrons. Their respective ground state electron configurations are

$$\mathrm{N}(^4S_{3/2}) : 1s^2 2s^2 2p^3 \tag{4.1}$$

$$\mathrm{O}(^3P_2) : 1s^2 2s^2 2p^4. \tag{4.2}$$

The electrons of both atoms combine to fill the molecular orbitals of NO in accordance with Tab. 4.1 to produce the electron configuration

$$\mathrm{NO}(X^2\Pi) : (\sigma 1s)^2(\sigma^* 1s)^2(\sigma 2s)^2(\sigma^* 2s)^2 \underbrace{(\sigma 2p)^2(\pi 2p)^4(\pi^* 2p)^1}_{2\,1/2\ \text{bond}}. \tag{4.3}$$

The subscripts that had previously been used to describe the N_2 molecule have been dropped, since a hetereonuclear molecule lacks an inversion center. Orbitals can neither be *gerade* nor *ungerade*. The meaning of the asterisk over an orbital, however, remains. Thus the unpaired electron of the oxygen atom that populates the $(\pi^* 2p)$ orbital cancels the bonding effect of one of the electrons in the $(\pi 2\mathrm{p})$ orbital. As a result, the NO molecule is compared to the N_2 molecule a little less strongly held together with a $2\,1/2$ bond and a slightly lower dissociation energy of $893.9\,\mathrm{kJ\,mol^{-1}}$ [129].

Table 4.1 Ground state electron configuration of NO. The atomic orbitals of the nitrogen atom with 7 electrons and the oxygen atom with 8 electrons combine to form a $2\,1/2$ bond. With one electron being unpaired, the ground state is a spin doublet and its term symbol is $X^2\Pi$.

N	O	NO : σ	NO : σ^*	NO : π	NO : π^*
$1s^2$	$1s^2$	$(\sigma 1s)^2$	$(\sigma^* 2s)^2$		
$2s^2$	$2s^2$	$(\sigma 2s)^2$	$(\sigma^* 2s)^2$		
$2p^3$	$2p^4$	$(\sigma 2p)^2$		$(\pi 2p)^4$	$(\pi^* 2p)^1$

The presence of an unpaired electron makes nitric oxide highly reactive and is the primary reason for its toxicity [130]. Unlike N_2, which has a similarly high ionisiation energy, the heat transformation of NO is endothermic and it thus readily decomposes into the elements via the reaction

$$2\mathrm{NO} \rightarrow \mathrm{O_2} + \mathrm{N_2}. \tag{4.4}$$

It is the primary means by which catalysts in combustion engine powered vehicles remove NO from exhaust gases before those are released [131]. Detection of nitric oxide commonly happens via its volatile reaction with ozone

$$\mathrm{NO} + \mathrm{O_3} \rightarrow \mathrm{NO_2} + \mathrm{O_2} + h\nu. \tag{4.5}$$

Upon reacting, a chemiluminescent photon with a wavelength between 430 and 630 nm [132] is emitted. By collecting photons created in the reaction with ozone, ppb levels of NO can be precisely detected [133].

The tight electronic bond causes the NO molecule to have deep potentials wells. They are illustrated in Fig. 4.2 using Morse potentials. They have been drawn for the ground and the first electronic state.

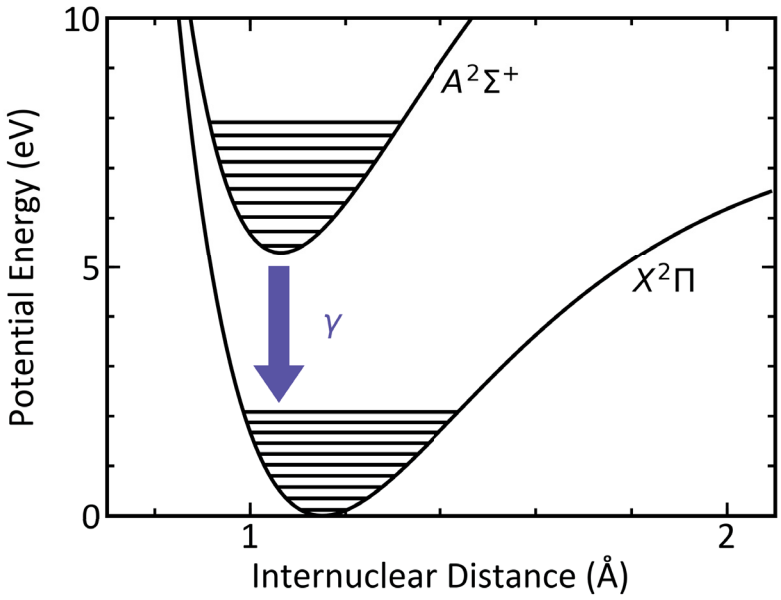

Figure 4.2 Morse potentials drawn for NO. Potentials, including the first 10 vibrational levels, are drawn for the ground and the first excited state. Radiative decay from the $A^2\Sigma^+$ state to the $X^2\Pi$ ground state creates UVC emissions that form the γ-band. The extensive compilations of molecular constants of Danielak [125] and Gilmore [134] had been used to create this figure.

Radioluminescence from NO is generated primarily during radiative decay from the electronic A state to the ground state. Those emissions form the γ-band and they are overwhelmingly located in the UVC. The NO radioluminescence spectrum that

had been recorded from the radioluminescence emissions in a gas mixture of 50 ppm of NO in purified N_2 Publication II is shown in Fig. 4.3. A summary of the most intense spectral lines is tabulated in Tab. 4.2.

The wavelengths given in Tab. 4.2 are estimates. In addition to making it chemically reactive and toxic, the unpaired electron also makes NO paramagnetic. The coupling of the electron's spin with the molecular vibration is called lambda-doubling and it causes the rotational levels to split [135]. As a result, every vibrational transition in the γ-band does not result in one spectral line, but four. They are commonly referred to as Q_{11}, P_{11}, P_{12} and P_{21}, where letters indicate the ro-vibrational branch and the subscripts the coupling of vibration and electron spin. However, much like for N_2, the rotational structure is ignored within the scope of this Thesis, as a finely resolved spectrum down to the rotational structure is not necessary for the intents and purpose in this Thesis. The displayed wavelengths then are a simple an average over all 4 band heads and the error introduced is of the order of pm [125].

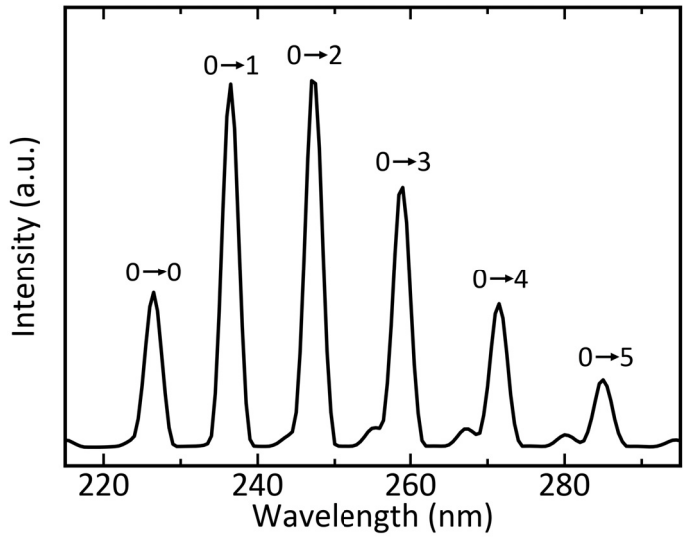

Figure 4.3 Spectrum of NO radioluminescence. This spectrum has been compiled using spectroscopic data that had first been presented in Publication II. Labels of the form $v' \rightarrow v''$ have been added to the most significant peaks to indicate the vibrational transitions that gave rise to them. The peaks have been identified with the displayed vibrational transition using the spectroscopic data tabulated in [125].

γ-band emissions are not the only type of radioluminescence that make up NO radioluminescence. If static electric fields were applied or certain levels of gas purity

had been achieved, then certain spectra in the work of Dondes and colleagues [77] would show both the γ- and the β-band. The β-band is a series of spectral lines located between 230 and 530 nm and it is created when NO radiatively decays from the B to the ground state [136, 137]. The study of the NO β-band is beyond the scope of this Thesis. However, much of it is located in the UVC and by this virtue would deserve a more detailed treatment. There is even reason to hypothesise that the NO β-band might exhibit intensities as strong as this of the γ-band, if conditons are set up correctly. However, for easier comprehension, the focus momentarily lies on the γ-band and the mechanism that give rise to it. The β-band will return into the description of NO radioluminescence in the discussion-part of this chapter.

Table 4.2 Relative intensities of the NO γ-band spectral lines. The relative intensities are given as fractions of the intensity of the $0 \rightarrow 2$ spectral line. Lines that are located in the UVC are marked with an asterisk. The table has been compiled from spectroscopic data presented in [125] and Publication II.

λ(nm)	v'	v''	I_{rel}(%)	λ(nm)	v'	v''	I_{rel}(%)
226.55*	0	0	41	259.09*	0	3	71
236.60*	0	1	97	271.70*	0	4	39
247.42*	0	2	100	285.38	0	5	18

Table 4.3 Quenching rates of the NO $A^2\Sigma^+(v'=0)$ state by molecules found in air. The list is compiled from quenching coefficients published in the extensive compilation of Settersten [119] and presented for quenching at room temperature.

Quenching Species X	$Q_X^{\mathrm{NO}(A,v'=0)}$ ($10^{-10}\,\mathrm{cm^3\,s^{-1}}$)
N_2	$< 10^{-4}$
NO	2.49 ± 0.01
O_2	1.71 ± 0.01
H_2O	8.96 ± 0.04

Part of the difficulty in observing NO radioluminescence comes from its rapid quenching by atmospheric gases. While the presence of N_2 is much less of a problem than it is for N_2 radioluminescence, the presence of O_2 and especially H_2O is much worse a problem for NO radioluminescence than it is for this of N_2. With a quenching coefficient of about $9 \cdot 10^{-10}\,\mathrm{cm^3 s^{-1}}$ at room temperature, even very small

amounts of water are uniquely well suited to remove almost all excitations from the *A*-state of NO before they have a chance to radiatively decay. As it has been noted already by Dondes and colleagues [77], O_2 is only slightly better in this regard. NO itself is a potent quencher, too. Thus, trying to produce more UVC radioluminescence by adding more NO to a gas mixture will not necessarily be met with success. A list of quenching coefficients that are relevant within the scope of this Thesis is given in Tab. 4.3. It draws on the extensive work of Settersten and colleagues [119] and it is their work that should be consulted to both find a more exhaustive list of quenching coefficients and a more nuanced description of the quenching processes.

4.2 Excitation Transfer

The excitation of NO molecules happens via two distinct mechanisms, both of which are mediated by electron bombardment. One mechanism is the direct interaction of an electron and the NO molecule, usually referred to as impact excitation. The other one is the transfer of an excitation from a different atom or molecule to the NO molecule. The transfer of excitations is a special case of radiationless transition [138].

Impact excitation requires the electrons to have sufficiently small kinetic energies in order to be able to excite the NO molecule. Schappe and colleagues [139] studied impact exciation by using an electron gun to precisely sample electron energies from the ionisation threshold up to electron energies of 740 eV. The found that the electron-scattering event [140]

$$\mathrm{NO}(X^2\Pi) + \mathrm{e}^- \rightarrow \mathrm{NO}(A^2\Sigma^+) + \mathrm{e}^-_{\text{scattered}} \tag{4.6}$$

has a total cross section of about $0.014\,\mathrm{a}_0^2$. Electrons with kineitc energies of about 30 eV were found to be most likely able to excite molecules into the *A* state whereas electrons with higher kinetic energies were found to be less likely to do so. The cross section quickly decreases for electrons with kineitc energies larger than 100 eV.

The second mechanism by which NO can reach the *A*-state is by transfer of an excitation from a different atom or molecule. Excitation transfer is a case of a radiationless transition where one atom or molecule loses energy which had been stored in an excitation, and this energy is then picked up by another atom or molecule and

stored again as an excitation. The transfer can happen between atoms or molecules of the same species or between atoms or molecules of different species. In the case of NO, an excited molecule can interact with another NO molecule, excited or not, and transfer some of if its electronic, vibrational and/or rotational energy. In the same process it can also lose some of the energy contained in the excitations to kinetic energy, thus increasing the gas temperature. Excitation transfer between atoms or molecules of the same species is part of the processes that thermalise a collection of identical atoms or molecules [141].

Excitation transfer that occurs between atoms or molecules of different species is a form of quenching. As an example, excited Ar is known to populate different states of NO, N_2 and H_2 by losing its excitation [142]. For what it matters to the Ar atom, it lost its excitation and can no longer radiatively decay, its light emission has been quenched. In the remainder of this chapter it is argued that if the only species exposed to an alpha source are N_2 and NO, then electron impact excitation of N_2 and subsequent transfer to NO are the dominant mechanism by which NO γ-band emissions are produced. Further, it is argued that those mechanism can be made to work in the favour of alpha imaging by efficiently converting an alpha particle's kinetic energy into UVC photons.

The first part of the argument rests on the observation that a mixture of N_2 and NO under electron bombardment will see much of the electron's kinetic energy deposited as excitations in the N_2 molecules. The kinetic energy of the electrons produced by the stopping of an alpha particle are for the most part below 1 keV [23]. In fact, the Bragg curve in Fig. 2.3 shows that the vast majority of the electrons is created with kinetic energies at the low end of the energetic spectrum. Electrons with those energies are more likely to interact via electron-scattering with ground state nitrogen than with nitric oxide. The ground state excitation by electron scattering of the N_2 triplet states A, B, C, D, W, and E, is with cross sections between 0.133 (E-state) and 4.354 a_0^2 (A-state) [95] orders of magnitude higher than the cross sections for the NO A-state with only 0.014 a_0^2 [139]. Thus, even in a gas mixture consisting in large parts of NO, most of the energy would be deposited as N_2 rather than as NO excitations. For gas mixtures where NO is only present in trace amounts, the energy deposited as NO excitations might be safely neglected in comparison to this deposited as N_2 excitations.

The second part of the argument rests on the observation that the N_2 molecules

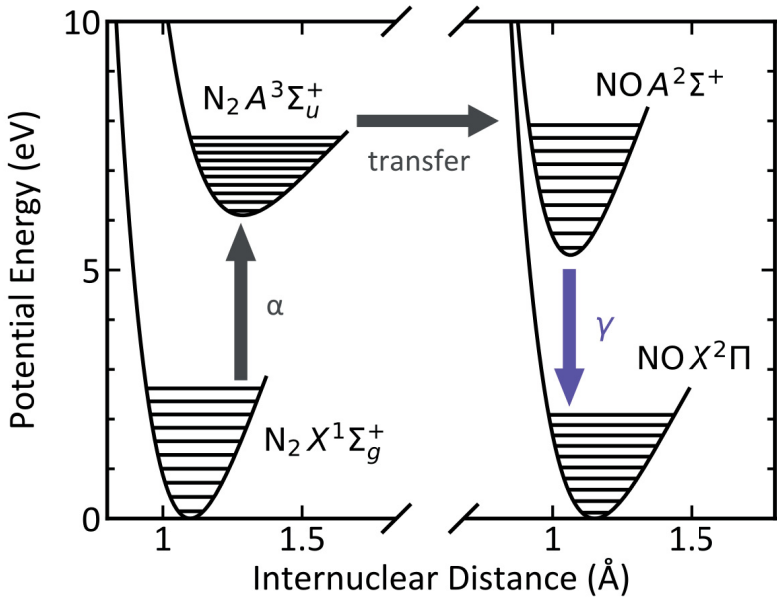

Figure 4.4 UVC radioluminescence generation by NO. An alpha particle causes the eventual population of the N_2 A-state, which is quenched by excitation transfer to the NO A-state. There the excitation radiatively decays producing UVC radioluminescence as part of the γ-band emissions. [125, 134, 143].

store much of this energy. The ground state of N_2 is a singlet state whereas many of the states excited by electron impact are triplet states, with the lowest energetic one being $^3\Sigma_u^+$. None of the triplet states can by means of a dipole transition decay into the ground state, they can only decay into lower-energetic triplet states. Thus, N_2 molecules in higher excited triplet states will eventually decay into the meta-stable A-state. In the absence of quenchers, they remain there with a natural lifetime of about 2.5 s [84]. Only then they decay over a forbidden transition and emit light in the UVA and UVB, where they form the Vegard-Kaplan system. In a pure N_2 atmosphere, the only quencher of the A-state is N_2 itself. In a reaction called energy-pooling, two N_2 molecules in the A-state interact to create one ground state and one B-state molecule. With a quenching constant of $0.77 \cdot 10^{-10}\,\mathrm{cm^3\,s^{-1}}$ [144], this reaction is not as impactful as quenching by oxygen or water, but significant nonetheless. Energy pooling empties the A-state, which then is repopulated via decay of the newly produced B-state molecule back to the A-state. Thus, it can be argued that the N_2 molecules in the A-state as a whole store much of the energy that has been released

in the stopping of an alpha particle. They function as a meta-stable energy reservoir.

The third part of the argument holds that the energy stored by the N_2 molecules is transferred to the NO molecules, from where they decay as UVC photons. The potential of the N_2 A-state is energetically similar this of the NO A-state and energy transfer from the former to the latter molecule is therefore possible. It is known to occur at least since 1980, when Clark and colleagues were among the first to throughly study the phenomenon [145]. The excitation transfer and the production of a UVC photon are described by the reactions

$$N_2(A^3\Sigma_u^+) + NO(X^2\Pi) \rightarrow N_2(X^1\Sigma_g^+) + NO(A^2\Sigma^+) \tag{4.7}$$

$$\rightarrow N_2(X^1\Sigma_g^+) + NO(X^2\Pi) + h\nu, \tag{4.8}$$

where the excitation transfer happens at a rate of $1.00 \cdot 10^{-10}\,\mathrm{cm^3\,s^{-1}}$ per NO molecule [143, 146] and the radiative decay at a rate of 5.16 MHz [119, 147, 148]. Much like energy-pooling, excitation transfer deactivates the N_2 A-state. Unlike energy-pooling, however, excitation transfer does not cause the A-state to become repopulated, it depletes it. It is only fair to point out, that energy-pooling also depletes the number of excitations in the A-state, since only one of the two involved excitations eventually returns to the A-state. However, transfer of an exciation to NO does not even allow for the possibility of repopulation by an exication transfer back to the N_2, since the excitation is quickly lost to radiative decay. Thus, the excitation transfer to NO can be interpreted as the emptying of the energy reservoir.

The mechanism that is proposed to create NO γ-band emissions rests on a sequence of three successive interactions. The sequence is sketched in Fig. 4.4 for easier comprehension. It uses once again the Morse potentials to illustrate the process and emphasise the energetic similarity of both molecule's respective A-states. Energy-pooling, electron impact excitation and other relevant details have been consciously omitted to highlight the chain of interactions that is thought to be relevant.

4.3 Evidence for Excitation Transfer

The arguably most important test of the theory is this for the levels of UVC radioluminescence intensity that can be achieved. The primary motivation to study

NO in the first place has been its purported superior qualities as a UVC radioluminescent species. To test the achievable levels of intensity and other features the theory around excitation transfer implies, an experimental arrangement like the one sketched in Fig. 4.5 had been put together.

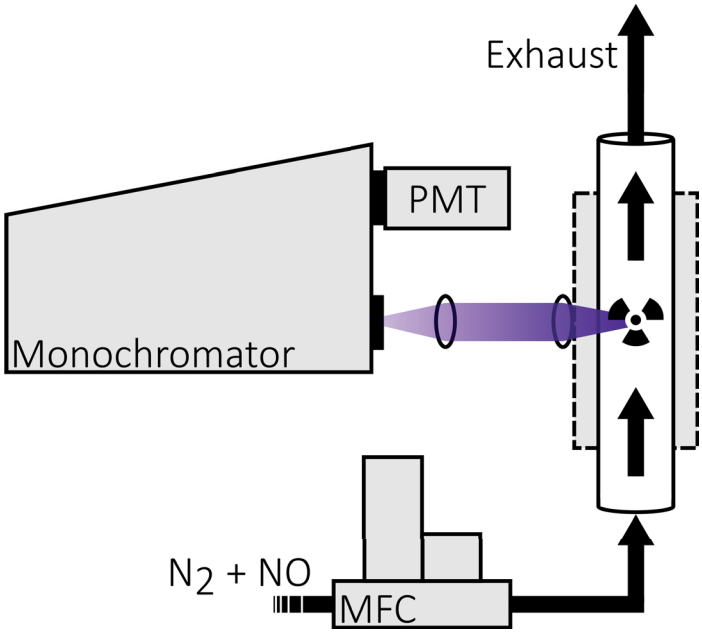

Figure 4.5 The experimental arrangement used to study NO radioluminescence. An Am-241 source rested inside the quartz glass tube. The atmosphere inside the glass tube was controlled with a system of mass flow controllers. Security precautions have been taken to protect personnel from exposure to both gamma radiation and NO. This drawing shows a system of monochromator, PMT and a telescope. A slightly altered version of this setup replaced those elements with an interference filter and a PMT. This figure has first been shown in slightly different form in Fig. 2 in Publication II.

There an alpha active Am-241 source with a total activity of 32 MBq, spread out over an area of 12.5 mm in width and 50 mm in length, rested on a rectangular source holder in the centre of a quartz glass tube. The quartz glass tube was 1 m long, had an outer diameter of 30 mm, 1.5 mm thick walls and flame polished ends (Robson Scientific, Product Code: RQT 30). A 21 mm thick steel mantle surrounded the glass tube, protecting personnel and equipment from gamma radiation. A cone shaped hole with an opening angle of 70° allowed light inside the tube to escape it. There the light was collected in one of two ways: in one arrangement it was guided

with a lens system (Thorlabs, Product Codes: LA4052-UV, 35 mm and LA4924-UV, 175 mm) to a computer-controlled monochromator (Horiba, Product Code: iHR 550) and then collected by a UV-sensitive PMT (Perkin-Elmer, Product Code: MP-1082, Dark Count: < 1 cps). In the other arrangement, the light escaping the tube passed an optical filter (Edmund Optics, Product Code: 67805, transmittance band: 239 nm $\pm$ 5 nm) and was then collected by the same PMT. The setup involving the monochromator was used to precisely measure the spectrum, the setup involving only a filter was used to study changes in intensity more accurately. The sketch in Fig. 4.5 shows the arrangement with the monochromator and lens system.

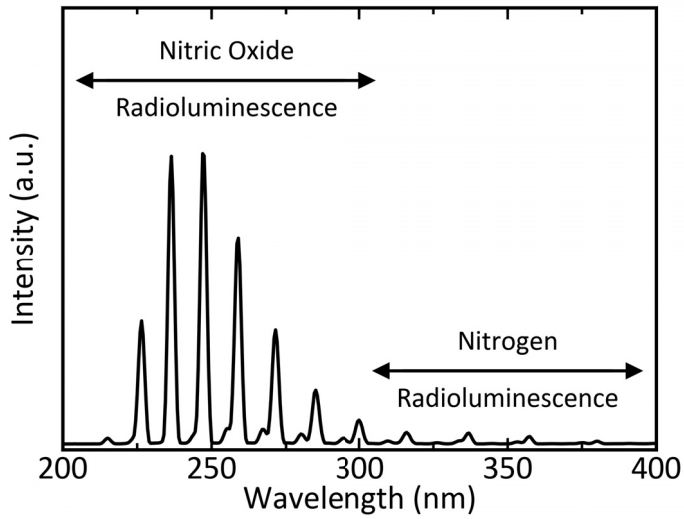

Figure 4.6 Radioluminescence spectrum of a gas mixture of 50 ppm of NO in N_2. The UV emissions of NO are about 25 times stronger than those of N_2. Additionally, the NO emissions are for the most part in the UVC, while the N_2 emissions are for the most part in the UVA. The data shown in this figure has been first presented in Fig. 4 in Publication II.

In both arrangements the atmosphere inside the glass tube had been controlled. A set of three mass flow controllers (MFC, Bronkhorst High-tech, Product Codes: 18BRF-201CV-1K0, 18BRF-201CV-10K and 18BRF-201CV-20K) enabled to control both the mass flow and the NO concentration in an otherwise pure N_2 atmosphere. The gases that had been used were N_2 containing 5 ppb of NO, N_2 containing 50 ppb of NO and N_2 containing 1500 ppm of NO. They were stored bottled and compressed in gas cylinders (AGA, Product Codes: 2093A7, 2098A7 and 621987). All concentrations were measured by volume and the ppb concentrations of NO had

been verified using a chemiluminescence analyser. The gas inside of the glass tube was isolated from the laboratory air and only connected to the system of mass flow controllers and an exhaust. This was in part to ensure an uncompromised measurement and in part to protect equipment from corrosion and personnel from intoxication through exposure to NO.

Table 4.4 UV radioluminescence intensity in different atmospheres. The intensity is expressed in relation to the intensity found in normal air. The fraction of light emitted in the UVC and the conversion efficiencies of an alpha particle's kinetic energy into UV photons ($\eta_{\alpha,\mathrm{UV}}$) have been added. The table is an extended version of this that had been shown in Tab. 1 in Publication II.

Atmosphere	I_{rel}	UVC	$\eta_{\alpha,\mathrm{UV}}$	Reference
Air	1	$< 1\,\%$	$1 \cdot 10^{-4}$	[27]
N_2	6	$< 1\,\%$	$6 \cdot 10^{-4}$	[27]
50 ppm of NO in N_2	150	$> 90\,\%$	$2 \cdot 10^{-2}$	Publication II

The experiment wholly confirmed the hypothesis that NO makes for an exquisite UVC radioluminescent species. Upon diluting 50 ppm of NO into N_2 an intense UVC radioluminescence had been created. Its spectrum is presented in Fig. 4.6. It can clearly be seen that the NO γ-band in the UVC and the N_2 2+ system in the UVA and UVB make up the bulk of the radioluminescence. Even though the radioluminescence produced by N_2 appears to be faint in comparison to this of NO, it has to be pointed out that in fact it is the same intensity as the one that would be created in a pure N_2 atmosphere. The radioluminescence produced by N_2 in this scenario is about 6 times more intense than this in air [27, 116]. Thus, the N_2 spectrum presented in Fig. 4.6 already shows amplified radioluminescence emissions. The fact that it appears faint in comparison to the emissions of NO shows just how intense the γ-band emissions can become.

Direct excitation of the NO molecules by electron impact cannot explain this phenomenon. By replacing 50 in a million N_2 molecules with NO molecules, the efficiency with which an alpha particle's kinetic energy had been converted into UV light had increased 25 times. The efficiencies in the different atmospheres are tabulated in Tab. 4.4. For electron impact excitation to explain this increase in intensity, the NO molecule's electron-scattering cross section would have to be about a million times higher than this of the N_2 molecule. The opposite is the case, the cross section is about 100 times smaller [140]. Thus, the intensity of NO radioluminescence

Table 4.5 Constants that govern NO radioluminescence production. Quenching constants and excitation transfer rates are expressed relative to a quencher's partial pressure.

Constant	Description	Value	Reference
k_α	Excitation Rate	$\ll 1\,\mathrm{s}^{-1}$	-
p	Pressure	760 Torr	-
T	Temperature	293.15 K	-
k_{f,N_2^A}	N_2^A fluorescence rate	400 mHz	[84]
k_{f,NO^A}	NO^A fluorescence rate	5.16 MHz	[119]
$\mathrm{Q}_{\mathrm{NO}^X}^{\mathrm{N}_2^A}$	excitation transfer	$3.29\cdot 10^6\,\mathrm{Torr}^{-1}\,\mathrm{s}^{-1}$	[143]
$\mathrm{Q}_{\mathrm{N}_2^X}^{\mathrm{NO}^A}$	NO^A quenching by N_2^X	$< 3\cdot 10^2\,\mathrm{Torr}^{-1}\,\mathrm{s}^{-1}$	[119]
$\mathrm{Q}_{\mathrm{NO}^X}^{\mathrm{NO}^A}$	NO^A quenching by NO^X	$8.17\cdot 10^6\,\mathrm{Torr}^{-1}\,\mathrm{s}^{-1}$	[119]

and the efficiency with which it is produced can be taken as first piece of evidence that the population of the upper state of the NO molecules happens by excitation transfer.

The second piece of evidence is provided by the value of the optimal NO concentration for which radioluminescence production is maximised. If electron impact were the dominant mechanisms by which NO would be excited, then an increase in NO concentration would result in a linear increase in radioluminescence up to the point where self-quenching would start to dominate the production of radioluminescent light. From this point onwards, a further increase in concentration would only result in a reduction of radioluminescence intensity. The rate equations governing such a system would be

$$\frac{\mathrm{d}}{\mathrm{d}t}[\mathrm{NO}^A] = k_\alpha[\mathrm{NO}^X] - k_{f,\mathrm{NO}^A}[\mathrm{NO}^A] - p\,\mathrm{Q}_{\mathrm{NO}^X}^{\mathrm{NO}^A}[\mathrm{NO}^X][\mathrm{NO}^A] \tag{4.9}$$

$$\frac{\mathrm{d}}{\mathrm{d}t}[\mathrm{NO}^X] = -k_\alpha[\mathrm{NO}^X] + k_{f,\mathrm{NO}^A}[\mathrm{NO}^A] + p\,\mathrm{Q}_{\mathrm{NO}^X}^{\mathrm{NO}^A}[\mathrm{NO}^X][\mathrm{NO}^A] \tag{4.10}$$

where $[X]$ is the volume concentration of species X. The NO molecules are assumed to be only present in either the ground or the excited state, thus their concentrations add up to the total nitric oxide concentration in the system [NO], i.e. $[\mathrm{NO}^X] + [\mathrm{NO}^A] = [\mathrm{NO}]$. The meaning and the value of the constants used in the equations

are tabulated in Tab. 4.5. The photon production efficiency is

$$[\Phi] = \underbrace{\frac{k_{f,\mathrm{NO}^A}}{k_{f,\mathrm{NO}^A} + pQ_{\mathrm{NO}^X}^{\mathrm{NO}^A}[\mathrm{NO}^X]}}_{\mathrm{QE}}[\mathrm{NO}^A], \tag{4.11}$$

where QE is the quantum efficiency. Under steady-state conditions, i.e. the rate equations can be assumed to be 0, the NO concentration at which this value is maximised is about 826 ppm. This is in clear contrast to result of the measurement where this maximum has been found at much smaller concentrations. If, however, excitation transfer would be the mechanisms by NO molecules are excited, then the rate equations describing the system are a bit more complex. They now need to account for the dynamics of the N_2 molecules and for the transfer of excitations to the NO molecules. The equations can be expressed in the form

$$\frac{\mathrm{d}}{\mathrm{d}t}[\mathrm{N}_2^A] = k_\alpha[\mathrm{N}_2^X] - pQ_{\mathrm{NO}^X}^{\mathrm{N}_2^A}[\mathrm{N}_2^A][\mathrm{NO}^X] - k_{f,\mathrm{N}_2^A}[\mathrm{N}_2^A] \tag{4.12}$$

$$\frac{\mathrm{d}}{\mathrm{d}t}[\mathrm{N}_2^X] = -k_\alpha[\mathrm{N}_2^X] + pQ_{\mathrm{NO}^X}^{\mathrm{N}_2^A}[\mathrm{N}_2^A][\mathrm{NO}^X] + k_{f,\mathrm{N}_2^A}[\mathrm{N}_2^A] \tag{4.13}$$

$$\begin{aligned}\frac{\mathrm{d}}{\mathrm{d}t}[\mathrm{NO}^A] = {} & pQ_{\mathrm{NO}^X}^{\mathrm{N}_2^A}[\mathrm{N}_2^A][\mathrm{NO}^X] \\ & - k_{f,\mathrm{NO}^A}[\mathrm{NO}^A] - pQ_{\mathrm{NO}^X}^{\mathrm{NO}^A}[\mathrm{NO}^X][\mathrm{NO}^A]\end{aligned} \tag{4.14}$$

$$\begin{aligned}\frac{\mathrm{d}}{\mathrm{d}t}[\mathrm{NO}^X] = {} & -pQ_{\mathrm{NO}^X}^{\mathrm{N}_2^A}[\mathrm{N}_2^A][\mathrm{NO}^X] \\ & + k_{f,\mathrm{NO}^A}[\mathrm{NO}^A] + pQ_{\mathrm{NO}^X}^{\mathrm{NO}^A}[\mathrm{NO}^X][\mathrm{NO}^A],\end{aligned} \tag{4.15}$$

where the quenching of the excited state of NO by N_2 has been neglected. The equation for the generated amount of photons per unit of time, Eq. (4.11), also holds true for this modified form of the rate equations. For those set of equations, the photon generation can be found to be at its maximum for a NO concentration of about 44 ppm. This is in much better agreement with the experimental finding. The curves that describe the photon yield as a function of the NO concentration for both excitation paths are presented in Fig. 4.7.

The theory laid down in the rate equations works with a lot of simplifications and omissions. It does not include include energy-pooling, entirely neglects quenching

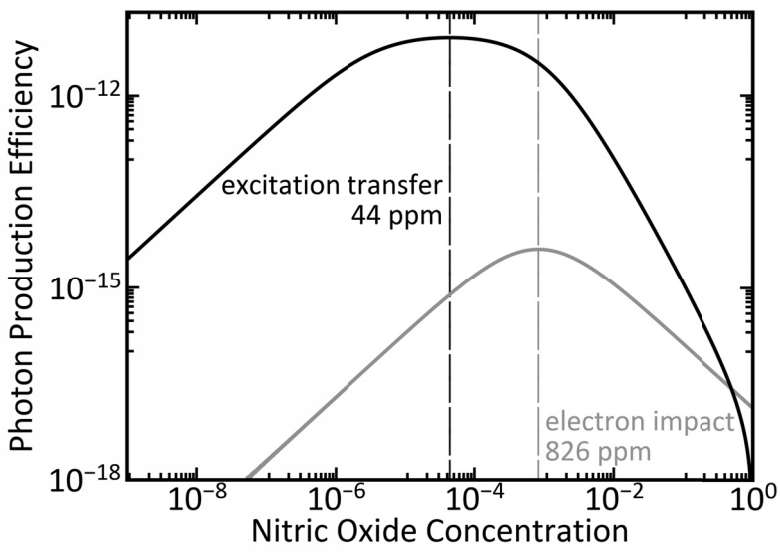

Figure 4.7 Photon production efficiency for two different mechanisms that excite the NO molecule. The curves have been obtained by numerically solving Eq. (4.11) for the two different set of equations describing the evolution of the upper state $[\mathrm{NO}^A]$. The theory holds that electron impact requires large amounts of NO to become an effective excitation mechanism, while transfer of excitations from N_2 molecules becomes an effective process for much smaller concentrations.

by common trace gases like O_2 and $\mathrm{H}_2\mathrm{O}$ and does not consider any electronic states other than the ground and respective *A*-states of both types of molecules. Further, it has been entirely omitted that quenching acts differently on different vibrational states. In short, the theory is much simplified and only considers the bare minimum of detail necessary to formulate an excitation by interaction with N_2. Including higher electronic states could give a more complete picture, since it would allow to properly account for different excitation transfer reactions that are known to occur [145]. This would also enable to include the excitation of the NO β-band, which has been observed to substantially contribute to the UVC radioluminescence if certain conditions are met [77]. Further, electron scattering could be included into the theory. The energy-distribution of the generated electrons upon stopping of an alpha particle has been extensively studied [22] and the scattering cross sections for both N_2 [95] and NO [140] are at the point where theory and experiment are in very good agreement.

Yet the much simplified theory comprises sufficient detail to rule out the possi-

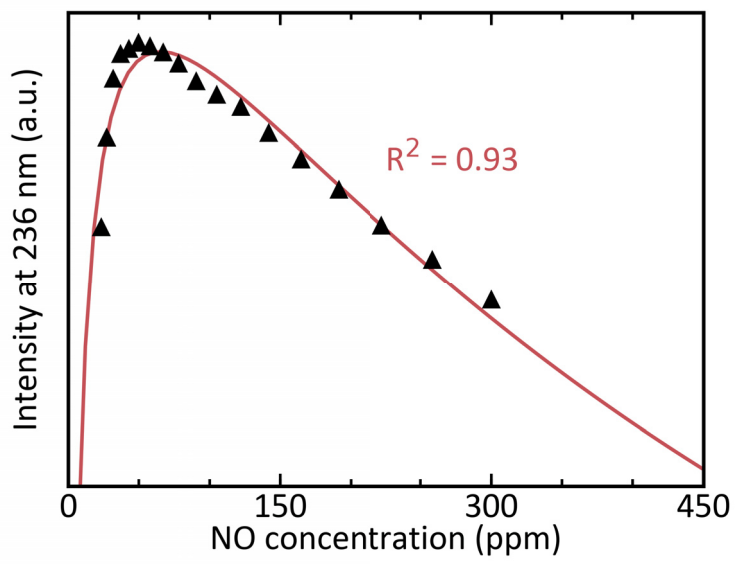

Figure 4.8 Dependence of γ-band emissions on NO concentration. The intensity of the 236 nm line of the γ-band had been recorded while the NO concentration had been step-wise increased. The intensity was maximised at about 50 ppm. The red line is a fit of the excitation transfer model to the data. The data and the fit presented in this figure have been presented first in Fig. 3 in Publication II.

bility that excitation by electron impact is the dominant mechanism. In Publication II the γ-band intensity as a function of the NO had been measured. The model had been fitted to the data in a setting where all parameters that are tabulated in Tab. 4.5 had been left as parameters for the optimiser to tweak. Only pressure and temperature were set to 760 Torr and 293.15 K, respectively. The theory fitted the data relatively well while returning reasonable values for the fitted parameters. Especially the dominance of NO self-quenching past the point of maximum intensity was very well reflected by the theory. The curve and the fit are once again shown in Fig. 4.8. However, the relevant feature of the theory for the purpose of this Thesis is that it can cleanly discriminate between two different excitation mechanisms by using nothing more than the information of the concentration at which the NO radioluminescence is maximised. It was found to be a low concentration with a value of about 50 ppm, which is a clear indicator that the dominant excitation mechanisms cannot be electron impact. This observation is evidence for the the the predominant mechanism that populates the NO A-state is transfer of excitations from N_2

molecules.

It has to be noted that at the time the experiments were conducted, the strong effects of water quenching were not known to the experimenters. Thus the effects of water quenching on the radioluminescence intensity remains an open question. It might be sensible to redo those experiments in a much more controlled environment where water concentration (and by extension oxygen concentration) are much more controlled. The conclusion that electron impact is unlikely the primary excitation mechanism, however, remains unchanged. Further, the data displayed in Fig. 4.8 does not show error bars. A thorough analysis of the measurement uncertainty necessarily must include uncertainties in NO concentration, uncertainties brought about by an unknown water content, uncertainties induced by a possibly not perfectly mixed gas and uncertainties coming from the photon counting statistics. In the experiment in Publication II on creating NO radioluminescence, those sources of error had not been analysed enough such that it would justify displaying error bars. Displaying them would give the false impression that the error sources had been analysed. Similar considerations apply to the other experiments that are presented in this chapter.

The third piece of evidence comes from the specific way the γ-band emissions form, once a NO/N_2 gas mix is exposed to an alpha radiation source. In Publication IV an experiment is described that went as follows: N_2 gas with either 5 ppb or 50 ppb of NO had been flown over an alpha active source for a duration of 30 min. At all times, the 236.60 nm line of the γ-band had been observed. When the flow had been stopped after 30 min, then the radioluminescence intensity produced by the gas containing 5 ppb of NO suddenly increased. The same could not be observed with the gas containing 50 ppb of NO. The experimental data is shown in Fig. 4.9.

Much of the behaviour of the radioluminescence intensity can be explained with changing water vapour concentrations in the tube. The apparent increase in intensity with an increase in flow rate is explained by the more efficient removal of water that diffuses into the optical volume. Water is an extraordinarily potent quencher of the NO A-state [119] and if a larger mass flow removes just a bit more water vapour than a smaller one, then this small improvement shows by yielding an increased γ-band intensity. Also, the overall higher intensity produced by the gas containing higher levels of NO is explained by more molecules being available to emit radioluminescent light.

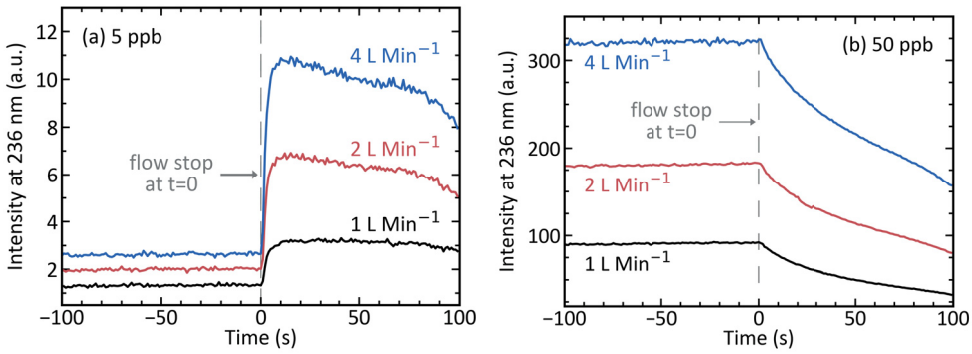

Figure 4.9 Dynamics of the γ-band emissions. N_2 gas containing either 5 ppb or 50 ppb of NO had been flown over an alpha source at different mass flow rates. Upon stopping the flow, radioluminescence produced by the gas containing 5 ppb of NO showed a sudden increase in radioluminescence (**a**), while the gas containing 50 ppb of NO did not (**b**). The data shown in this figure has been first presented in Fig. 3 in Publication IV.

The feature that can not be explained with either changes in water vapour concentration or a higher abundance of NO is the jump-like behaviour that only one of the two the gas mixtures exhibits. Excitation transfer, however, does provide an explanation. The rate equation that governs the population and depletion of the energy reservoir, Eq. (4.12), is

$$\frac{\mathrm{d}}{\mathrm{d}t}[\mathrm{N}_2^A] = k_\alpha[\mathrm{N}_2^X] - pQ_{\mathrm{NO}^X}^{\mathrm{N}_2^A}[\mathrm{N}_2^A][\mathrm{NO}^X] - k_{f,\mathrm{N}_2^A}[\mathrm{N}_2^A]. \tag{4.16}$$

With NO concentrations as small as a few ppb it is safe to assume that self-quenching of NO plays only a minor role. In the absence of self-quenching, every excitation that is transferred from N_2 to NO is made into a photon, which is to say that $[\Phi] \propto [\mathrm{N}_2^A]$. Thus the evolution of the γ-band intensity is indicative of the evolution of the energy reservoir. The equation for the evolution of the reservoir, Eq. (4.12), can be decoupled from the other equations and solved independently if it can be approximated that most of the NO is commonly found in the ground state, i.e. $[\mathrm{NO}^X] \approx [\mathrm{NO}]$. Then the rate equation for a time t after first exposure to an alpha source is solved by a simple exponential function

$$[\mathrm{N}_2^A](t) = \frac{k_\alpha}{\xi}\left(1 - e^{-\xi t}\right)[\mathrm{N}_2], \tag{4.17}$$

where $\xi = k_\alpha + k_{f,\mathrm{N}_2^A} + pQ_{\mathrm{NO}^X}^{\mathrm{N}_2^A}[\mathrm{NO}]$ is the speed by which the equilibrium concentration is approached and $[\mathrm{N}_2]$ the nitrogen concentration.

With this simple expression, the explanation for the difference in behaviour upon stopping the flow becomes clear. Energy reservoirs of gas mixes containing larger NO concentrations reach the equilibrium faster than gases with smaller NO concentrations. Then the interpretation of the jump-like behaviour upon stopping is simply that the energy reservoir of the low-concentration gas did not have sufficient time to equilibrate. That changed when the flow was stopped and the gas that was just flowing over the source now stayed there for much longer. The jump-like behaviour can be explained fully within the bounds of the theory of excitation transfer, which is a yet another piece of evidence that it is the primary mechanism that drives NO radioluminescence production.

A peculiarity of the intensity increase upon stopping the flow is that it allows to estimate the speed with which the gas was flowing over the source. The intensity before stopping the flow shows how much the reservoir had built up over a time t, whereas the intensity after stopping the flow shows the reservoir at equilibrium. Those two values are linked by Eq. (4.17) by a combination of NO concentration and exposure time t. This link can be exploited to estimate the time t_0 the gas was actually spending over the source. In this experiment, the PMT was placed next to the source, thus it picked up light emanating from all parts of the source. If they are approximated to equally contribute to the measured radioluminescence, then the equation of the total radioluminescence intensity can be written in the form

$$I(t_0) = C \cdot \frac{1}{t_0} \int_0^{t_0} [\mathrm{N}_2^A](t)\mathrm{d}t = \underbrace{C \cdot \frac{k_\alpha}{\xi}[\mathrm{N}_2]}_{I_{\mathrm{eq}}} \left(1 - \frac{1 - e^{-\xi t_0}}{\xi t_0}\right), \tag{4.18}$$

where C is a constant accounting for geometry and source activity and I_{eq} the measured intensity after the flow had been stopped. This equation had been numerically solved for t_0 for all three mass flows and the results are displayed in Fig. 4.10.

The estimated exposure times t_0 follow a pattern that indicates that an increased mass flow results in a shorter time of exposure. The relation of the exposure time t_0 to the mass flow Q is this of an inverse proportionality, which has been verified with regression analysis having a quality of fit of $\mathrm{R}^2 = 0.97$. It has been added as a red line to the figure. N_2 gas is a Newtonian fluid and as such travels over the

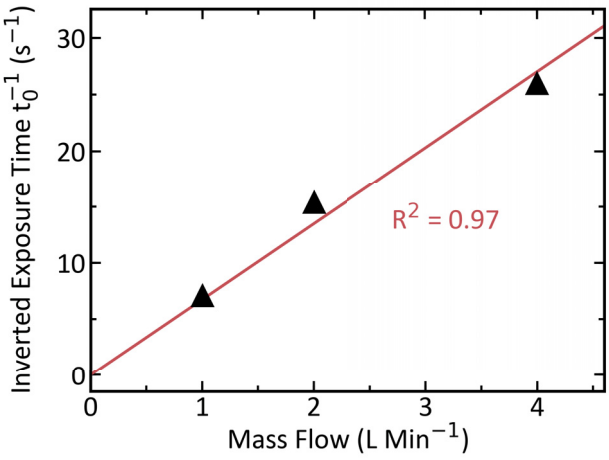

Figure 4.10 The time t_0 the low NO concentration gas is exposed to the source. The radioluminescence increase in each dataset shown in Fig. 4.9 had been evaluated for the time the gas had spent over the source by numerically solving Eq. (4.18) (black). The calculated times show a reciprocal dependence on the mass flow, which has been highlighted with a linear regression crossing the coordinate origin (red). The data shown in this figure has been first presented in Fig. 4 in Publication IV.

length of the source in a time $t_0 \sim Q^{-1}$, if the flow is laminar [149]. In the studied system, the Reynolds numbers were $48\,(Q = 1\,\mathrm{L\,Min^{-1}})$, $95\,(Q = 2\,\mathrm{L\,Min^{-1}})$, and $190\,(Q = 4\,\mathrm{L\,Min^{-1}})$ and thus well below the numbers at which transitions to turbulent flows might start to occur [150]. Thus, the flow is laminar and the predictions made by comparing radioluminescence intensities alone are congruent with the theory of fluid dynamics. Those predictions had been made based on an understanding that the radioluminescence is produced as a result of excitation transfer from N_2 to NO. Hence, the agreement between fluid dynamics and the model of radioluminescence production is further evidence that excitation transfer adequately describes the population of the NO A-state.

In this section of the Thesis, four pieces of evidence have been provided that excitation transfer from N_2 to NO is the dominant mechanism that efficiently converts an alpha particle's kinetic energy into UVC radioluminescence. The first piece of evidence has been the creation of intense UVC radioluminescence, whose spectrum has been identified with the NO γ-band. It has been shown that that replacing ambient air with a mixture of 50 ppm of NO in N_2 increased the radioluminescence yield by a factor of more than a hundred. Almost all of the additionally generated

light is located in the UVC. The second piece of evidence that has been provided is the relatively small concentration of NO that was required to create this effect. It had been shown that impact excitation cannot explain this behaviour. As third piece of evidence it has been shown that the evolution of the γ-band intensity can be purely explained with the evolution of the energy-reservoir, from which excitations are drawn to create NO radioluminescence. As last piece of evidence, it has been shown that the an excitation transfer based understanding of NO radioluminescence enables to estimate kinematic properties of the gas creating the radioluminescence by optical means alone. It has been shown that those estimates are congruent with the predictions of the established theory of fluid dynamics.

The following section of this chapter presents demonstrations of NO radioluminescence in settings relevant for nuclear decommissioning.

4.4 Applications

NO radioluminescence enables to detect weak sources in broad daylight. In environments where the atmosphere and its contents can be precisely controlled, replacing the air around an alpha emitter with a carefully prepared mixture of NO and N_2 results in the emisson of UVC light. In a measurement campaign at the Photonics Laboratory at Tampere University, this ability to resolve weak alpha sources with UVC light alone has been demonstrated by placing a 9.9 kBq Am-241 alpha source, taken from a smoke detector, in an air-tight chamber whose atmosphere was manipulated with a set of mass flow controllers. A quartz-glass window allowed UVC light in the chamber to leave it. An ICCD camera (Andor, Product Code: iStar 320T) equipped with a solar blind filter (Materion, Product Code: None - Custom Design) was placed at half a meter distance at the other side of the quartz glass window. Images of the chamber and the source as well response curves of the ICCD and filter are shown in Fig. 4.11.

The radioluminescence was produced by taking 30 individual images with 60 s exposure time each. The gain settings of the camera, binning and other internal parameters have been taken from the study on different camera systems by Sand and colleagues [32]. The image processing followed the procedure of background subtraction and noise removal by Lamadie and colleagues [28]. The gas was prepared to be a mixture of 3 ppm NO in N_2 of industry-grade purity. It flowed at a speed of

$5\,\mathrm{L\,min^{-1}}$ through the chamber. Much like in the previous experiments, it is important to stress that the measurement uncertainty has not been thoroughly analysed. The experiments are designed to be proof of principle. Those experiments do not constitute a carefully prepared analysis to fully determine the capabilities of NO amplification. They are meant to show that NO can overcome the daylight problem, that the amplification can be employed in relevant scenarios, and that it is worth to invest more time to assess the said capabilities.

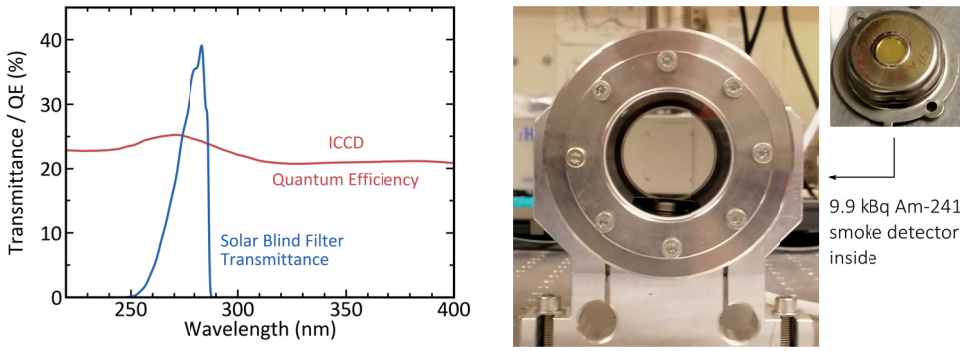

Figure 4.11 Imaging of a $9.9\,\mathrm{kBq}$ source using UVC light only. **Left**: The quantum efficiency of the ICCD camera [151] and the transmittance curve of the filter show that only UVC light was imaged. **Right**: The gas-controlled chamber contains a $9.9\,\mathrm{kBq}$ Am-241 source. The golden surface is the alpha active area.

The overlay image in Fig. 4.12 clearly identifies the smoke detector source. This experiment demonstrates the efficacy of NO radioluminescence for the purpose of enhancing UVC radioluminescence. Up to now, only alpha imaging system that collect air radioluminescence in a completely dark environment were able to produce radioluminescence images of sources with activities as small as $9.9\,\mathrm{kBq}$ [28, 102]. By diluting an amount of NO as small as $3\,\mathrm{ppm}$ into N_2, however, an UVC imaging system was enabled to do the same. It can be speculated that concentrations smaller than $1\,\mathrm{ppm}$ enable to produce UVC alpha images of similar quality, since the model of excitation transfer depicted in Fig. 4.7 predicts a linear decrease in intensity with a decrease in concentration. Thus, a reduction of the intensity by a factor 3 could be counterbalanced by imaging with longer exposure time.

It is important to stress that it has to be considered good practice to keep the NO concentrations as small as possible. As pointed out earlier in the chapter, an unbounded electron makes NO highly reactive, which, among other things, means

that it easily corrodes the equipment it comes into contact with it [152]. Using small concentrations can result in the desired increase of UVC radioluminescence, all the while ensuring the longevity of devices and equipment. The benefits of low levels of NO in the gas mix is obvious, should the situation arise that personnel is accidentally exposed to it [130]. Concentrations as small as 100 ppm are immediately dangerous to life and health and the maximum admissible concentration is only 500 ppb [153]. Depending on the legislator, the occupationally admissible concentration might be different from the maximum admissible concentration. The danger NO poses to life and health, however, is clear.

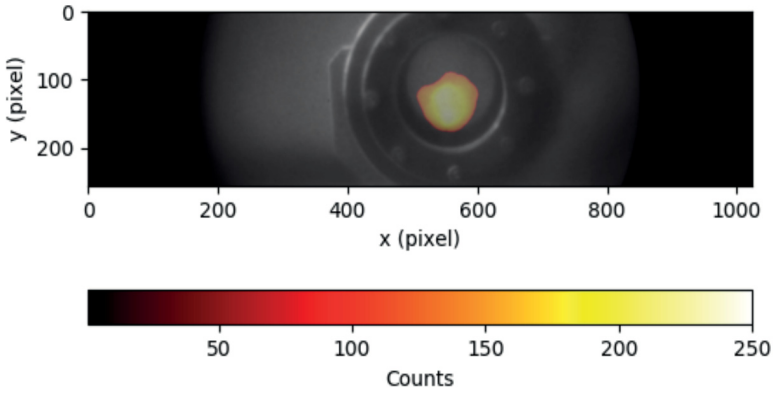

Figure 4.12 Alpha image of the smoke detector source using only UVC light. The overlay shows a grey-scale background image and a red overlay on top displaying the emission of UVC light just above the source.

Potential use cases for the technique are installations and facilities where nuclear material is processed. There, treatment or radioactive material typically happens in gloveboxes and alteration of the gas atmosphere inside is relatively easy. Solar blind imaging systems could be used to identify alpha contamination without the need to darken the box. Sufficiently strong sources could be tracked in real-time.

The use of NO radioluminescence is not only restricted to precisely controlled environments. Two properties of NO radioluminescence production make it possible to generate it in ambient air using nothing more than an N_2 purge with a sufficient but small amount of NO. First, NO radioluminescence is intense, provided that quenchers are absent. Second, it has been shown that the reservoir reaches equi-

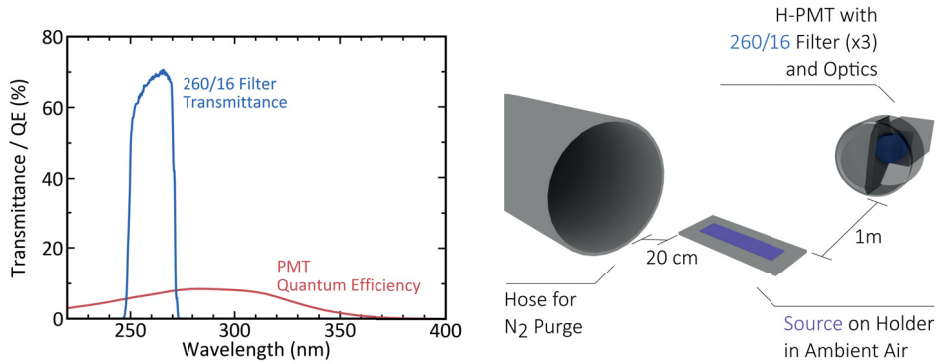

Figure 4.13 Experimental arrangement to create and detect NO radioluminescence in ambient air. **Left**: The quantum efficiency of the PMT [154] and the transmittance curve of the interference filter [155] show that only UVC light around 260 nm was collected. **Right**: A 32 MBq Am-241 source has been placed in ambient air and a hose blew nitrogen of varying purity over it. A system of PMT and filters collected UVC light under bright illumination. This figure was first presented in modified form in Fig. 1 in Publication IV.

librium concentration in a short amount of time, provided that a sufficient amount of NO is present. Thus, applying a N_2 purge for a brief moment should create intense UVC radioluminescence. In Publication IV this hypothesis had been tested by using an experimental arrangement as shown in Fig. 4.13.

A 32 MBq Am-241 source had been placed in ambient air under normal fluorescenct lighting on a table in a laboratory. A UVC sensitive PMT, which had been rendered solar blind by attaching a stack of three 260 nm bandpass filters, measured the UVC radioluminescence emanating around the source at 1 m distance. A hose at 20 cm distance applied an N_2 purge. The N_2 gas contained either 5 ppb or 50 ppb of NO. These low levels of NO are considered safe and are well below the various levels of NO a human lung produces [156]. Thus, applying an N_2 purge with prepared levels of NO can be considered safe for humans.

In the recorded radioluminescence intensities in Fig. 4.14 it can be seen that only the purge containing higher amounts of NO lead to a temporary significant increase in UVC light production. This behaviour is congruent with the jump-flow behaviour presented in the previous section of this chapter. There it had been argued that the speed with which the reservoir builds up is dependent on the NO concentration. During a flush, the exposure time is very limited, which does not give the N_2 containing little NO nearly enough time to build up a reservoir. Thus, an N_2

purge with small amounts of NO does not result in a significant increase in UVC radioluminescence.

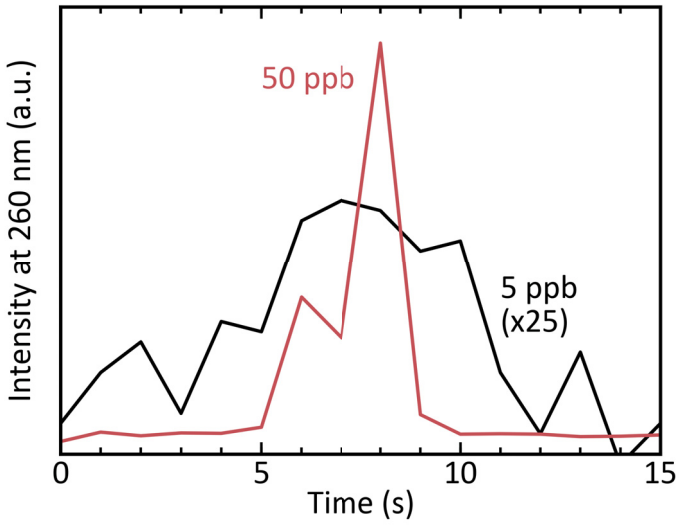

Figure 4.14 Dynamic enhancement of UVC radioluminescence. The radioluminescence had been measured in broad daylight and ambient air. The brief exposure of the source to an N_2 purge containing 50 ppb resulted in a brief but intense increase in UVC radioluminescence. This was only the case to a much lesser degree for a purge with N_2 containing 5 ppb of NO, which is displayed with 25-fold magnification to make the slight increase visible. The data presented in this figure has been first presented in Fig. 5 in Publication IV.

A purge with slightly elevated levels of NO is more successful in creating γ-band emissions. In general, the degree to which UVC radioluminescence can be created depends on the NO concentration, the time the gas mixture remains around the source and the speed by which quenchers diffuse into the flushed volume after the purge ends. In this particular case, the application of an N_2 purge with 50 ppb of NO lead to a few second long lasting thousand-fold increase in UVC radioluminescence. This is sufficient to detect even weaker source from a long distance in broad daylight. This experiment demonstrates that NO radioluminescence can work in ambient air. The most important aspects of this technique are the temporary absence of quenchers and addition of sufficiently high levels of NO, which themselves can be well below the limits where NO might become a health concerns.

This section has shown that NO radioluminescence can be applied both in a controlled environments and in ambient air. It enables solar blind imaging of alpha

radiation. These demonstrations conclude the chapter on NO radioluminescence and they make it clear that the utility of NO radioluminescence transcends this of an academic exercise. It stands to reason that the proven efficiency with which it can convert an alpha particle's kinetic energy into UVC radioluminescence make it a key luminescent species in new technologies in the field of alpha imaging. Especially the application in nuclear decommissioning seems apt, as the slight modification of the atmosphere in the commonly employed gloveboxes is simple. Further, the camera technology that is required for UVC imaging has been thoroughly tested [32] and is in large parts available off-the shelf.

5 RADIOLUMINESCENCE IN WATER

The contents of this chapter touch on the subject of radioluminescence in water. Like most topics discussed in this Thesis, the need to study radioluminescence in water is mostly application-driven. Radioluminescence produced in air has proven to be a reliable indicator for the presence of alpha contamination and thus enabled the development of optical systems that exploit this feature for remote alpha radiation detection. In addition to the obvious radiation-security-related advantages optical detection provides, it also promises to be a much more rapid process [33] in detection alpha contamination than the more traditional approaches based on swipe tests and Geiger-Müller counters [56]. The key insight that forms the physical basis of the technique is the realisation that alpha contamination located in normal air always produces UV light. The existance of UV light around an alpha source can be taken as a given. Hence, the development of optical detection of alpha radiation focuses on the technology that detects the light.

From this point of view it is easy to understand that the knowledge of the radioluminescence spectra of various materials is the foundation on which all optical detection of alpha radiation rests. Once the radioluminescence spectrum in a given medium is known, then it can be exploited. If the scintillating material is a gas, then the scientific literature provides a rich collection of articles that catalogues the spectra of radioluminescence in all manner of gas mixtures. The earliest studies reach as far back as into the 1960s, when nuclear research was opened to civilian institutes and at the same time some of the military work was declassified [77, 114]. Since then, the number of recorded spectra has only grown, with the latest contributions having been made in the late 2010s [78, 116]. The articles published between those two time periods are too numerous to discuss within the scope of this Thesis. However, if the scintillating material is a liquid, then the scientific literature has much less to offer. The reasons for this are two-fold and have important consequences for technologies that aim to utilise this form of radioluminescence in one way or another.

One of the earliest studies on radioluminescence in liquids has been conducted by Duquesne and colleagues [25] in the 1960s. They observed that the immersion of Po-210 in water caused the production of light. In the same study they found that the same emitter also produced luminescence in air, however, the emissions in water were of much lower intensity. Shortly thereafter a different group hypothesised that the light that was observed in water were a type of luminescence generated by intermediary species produced during water radiolysis [157]. Since then, there have been few reports on the phenomenon. Radioluminescence in water gained renewed interest when Yamamoto and colleagues [158] found in 2016 that by immersing an Am-241 source in water, very faint light emission were produced. Their findings and observations are in complete agreement with the observations made by Duquesne. The authors conclude the abstract of their contribution with the statement "The luminescence of water with alpha particles would be a new method for alpha particle detection and distribution measurements in water".

Before radioluminescence in water can be used for alpha imaging, however, its spectrum has to be known. Further, if the mechanisms that give rise to it can be found, then its precise shape can be predicted. In another study, Yamamoto and colleagues [159] used a set of optical long-pass filters to get a rough estimate of the radioluminescence's spectral shape. They found that the spectrum is mainly located in the UV and estimated that the spectral pattern follows a λ^{-2} law for wavelengths longer than 350 nm. With this estimate of the spectral shape, Yamamoto and colleagues convincingly showed that the radioluminescence in water occurs in the UV and thus low-noise and high-sensitivity equipment that has already been successfully applied to image N_2 and NO radioluminescence can also be applied to radioluminescence in water. However, the light output is reportedly much less intense than this in air [25, 158], yet with proper choice and arrangement of equipment this could be a manageable problem, much like the problem of the small light yield of radioluminescence in air was managed by Lamadie [28] and the many researchers after him. Before work on the detection can be started, however, the spectrum of the radioluminescence has to be known.

The rest of this chapter concerns itself mostly with the means by which the spectrum of radioluminescence in water can be recorded. The mechanism by which it is produced are largely unknown and the best guesses so far are mostly based on speculation. Some authors hypothesise it to be a form of luminescence of radioly-

sis products [157] while others see it more as a broadband light emissions born of a dipole displacement inside the water molecules [159]. Up to now, however, there is no conclusive evidence to bolster either hypothesis. Thus, the content that it is about to follow concerns itself mostly with the optical techniques that are necessary to accurately measure those spectra. This information hopefully helps to produce high quality spectra that provide clues and hints pointing to the true mechanism of radioluminescence production. The following descriptions draw largely on the work that has been described in Publication III, which might be consulted for more information on experimental details.

5.1 Measuring the Spectrum

The spectroscopic study of radioluminescence in water is technologically more challenging than the study of radioluminescence in air. In both scenarios, a minimal working experimental arrangement requires one device to physically separate the radioluminescent light into its spectral components and another device to measure the intensity of each separated component. The procedure is straightforward and has been used in Publication I and II to record the spectra of N_2 and NO radioluminescence, respectively. Additional equipment like a computer and automatised measurement scripts are convenient additions, but not strictly necessary. The difficulty comes with the means that have to be employed to guide the radioluminescent light to the experimental arrangement. A solid source like sealed Am-241 can simply be placed in front of the monochromator entrance slit to guide some of the radioluminescent light to the spectroscopic arrangement. If a higher throughput is desired, than a system of carefully selected lenses can be put between source and monochromator to maximise the light collection efficiency. This ease with which radioluminescent light from solids can be brought to the monochromator does not apply to liquids. There are three additional complications that come with using a liquid source and they are addressed in the following point by point.

The first complication comes with the dangers of handling radioactive liquids. Contamination in liquid form spreads much more easily than contamination in solid form, which is why radiation protection laws commonly only permit their handling in specially prepared gloveboxes in designated laboratories that follow a strict security protocol [47]. It was for this reason that the recording of the spectrum described

in Publication III had been carried out in the premises of the Joint Research Centre (JRC) in Karlsruhe, Germany. Further, the security protocol around contaminated liquids requires that any device, material or object that has once entered the glovebox is from that moment on considered highly contaminated nuclear waste and must be disposed of as such [47]. Thus, putting the spectroscopic arrangement into the glovebox is not an option and the radioluminescent light has to be guided out of the box and to the spectroscopic arrangement. This can either be done by replacing one of the gloves with a quartz window, which is useful for imaging applications like the one presented in Publication I. Or it can be achieved with a system of UV transparent light guides for an optimised throughput. For the work in Publication III, both a quartz glass window and liquid light guides (Lumatec, Product Code: Series 300, 8 mm core diameter, [160]) were used for two different set of experiments. For what it matters to the measurement of the spectrum, the security precautions make it necessary to introduce optical elements into the system which complicates the calibration of the spectrum, thereby adding a layer of complication to the task.

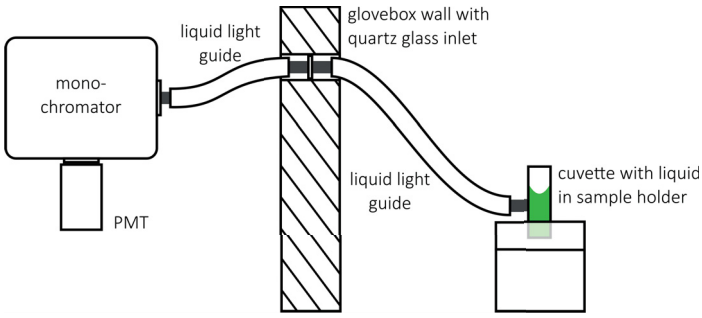

Figure 5.1 Setup to resolve the spectrum of radioluminescence in water. An alpha contaminated liquid (green) was filled into a quartz glass cuvette and then placed on a height-adjustable sample holder. A system of liquid light guides transported the radioluminescence emanating from the bottom of the cuvette to a system of monochromator and PMT. This figure has been first shown in a slightly different form in Fig. 3 in Publication III.

The second complication comes with need to keep the liquid confined in a container. This introduces yet another optical element into the system and thus it is desirable for the container to both be UV transparent and to exhibit an ideally flat transmittance spectrum. Solutions for this challenge are typically readily available in the form of cuvettes made of high-quality quartz glass. In the case of the measurements at the JRC, a cuvette made of glass with a flat spectral transmission in

the UV had been used (Hellma analytics, Product Code: 101-QS, Glass type: QS, Dimensions: 12.5 mm x 12.5 mm x 45 mm, [161]).

The third complication is presented by alpha particles that leave the liquid and are being stopped in air. If the liquid has a boundary layer with air and at the same time alpha particles are emitted close to this layer's surface, then alpha particles leave the liquid and get stopped in ambient air where they produce radioluminescence [162]. The radioluminescence in air can interfere with the measurement of the radioluminescence in water, which incidentally is also located in the UV [159]. Radioluminescence in water has been shown to be much less intense than this in air [25, 158], thus radioluminescence in air potentially supersedes this in water. As a result, if an alpha-active liquid has a boundary layer with water, then the light that is guided to the spectroscopic setup has to be taken from the parts of the liquid that is far away from the surface. This and the other two complications had been kept in mind when the measurement at the JRC was set up, which is shown in Fig. 5.1.

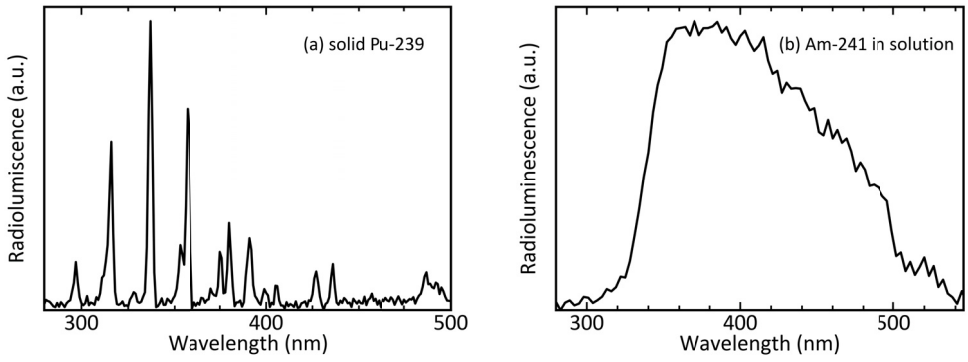

Figure 5.2 Spectra of radioluminescence in air and water. (**a**) Spectrum of the radioluminescence in air created by solid Pu-239. (**b**) Spectrum of the radioluminescence in water created by Am-241 dissolved in a 3 M aqueous nitric acid solution. These spectra have been first presented in Fig. 7 in Publication III.

The radioluminescence spectra of both radioluminescence in air and of radioluminescence in water were recorded. Radioluminescence in air had been guided to the monochromator by putting a solid sample of Pu-239 in front of the light guide. Radioluminescence in water had been guided to the monochromator by putting the cuvette, which had been filled with 2 mL of Am-241 dissolved in a 3 M aqueous nitric acid solution, in front of the light guide. The procedure to record the spectrum of radioluminescence in air was the same as in Publication I.

The measurement of the spectrum of the radioluminescence in water required large changes in the procedure, largely because the radioluminescence yield had been found to be very low. To increase the amount of light, a highly active solution of 95 MBq cm^{-3} had been used. Further, the throughput had to be increased, which came at the expense of spectral resolution. For that the monochromator had been equipped with a UV-sensitive grating with few grooves per mm (Horiba, Product Code: 51050, 300 gr mm^{-1}, 250 nm blaze) and the entrance slit width had been put to its maximum of 2 mm. This way a spectral resolution was reduced to 6 nm, while the throughput was enhanced by about an order of magnitude. Still, a total integration time of about 22 hours was necessary to resolve the spectrum.

Both spectra are presented side-by-side in Fig. 5.2. The spectrum of radioluminescence in air had been measured in part to test the spectral response of the system. In part it served to verify that the experimental arrangement is capable of correctly recording the spectrum of radioluminescence in air down to 280 nm. The spectrum of radioluminescence in air that had been found closely resembled this found by other authors [33, 82] and thus helps to trust in the correct representation of the spectrum of radioluminescence in water. More details on the verification of the spectra and the system response corrections for this particular experiment are discussed in great detail in Publication III.

The recorded spectrum shows that radioluminescence in water is spectrally broad, which explains part of the difficulties that had been encountered when recording it. It shows a broad maximum between 350 and 400 nm with a gradual decrease until 550 nm at the longer wavelength side. On the other hand, the spectrum exhibits a pronounced decrease at the shorter wavelength side which reaches down to the background level already at 300 nm. The increase with shorter wavelengths is in agreement with the studies done with long-pass filters of Yamamoto and colleagues [159]. It is also in agreement with their finding that the radioluminescence is mostly found in the UV. However, it does contrast with their study in that the authors estimated that the behaviour of increasing intensity with decreasing wavelength continues past the point of 350 nm. Thus the radioluminescence in water might be Cerenkov radiation. However, the steep decrease found in the spectrum clearly contrasts with this hypothesis.

It is worthwhile to show why Cerenkov radiation is unlikely the cause for the appearance of UV and blue light. Cerenkov radiation is a form of electromagnetic

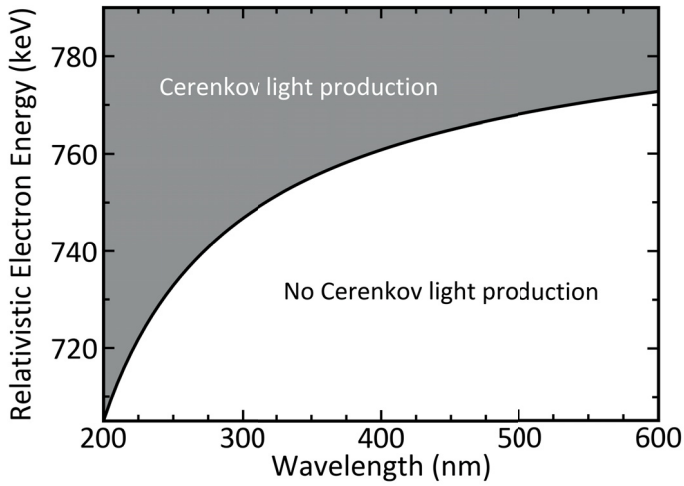

Figure 5.3 Cerenkov light production in water as a function of electron energy and wavelength. The grey part of the figure indicates the kind of electrons that are sufficiently energetic to produce Cerenkov light. The white part indicates the opposite. The black curve separating the two areas connects the points of mininum electron energy that is required to produce Cerenkov light. It shows that electrons need to have relativistic energies of more than 700 keV to produce UV and VIS Cerenkov light in water. The curve has been compiled using the extensive collection refractive indices of water by Segelstein [163]. The black curve has been computed by using the mass-energy equivalence $E_{\text{min}}(\lambda) = {}^{m_e c^2}/\sqrt{1-n^{-2}(\lambda)}$.

radiation that is emitted when a charged particle passes through a dielectric medium at speed greater than the phase velocity of light in that medium [60]. As such, it is the electromagnetic analogue to a sonic boom [61]. Thus, in principle, it can be assumed that the an alpha particle, or one of the free electrons it creates, are sufficiently energetic to cause the creation of Cerenkov light. Cerenkov light appears as a continuum, where the number of created photons N of wavelength λ over a length x is [164]

$$\frac{\partial N}{\partial \lambda \partial x} = \frac{2\pi\alpha_f}{\lambda^2}\left(1 - \frac{c^2}{v^2 n^2(\lambda)}\right), \tag{5.1}$$

where in this case $\alpha_f \approx \frac{1}{137}$ [165] is the fine structure constant and $n(\lambda)$ the medium's index of the refraction at wavelength λ. The equation requires the charged particle's velocity to be greater or equal than the speed of light in the medium ${}^{c}/_{n(\lambda)}$ for Cerenkov radiation to be emitted. Alpha particles are way too massive to achieve high enough velocities, given the few MeV of kinetic energy they typically carry

[166]. Electrons, on the other hand, are much lighter and can potentially achieve sufficiently high velocities to create Cerenkov radiation in water. A picture showing the characteristics blue light emanating in the moderator around a nuclear reactor is shown in Fig. 2.2. The mininum relativistic energies electrons need to have in order to cause the creation of UV and VIS Cerenkov light are shown in Fig. 5.3. There it becomes apparent that an electron needs to have more than 700 keV of relativistic energy in order to create Cerenkov light in water. The stopping of an alpha particle in water does not produce electrons with those kind of energies [166, 167]. Thus, it is unlikely that Cerenkov radiation is produced by the stopping of an alpha particle.

The other mechanisms that could create sufficiently energetic electrons is β^--decay. Am-241 itself only undergoes α-decay, γ-decay, spontaneous fission and cluster decay [41]. The next likely candidate in the Am-241 decay chain that does produce electrons carrying sufficiently high energies is the β^--decay of Bi-213 to Po-213, which releases an electron with 1.423 MeV of relativistic energy [41]. However, Am-241 decays to Po-213 with a half-life of millions of years, so it is unlikely that within the few hours of measurement a detectable amount of Am-241 had completed the decay all the way to Po-213 and thereby produced Cerenkov light.

The only possibility that remains for the light not to be a form of radioluminescence in water, is to be a form of quartz glass scintillation brought about by the cuvette. To test for this possibility, the radioluminescence has been imaged. Imaging of weak UV light sources is an exercise that has been thoroughly studied by previous authors [28, 76] and the best practices for this procedure are now well understood. However, the details and the findings that had been made during this particular implementation of radioluminescence imaging warrant a slightly more comprehensive discussion.

5.2 Imaging the Radioluminescence

The imaging of alpha active material that is inside a glovebox made it necessary to apply a few alterations to the box itself. The radioluminescence had to be guided out of the box without distorting its spacial distribution. Gloveboxes, however, are typically made of acrylic which does not transmit UV light [168]. Hence, one of the glove ports was replaced with a UV transmissive quartz glass window, which had a flat transmittance down to 180 nm (Sico Technology, Product Code: SQ1, [169]).

Thus, no distortion of the radioluminescence image by the quartz glass window was to be expected. The used camera was an EMCCD camera (Andor, Product Code: iXon3 897) equipped with a UV transmissive objective (Universe Kogaku, Product Code: UV1228CM, f/2.8, 12 mm) and was placed such that it imaged the inside of the glovebox through the quartz glass window. The camera sensor was cooled to −80° C to reduce thermal noise. At about 30 cm distance from the camera, inside the glovebox at the other side of the window, the cuvette containing the alpha active liquid was placed inside a light-tight PVC tube. At all times, both camera and cuvette were completely shielded from ambient light using black rubberised fabric (Thorlabs, Product Code: BK5). The low light yield of radioluminescence in water made it necessary to be extra thorough with the shielding by using multiple layers of cloth, as any light entering from the outside would have easily disturbed the measurement. A drawing of the setup is shown in Fig. 5.4 for easier comprehension.

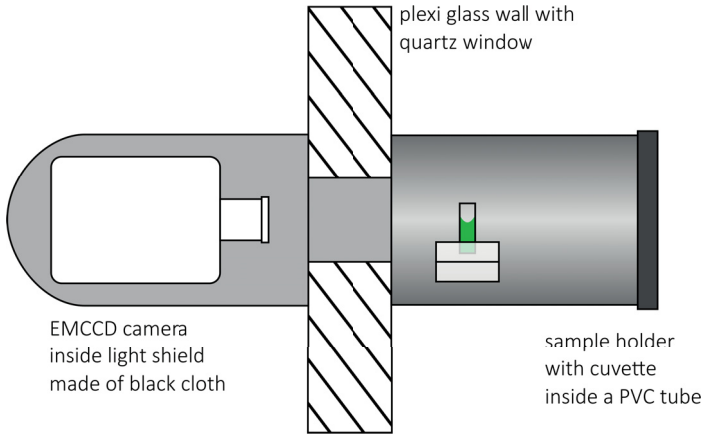

Figure 5.4 Setup to image radioluminescence in water. Water containing Am-241 (green) dissolved in nitric acid was filled into a quartz glass cuvette and then placed on a height-adjustable sample holder inside a light-tight PVC tube. Light emanating from the liquid left the glove box through a quartz glass window where it was picked up by an EMCCD camera. The camera was shielded from ambient light with black fabric. This figure has been first shown in a slightly different form in Fig. 1 in Publication III.

A variety of alpha contaminated liquids was imaged. All liquids had in common that they were prepared by dissolving Am-241 into nitric acid and then into deionised water. Dissolving the Am-241 in nitric acid first was necessary to keep the Am-241 in solution and prevent it from sedimenting out. The samples only varied in nitric acid concentration (1, 3 and 7 M) and activity (6.5, 9.5, 19 and 95 MBq cm^{-3}). The

cuvette only held 2 mL of a given liquid at a time. In addition to the liquids, a Po-210 planchet had been imaged. Much like for the verification of the radioluminescence spectrum, the correct reproduction of an image of radioluminescence in air helps to trust that the liquid samples had been correctly imaged.

The imaging protocol followed the approach of creating an overlay of a VIS and a UV image [28]. The only modification to the procedure was that the UV image had been created as a median of 30 consecutive captures, each with 60 s exposure time, instead of taking a single capture with 30 min exposure time. This was necessary to remove artifacts in the image material brought about by the 59.6 keV gamma rays of Am-241 [41] hitting the camera sensor, thereby creating overexposed parts of the CCD sensor commonly referred to as "hot pixels". Those hot pixels were efficiently removed by applying a pixel-wise median over all 30 indivudal captures. The same median filter also improved the signal-to-noise ratio, since it increased the total exposure time of the filtered image to 30 min. An illustration of the hot pixel removal is demonstrated in Fig. 5.5. The postprocessing had not be applied to the image of radioluminescence in air, where UV image was created with a single 100 s exposure.

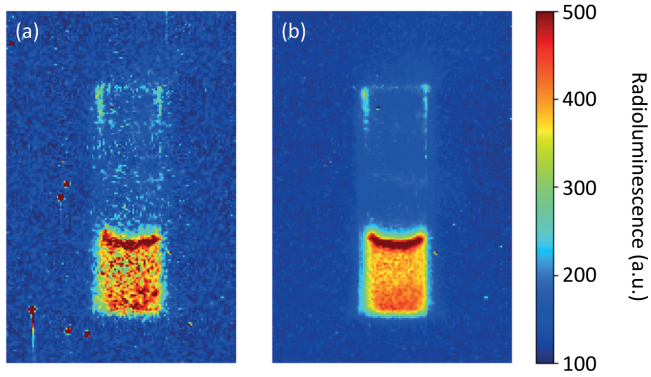

Figure 5.5 Demonstration of hot pixel removal using 30 images of 60 s exposure time each. (**a**) A single capture, raw data. The cuvette and the liquid are clearly visible, hot pixels and noise obscure the view. (**b**) The pixel-wise median over the total of 30 images. The z-scale shows raw pixel values. This figure has first been shown in Fig. 2 in Publication III.

The VIS, UV and overlay images of radioluminescence in air and in water are shown in Fig. 5.6. The liquid that had been used had an acidity of 3 M and an activity of 95 MBq cm^{-3}. In the images it can be seen that the radioluminescence in air is correctly depicted. The UV image clearly resembles those that had been found by

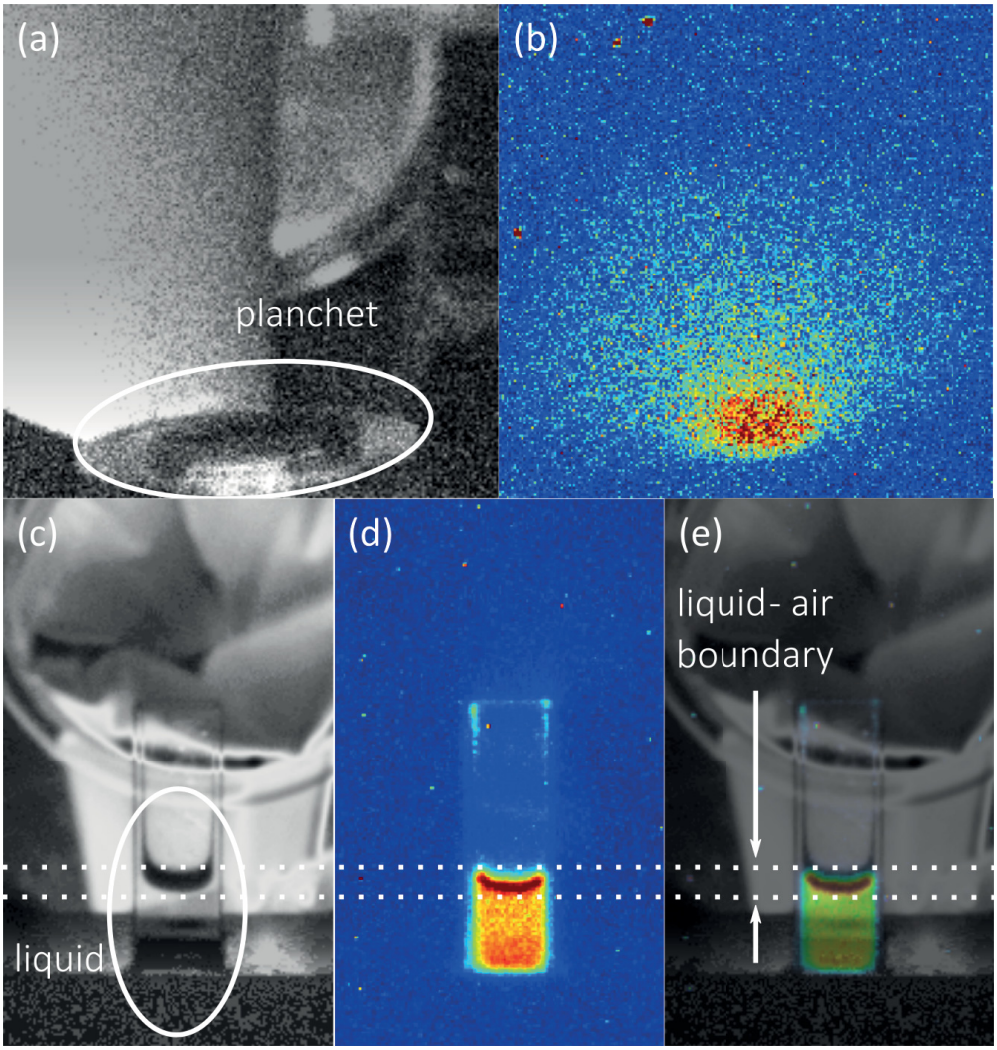

Figure 5.6 Images of radioluminescence in air and in water. They grey scale images show a single 0.1 s image taken under normal lighting conditions. The colourful images next to them are the radioluminescence images displayed as a colour-coded intensity-map. Their scales are the same scale that had been used in Fig. 5.5. (**a**) VIS image of a Pu-239 coated planchet. (**b**) UV image of the same scene. (**c**) VIS image of the sample holder, the cuvette and a transparent liquid. (**d**) UV image of the same scene. (**e**) Overlay of images (c) and (d). (**c-e**) Dotted lines frame the area where the surface of the liquid with air is visible. This figure has first been shown in Fig. 4 in Publication III.

other authors in similar settings [28, 32, 35]. The UV image of the cuvette shows that the water homogeneously emits radioluminescence. Inhomogeneities are found at the bottom part of the cuvette and at the liquid-air boundary. The apparent intensity increase at the bottommost part of the cuvette is likely caused by the reflection of radioluminescent light from the sample holder towards the camera. This can be inferred from the fact that only the parts of the cuvette that are immersed into the holder exhibit this apparent increased radioluminescence intensity. That means that light that otherwise would have never reached the camera now does and it gives the impression of an increased radioluminescence production, though it is nothing but a reflection.

The pronounced inhomogeneity at the liquid-air boundary is either an optical effect or it is an actual increase radioluminescence intensity. Both cases seem likely, since light can refract at the curved surface and thus give the impression of increased light production. On the other hand, it is also known that alpha particles which are emitted close enough to the liquid-air boundary leave the liquid [162]. Alpha particles that left the liquid would then create the more intense radioluminescence in air. In the experiments and in these carried out by Yamamoto and colleagues [158], it was found that radioluminescence in air is produced much more efficiently than this in water. In this particular work it could be estimated from Fig. 5.6 that the radioluminescence production in air was about 150 times more efficient than this in water. Hence, even few alpha particles escaping the liquid could create enough radioluminescence in air that would compete in intensity with this in water.

The homogeneously illuminated parts of the cuvette show that its walls do not have an influence on the radioluminescence production. If it were the case, then the walls would show a distinct glow that would reveal their radioluminescent properties. However, they do not show such an effect and thus it can be concluded that the radioluminescence emanates from within the liquid.

The possibility that the nitric acid rather than the water gave rise to the observed radioluminescence had also been investigated. To do so, UV images were taken of liquids where the activity was always 19 MBq cm^{-3} but the nitric acid concentration was either 1, 3 or 7 M. The radioluminescence of each sample was measured by averaging over the homogeneously illuminated part of the cuvette in each UV image. The same had been done for a series of images taken from a series of liquids with a constant nitric acid concentration of 3 M but varying activities of 6.5, 9.5, 19 and

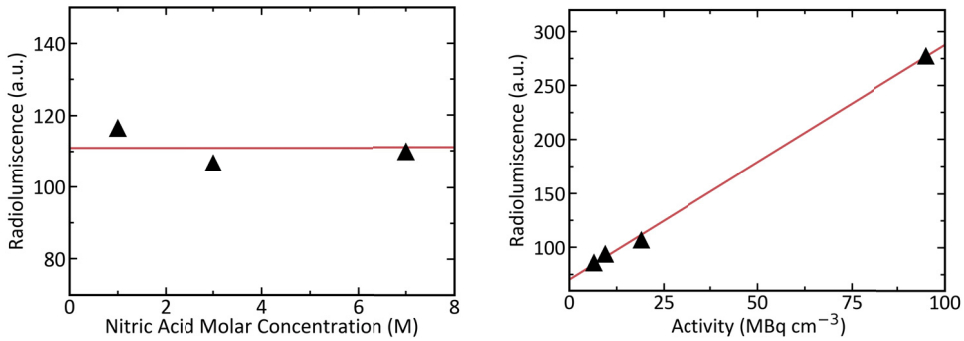

Figure 5.7 Radioluminescence dependence on acidity and activity. The radioluminescence intensities are displayed as pixel values which have been corrected for the image background. (**a**) Change of the radioluminescence intensity with a varying nitric acid concentration (black). The activity of all liquids was $19\,\mathrm{MBq\,cm^{-3}}$. A constant function has been fitted to the data (red). (**b**) Change of the radioluminescence intensity with a varying activity (black). The nitric acid concentration in all liquids was $3\,\mathrm{M}$. A linear function has been fitted to the data (red). This figure has been shown in slightly different form for the fist time in Fig. 6 in Publication III.

$95\,\mathrm{MBq\,cm^{-3}}$. The measured radioluminescence intensities are shown in Fig. 5.7. There it can be seen that the change in nitric acid concentration had no effect on radioluminescence intensity, while an increase in activity lead to a linear increase in intensity. Thus it can be concluded that nitric acid does not give rise to the radioluminescence, either.

It remains to conclude that the radioluminescence in water is likely a UV emission created in an interaction of alpha particles with water. It has been shown that this interaction is unlikely to be a form of superluminal travel of charged particles through water, which would result in the production of Cerenkov radiation. It has also been shown that it is not a form of quartz glass scintillation or emissions created by the interaction with nitric acid, either. At this point, it might be reasonable to speculate that the radioluminescence is form of luminescence from one of the radiolysis products. The number of generated species during radiolysis is vast and it involves the creation of species like OH, H_2 and H_2O_2 [170], all of which are known to emit radioluminescence in one form or another [77]. Their radioluminescence production has been observed in the gas phase, however, the excitation mechanism that creates the radioluminescence could potentially also be present in the liquid phase. However, so far this speculation is nothing more than that: a speculation, pure conjecture, guesswork. It would require an extensive literature study or more experimental re-

search on radioluminescence in water to formulate a reasonable hypothesis.

The existence of radioluminescence in water, however, is proven. For the most part, the measured spectrum is in agreement with earlier works. It remains to find the origins of this ultraviolet light that is produced when water contains alpha contamination. This research, however, opens the door for a whole new study of alpha contamination detection in liquids. To put it once again in the words of the colleagues in Japan who where the first to extensively report on the phenomenon: "The luminescence of water with alpha particles would be a new method for alpha particle detection and distribution measurements in water" [158].

6 CONCLUSIONS

This Thesis has started out by showing that a growing number of upcoming nuclear power plant decommissioning projects will require the attention of professionals. More so, it has shown that one of the largest cost drivers is the decontamination of materials and facilities. This fact has been known since the first nuclear power plant had been commissioned in 1948 [171], and typically the operators of nuclear power plants are required to withhold funds to finance the plant's eventual takedown. What was not known at the time, however, were the dangers of nuclear radiation. Increasing public awareness and a series of accidents resulted in stricter security protocols around nuclear waste and nuclear contamination in general [3]. Some countries have gone as far as opting out of nuclear power completely. Stricter regulations and reduced levels of acceptable radiation levels have substantially driven up the prices for finding and disposing of nuclear contamination. Europe alone is "facing [a] €253bn nuclear waste bill" [9].

The need for new technology that can comply with the new standards is obvious. While the technology to detect beta and gamma radiation has made steady progress in the past 50 years [172], the same can not be said of the technology that detects the arguably most pernicious type of radiation, alpha radiation. For the most part, this is a direct consequence of its limited travel distance in ambient air. Even today, swipe tests are industry standard and it is those tests that are being used in decommissioning of nuclear power plants [47]. It is difficult to overstate the laboriousness of carefully swiping through every nook, notch and neck of every part of the entire power plant that might have been in contact with radiation. And yet it is the only way by which alpha contamination can be detected such that compliance with government regulations can be achieved. And even then the possibility of proliferation of alpha active material can not be eliminated [21].

The outlook on technological progress in alpha detection wholly changed with the landmark experiments of Baschenko [24]. It were his experiments that started a

whole new line of research that uses the scintillation in ambient air to detect alpha radiation from a large and safe distance. By 2006, the technique had improved to levels that permitted first experimental uses in industrial settings [103]. As of 2019, the use of ICCD and EMCCD cameras are the best-known types of cameras to rapidly image alpha contamination [76]. However, sensitivity to daylight and the inability to resolve alpha sources as small as mandated by regulations ($0.1\,\mathrm{kBq\,kg^{-1}}$ [16] for Finland) keep the otherwise mature technology from being employed in nuclear decommissioning tasks.

In this Thesis, it has been argued that those challenges can be overcome by making the appropriate changes to the gas atmosphere around the alpha emitters. It has been shown that the radioluminescence of NO possesses characteristics that overcome both limitations at once. Its intensity can far surpass this of radioluminescence in ambient air and it is mostly emitted in the UVC, thus rendering the detection scheme resistant to influences of daylight. It has been demonstrated that replacing ambient air around an alpha emitter with 50 ppm of NO diluted in N_2 increases the production of UVC radioluminescence by more than four orders of magnitude. The imaging of a 9.9 kBq with solar blind optics served as proof of principle that NO radioluminescence can be used to detect weak radiation source.

It has been argued that the efficient generation of NO radioluminescence can be fully explained by the molecule's unique access to a storage of energy that is held by electronically excited N_2 molecules. By conducting a literature study, it has been shown that much of the energy that an alpha particle deposits in ambient air is stored in the A-state of N_2 molecules. The theory that has been laid down holds that transfer of excitation from this state to the NO molecules sufficiently well explains the high intensities the γ-band can achieve. More so, it has been argued that the direct excitation of the NO molecules by electron bombardment is insignificant in comparison. A minimal working theory that encapsulates these aspects has been presented. It has been shown to predict conditions under which the NO radioluminescence can even be used in ambient air by using nothing more than a purge of N_2 which has been dosed with a few tens of ppb of NO.

One of the main results in this Thesis has been the demonstration of just how intense the NO radioluminescence can become. For what it concerns this Thesis, this quality is its defining characteristic and one of the two factors that make it relevant for decommissioning tasks. The high UVC radioluminescence intensity makes NO

as a luminescent species stand out among others that have been proposed in the past years. For example, it has been found that by flowing Xe gas over an alpha source located in ambient air, the UVC radioluminescence intensity could be increased by about a factor of 6 [78]. Improvements of this kind of magnitude are common in the recent literature on the matter [34, 116]. This Thesis holds that this factor can be more than 10 000, if NO in a carefully prepared setting is used.

To a lesser degree, this Thesis investigated the radioluminescence in water. Much like radioluminescence in gases, it is relevant for the remote detection of alpha contamination. Nuclear fuel is processed in liquid form [38] and contamination by spill or leakage is a common concern in nuclear facilities. The benefits of an optical detection scheme of such contamination are just as large as if the contamination were present in solid form. However, no technology is available to collect radioluminescence from alpha contaminated liquids for the simple reason that the spectrum of the radioluminescence, sometimes the existence of the phenomenon itself, was unknown. This, the unavailability of the spectral data, changed with the full resolved spectrum that has been shown in this Thesis.

Radioluminescence in water has been shown to occur as broadband emissions between 330 and 500 nm. This confirms what Duquesne in 1960 [25] had suspected and Yamamoto in 2016 [158] had observed: Alpha emitters immersed in water produce light blue and UV light. And they do so remarkably inefficiently. This Thesis and the work of Yamamoto estimate [158] the radioluminescence yield per alpha particle to be at least two orders of magnitudes less compared to this in air. This makes it principally detectable with single-photon counting devices, but the measurement of the spectrum is a whole different challenge. Much of the related parts of the Thesis and Publication III have been spent on discussing how to measure the spectrum. The radioluminescence has been shown not to be a form of Cerenkov radiation [60] and not a form of quartz glass scintillation either. Rather, its origins are speculated to be related to a form of light emission created by one of the intermediary and short-lived species that are being produced during water radiolysis [157]. However, at this point, there is no evidence that either supports or falsifies the hypothesis.

In concluding this Thesis and before moving on to the outlook, it is sensible to summarise all experiments in a brief and concise form. This is best done in the form of a table, which can be used for quick reference to access the relevant information of a given experiment. The table is presented in Tab. 6.1.

Table 6.1 List of all experiments presented in this Thesis. Radioactive samples that were prepared in solution are marked with an asterisk.

Experiment	Equipment	Sources	References
N_2 Spectrum	PMT, lenses, monochromator	32 MBq Am-241	Publ. I, Chap. 3.1
N_2 Imaging: Crime Scene	EMCCD, interference filters	10 MBq Am-241	Publ. I, Chap. 3.2
N_2 Imaging: Hot Cell	EMCCD, interference filters	unknown	Publ. I, Chap. 3.2
NO Spectrum	PMT, gases, monochromator	32 MBq Am-241	Publ. II, Chap. 4.1
Optimal NO Concentration	PMT, gases, monochromator	32 MBq Am-241	Publ. II, Chap. 4.3
NO Dynamics	PMT, gases, interference filters	32 MBq Am-241	Publ. IV, Chap. 4.3
NO Detection: Controlled Env.	ICCD, gases, solar blind filter	9.9 kBq Am-241	Chap. 4.4
NO Detection: Ambient Air	PMT, gases, interference filters	32 MBq Am-241	Publ. IV, Chap. 4.4
Liquid Spectrum	PMT, glove box, monochromator, liquid light guides	190 MBq Am-241*	Publ. III, Chap. 5.1
Liquid Imaging	EMCCD, glove box	190 MBq Am-241*	Publ. III, Chap. 5.2
Concentration Dependence	EMCCD, glove box	13 MBq Am-241* 19 MBq Am-241* 38 MBq Am-241* 190 MBq Am-241*	Publ. III, Chap. 5.2
HNO_3 Dependence	EMCCD, glove box	38 MBq Am-241*	Publ. III, Chap. 5.2

6.1 Outlook

The primary aim of this Thesis has been to study the radioluminescence of species that could help to overcome the problems that keep alpha imaging from being used in decommissioning tasks. The demonstration of NO radioluminescence has certainly shown that there are types of radioluminescence that can do that. Not only did it enhance UVC radioluminescence in a controlled gas environment, but it also succeeded in revealing alpha sources in ambient air via UVC light collection by using a N_2 flush. The potential for the application of NO radioluminescence by engineering of the gas atmosphere is apparent and the possibilities to further the studies abound. However, when deciding to do so, the allocation of the commonly limited resources for research makes it sensible to prioritise some fields of research over others. The ones that in the opinion of the author will likely be blessed with success are

- Search for a more suitable radioluminescent species
- Optimisation of the NO radioluminescence intensity
- Designing detection systems around NO radioluminescence

The reasoning to prioritise those fields of inquiry over others is explained point by point in the following.

Search for a more suitable radioluminescent species

The high intensity of the NO radioluminescence has been argued to be a result of the NO molecule's unique access to a storage of energy that is being held by the N_2 molecules. In this description, the N_2 molecules only appear as intermediaries that have the ability exchange their own electrons with those of slightly higher kinetic energy and thereby become excited. Those excitations are then passed on to the NO molecules. Even though an inherently correct description of the process, it slightly undervalues the role of the N_2 molecules. From what has been found in the literature review, N_2 is unique in its ability to gain energy from low-energy electrons by incorporating them into their own molecular makeup. An efficient electron exchange and a dipole-forbidden transition from the *A*- to the ground state make the N_2 molecules stable storages for the energy they gained in the exchange process. Better still, the peculiar nature of the self-quenching process, the energy-pooling, causes

the molecules to regain a large fraction of the excitations which they would otherwise lose. All those mechanisms conspire to create a reservoir of energy, ready to be harvested.

From this vantage point, it is perhaps easy to see that NO might not be the only species that can be made to exhibit intense radioluminescence. Safety-wise it is not an ideal species, to begin with. It is highly reactive, intoxicating personnel and corroding equipment alike. Application-wise it presents the challenge of keeping it isolated from oxygen and water vapour, as the presence of either one of those quenchers makes the emergence of the γ-band impossible and thus subverts the entire endeavour of creating UVC radioluminescence. Perhaps it might be possible to find a luminescent species that is less of a security concern and at the same time more robust against quenching of common atoms and molecules found in ambient air. Whatever this other species might be, it will have one characteristic in common with NO. It will be able to efficiently empty the energy reservoir. This insight significantly changes the search for a suitable species, as such a species is no longer required to efficiently interact with low-energy electrons themselves, an energy structure similar enough to this of the N_2 molecule will do. A suitable candidate just needs to convert excitations into UVC light and at the same time perhaps be a little bit less of a security concern.

Optimisation of the NO radioluminescence intensity

Whatever the difficulties in using NO radioluminescence might be, it has been demonstrated to work. It has been demonstrated to overcome both the sensitivity and the daylight problem at once. However, with the wisdom of the hindsight, it can be said that the demonstration in this Thesis did not properly take into account the role of water quenching. It was not much of an issue at the time and only became apparent when the levels of NO changed from a few ppm to a few ppb during the NO dynamics experiments. By what is now known, small amounts of water heavily quench the γ-band emissions and make the emergence of the β-band impossible [77]. Thus, it might be sensible to redo those studies and this time account for quenching by H_2O to truly gain a measure of what is possible with NO radioluminescence. It is to be suspected that the results will be even higher than what has been found in this Thesis. Proper elimination of this kind of quenching could enable the excitation

transfer from N_2 to NO on electronic states higher than the *A*-state. The processes are known to exist [145] and it might be the careful removal of water that enables the production of radioluminescence on different bands than γ and β.

The means to optimise NO radioluminescence production are not limited to the engineering of the gas atmosphere. The application of electric fields has been shown to increase the β-band emissions [77]. The mechanism by which this happens is not well understood, but is known, however, that it modifies the intensity with which UVC light is emitted. The extent to which this is useful or even applicable to the various use cases of alpha imaging is unknown. What is nonetheless apparent is that NO radioluminescence can be engineered to become even more intense than this Thesis demonstrated. It might not be too outlandish a hypothesis that one could concoct a carefully prepared mixture of NO, N_2 and perhaps other gases to enhance UVC radioluminescence, all the while outer circumstances like electric or magnetic fields are modified to convert a maximum of excitations into UVC radioluminescence. At least as a hypothesis, it seems feasible.

Designing detection systems around NO radioluminescence

Imaging alpha sources in daylight by using NO radioluminescence has been shown to work. The logical conclusion is to employ this technique in nuclear facilities in a scheme that tracks alpha sources without interfering with the normal workflow around the glove box. The design would be mostly an engineering effort and revolve around picking appropriate cameras, designing solar blind optics and mixing the gases. A glovebox could be filled with gas made of 500 ppb of NO diluted in N_2. This should be feasible, given that many gloveboxes used in nuclear facilities are filled with N_2 by default. Suitable cameras and optics have been shown to be available off-the-shelf [76], which further helps to implement the technique. In such a scenario, a camera would constantly track the position of alpha sources by following the movements of the clouds of UVC light that it would detect. It is likely that some software engineering might be required to evaluate the video stream in real-time. Perhaps this could rely on the image processing that has been presented in the works of Lamadie [28], Sand [32] and in Publication III.

It is perhaps not too bold a statement to make that NO amplification might bring the much-needed improvement to the technique of radioluminescence imaging to

finally be able to comply with government regulations. In Finland, where this Thesis has been written, the free waste limit is $0.1\,\mathrm{kBq\,kg^{-1}}$ [1] and thus defines the target figure for the sensitivity any radioluminescence detection system, that is to be used in nuclear decommissioning, must meet. The current N_2-based solar blind detection approach found its preliminary high point with a technology developed in Tampere, when Sand and colleagues constructed a scanner based on a caesium-telluride PMT and appropriate optical filters to find alpha active sources with activities as low as 800 kBq from 1 m distance in broad daylight [33]. The results laid out in this Thesis suggest that NO amplification can potentially improve the sensitivity to 80 Bq. With optimised optics tailored to NO radioluminescence and a better understanding of water quenching, the sensitivity might be much better than this. Whatever the real number turns out to be, the potential is clear. The radioluminescence scanner and NO amplification combine to an optical technology that comes close to remotely detecting alpha radiation such that government requirements are met.

REFERENCES

[1] Organisation for Economic Co-operation and Development. *Decommissioning Nuclear Power Plants: Policies, Strategies and Costs*. OECD Publishing, 2003.

[2] International Atomic Energy Agency. *Power Reactor Information System*. 2019. URL: https://pris.iaea.org/PRIS/home.aspx (visited on 05/10/2019).

[3] E. Neri, A. French, M. E. Urso, M. Deffrennes, G. Rothwell, I. Rehak, I. Weber, S. Carroll and V. Daniska. *Costs of Decommissioning Nuclear Power Plants*. Tech. rep. Organisation for Economic Co-Operation and Development, 2016.

[4] T. Inajima and Y. Okada. Nuclear Promotion Dropped in Japan Energy Policy After Fukushima. *Bloomberg* (2011).

[5] Babbage. Difference Engine: The nuke that might have been. *The Economist* (2013).

[6] J. Kanter. Switzerland Decides on Nuclear Phase-Out. *The New York Times* (2011).

[7] A. Breidthardt. German government wants nuclear exit by 2020 at latest. *Reuters* (2011).

[8] L. Wood. *Research and Markets: Nuclear Reactor Decommissioning Industry-Global Market Size and Competitive Landscape Analysis to 2030*. 2013.

[9] A. Neslen. Europe faces €253bn nuclear waste bill. *The Guardian* (2016).

[10] Ed Malley. *Coal Power Plant Post Retirement Options*. 2016. URL: https://www.powermag.com/coal-power-plant-post-retirement-options/?pagenum=2 (visited on 08/22/2019).

[11] D. C. Invernizzi, G. Locatelli and N. J. Brookes. How benchmarking can support the selection, planning and delivery of nuclear decommissioning projects. *Progress in Nuclear Energy* 99 (2017), 155–164.

[12] B. K. Sovacool. A critical evaluation of nuclear power and renewable electricity in Asia. *Journal of Contemporary Asia* 40 (2010), 369–400.

[13] Loviisan voimalaitos. *Fortum* (2017).

[14] L. Langlois. IAEA Action Plan on nuclear safety. *Energy Strategy Reviews* 1 (2013), 302–306.

[15] M. Laraia. Nuclear decommissioning. *Planning, Execution and International Experience* (2012).

[16] Hallinnonala: Kauppa- ja teollisuusministeriö. *Ydinenergialaki, Voimaantulo: 01.03.1988*. 1987.

[17] H. Geiger and J. Nuttall. LVII. The ranges of the α particles from various radioactive substances and a relation between range and period of transformation. *The London, Edinburgh, and Dublin Philosophical Magazine and Journal of Science* 22 (1911), 613–621.

[18] P. Peura, C. Bélanger-Champagne, T. Kerst, P. Eerola, P. Dendooven and J. Toivonen. The NINS3 Research Project. *Nuclear Science and Technology Symposium NST2016*. Finnish Nuclear Society. 2016.

[19] E. Rutherford and H. Geiger. An electrical method of counting the number of α-particles from radio-active substances. *Proceedings of the Royal Society of London. Series A, Containing Papers of a Mathematical and Physical Character* 81 (1908), 141–161.

[20] J. E. Martin. *Physics for radiation protection: a handbook*. John Wiley & Sons, 2006.

[21] International Atomic Energy Agency. *Am-241 source melting*. 2012. URL: `https://www-news.iaea.org/ErfView.aspx?mId=b32411e3-a847-443f-86d4-abb911059e97` (visited on 05/30/2019).

[22] F. Arqueros, F. Blanco and J. Rosado. Analysis of the fluorescence emission from atmospheric nitrogen by electron excitation, and its application to fluorescence telescopes. *New Journal of Physics* 11 (2009), 065011.

[23] G. F. Knoll. *Radiation detection and measurement*. John Wiley & Sons, 2010.

[24] S. M. Baschenko. Remote optical detection of alpha particle sources. *Journal of radiological protection* 24 (2004), 75.

[25] M. Duquesne and I. Kaplan. Mesure de la luminescence induite par le rayonnement α du 210Po dans l'air et dans l'eau. *Journal de Physique et le Radium* 21 (1960), 708–716.

[26] D. L. Chichester and S. M. Watson. Multispectral UV-visual imaging as a tool for locating and assessing ionizing radiation in air. *IEEE Transactions on Nuclear Science* 58 (2011), 2512–2518.

[27] J. Sand, S. Ihantola, K. Peräjärvi, H. Toivonen and J. Toivonen. Radioluminescence yield of alpha particles in air. *New Journal of Physics* 16 (2014), 053022.

[28] F. Lamadie, F. Delmas, C. Mahe, P. Girones, C. Le Goaller and J. Costes. Remote alpha imaging in nuclear installations: New results and prospects. *IEEE Transactions on Nuclear Science* 52 (2005), 3035–3039.

[29] O. P. Ivanov, V. E. Stepanov, S. V. Smirnov and A. G. Volkovich. Development of method for detection of alpha contamination with using UV-camera "DayCor" by OFIL. *2011 IEEE Nuclear Science Symposium Conference Record*. IEEE. 2011, 2192–2194.

[30] J. S. Feener and W. S. Charlton. Preliminary results of nuclear fluorescence imaging of alpha and beta emitting sources. *2013 3rd International Conference on Advancements in Nuclear Instrumentation, Measurement Methods and their Applications (ANIMMA)*. IEEE. 2013, 1–8.

[31] C. Mahé. Alpha imaging: recent achievements and glove box characterization. *Proccedings of DD&R* 10 (2010).

[32] J. Sand, S. Ihantola, K. Peräjärvi, A. Nicholl, E. Hrnecek, H. Toivonen and J. Toivonen. Imaging of alpha emitters in a field environment. *Nuclear Instruments and Methods in Physics Research Section A: Accelerators, Spectrometers, Detectors and Associated Equipment* 782 (2015), 13–19.

[33] J. Sand, A. Nicholl, E. Hrnecek, H. Toivonen, J. Toivonen and K. Peräjärvi. Stand-off radioluminescence mapping of alpha emitters under bright lighting. *IEEE Transactions on Nuclear Science* 63 (2016), 1777–1783.

[34] A. Crompton, K. Gamage, A. Jenkins and C. Taylor. Alpha particle detection using alpha-induced air radioluminescence: a review and future prospects for preliminary radiological characterisation for nuclear facilities decommissioning. *Sensors* 18 (2018), 1015.

[35] O. Ivanov, A. Danilovich, V. Stepanov, S. Smirnov and A. Volkovich. Visualization of Radioactive Sources without Gamma-Radiation with UV Imaging Systems. *ASME 2009 12th International Conference on Environmental Remediation and Radioactive Waste Management*. American Society of Mechanical Engineers. 2009, 321–325.

[36] Ofil Systems. *2019 Catalog - English Animated Catalog*. 2019.

[37] F. Arqueros, J. R. Hörandel and B. Keilhauer. Air fluorescence relevant for cosmic ray detection: Review of pioneering measurements. *Nuclear Instruments and Methods in Physics Research Section A: Accelerators, Spectrometers, Detectors and Associated Equipment* 597 (2008), 23–31.

[38] G. Choppin, J.-O. Liljenzin and J. Rydberg. *Radiochemistry and nuclear chemistry*. Butterworth-Heinemann, 2002.

[39] K. Kamiya, K. Ozasa, S. Akiba, O. Niwa, K. Kodama, N. Takamura, E. K. Zaharieva, Y. Kimura and R. Wakeford. Long-term effects of radiation exposure on health. *The lancet* 386 (2015), 469–478.

[40] N. N. Greenwood and A. Earnshaw. *Chemistry of the Elements*. Elsevier, 2012.

[41] JRC Karlsruhe. *Americium Am*. 2019. URL: `https://nucleonica.com/wiki/index.php?title=Americium_Am` (visited on 05/09/2019).

[42] International Atomic Energy Agency. *Live Chart of Nuclides*. 2019. URL: `https://www-nds.iaea.org/relnsd/vcharthtml/VChartHTML.html` (visited on 05/09/2019).

[43] H. Sicius. *Radioaktive Elemente: Actinoide: Eine Reise durch das Periodensystem*. Springer-Verlag, 2015.

[44] J. McInroy, R. Kathren and M. Swint. Distribution of plutonium and americium in whole bodies donated to the United States Transuranium Registry. *Radiation Protection Dosimetry* 26 (1989), 151–158.

[45] W. Demtröder. *Kern-, Teilchen-und Astrophysik.(Experimentalphysik 4)*. 2005.

[46] K. Fajans. Radioactive transformations and the periodic system of the elements. *Berichte der Deutschen Chemischen Gesellschaft* 46 (1913), 422–439.

[47] M. G. Stabin. *Radiation protection and dosimetry: an introduction to health physics*. Springer Science & Business Media, 2007.

[48] Mirion Technologies. *Types of Ionizing Radiation*. 2019.

[49] G. Marr and S. Wherrett. The ionization of caesium vapour by the method of space charge amplification. *Journal of Physics B: Atomic and Molecular Physics* 5 (1972), 1735.

[50] W. Tobiska and A. Nusinov. ISO 21348-Process for determining solar irradiances. *36th COSPAR Scientific Assembly*. Vol. 36. 2006.

[51] J. M. Hollas. *Modern spectroscopy*. John Wiley & Sons, 2004.

[52] E. Fields, R. F. Cleveland and J. L. Ulcek. Questions and answers about biological effects and potential hazards of radiofrequency electromagnetic fields. *Oet Bulletin*. Citeseer. 1999.

[53] H. B. Stone, C. N. Coleman, M. S. Anscher and W. H. McBride. Effects of radiation on normal tissue: consequences and mechanisms. *The lancet oncology* 4 (2003), 529–536.

[54] K. Vij. *Textbook of forensic medicine and toxicology: principles and practice, 5/e*. Elsevier India, 2011.

[55] A. B. Chilton, J. K. Shultis and R. E. Faw. Principles of radiation shielding. (1984).

[56] J. K. Shultis, R. E. Faw and K. R. Kase. *Radiation shielding*. Prentice Hall PTR Upper Saddle River, New Jersey, 1996.

[57] M. F. Kaplan. Concrete radiation shielding. (1989).

[58] Custom Neutron Radiation Shielding. *Frontier Technology Corporation* (2019).

[59] Kansas State University. *TRIGA II Cerenkov*. 2019. URL: `https://www.mne.k-state.edu/research/reactor/` (visited on 05/10/2019).

[60] P. A. Cherenkov. Visible emission of clean liquids by action of γ radiation. *Doklady Akademii Nauk SSSR* 2 (1934), 451.

[61] J. V. Jelley. Cherenkov radiation and its applications. (1958).

[62] G. M. Hale and M. R. Querry. Optical constants of water in the 200 nm to 200 μm wavelength region. *Applied optics* 12 (1973), 555–563.

[63] H. A. Bethe. Passage of radiations through matter. *Experimental nuclear physics* (1953).

[64] E. Rutherford. The scattering of α and β particles by matter and the structure of the atom. *Philosophical Magazine* 92 (2012), 379–398.

[65] H. Geiger and E. Marsden. On a diffuse reflection of the α-particles. *Proceedings of the Royal Society of London. Series A, Containing Papers of a Mathematical and Physical Character* 82 (1909), 495–500.

[66] M. J. Berger, J. Coursey, M. Zucker, J. Chang et al. *Stopping-power and range tables for electrons, protons, and helium ions*. NIST Physics Laboratory Gaithersburg, MD, 1998.

[67] P. Olive. DNA damage and repair in individual cells: applications of the comet assay in radiobiology. *International journal of radiation biology* 75 (1999), 395–405.

[68] F. Ullmann, W. Gerhartz, Y. S. Yamamoto, F. T. Campbell, R. Pfefferkorn, J. F. Rounsaville et al. *Ullmann's encyclopedia of industrial chemistry*. VCH publishers, 1985.

[69] J. D. Spengler and K. Sexton. Indoor air pollution: a public health perspective. *Science* 221 (1983), 9–17.

[70] Environmental Protection Agency. The National Radion Action Plan: A strategy for saving lifes. *EPA 402/R-15/001* (2019).

[71] E. B. Podgorsak. Review of radiation oncology physics: a handbook for teachers and students. *Vienna, International Atomic Energy Agency. Educational reports series* (2003).

[72] F. Arqueros, J. R. Hörandel and B. Keilhauer. Air fluorescence relevant for cosmic ray detection: Summary of the 5th fluorescence workshop, El Escorial 2007. *Nuclear Instruments and Methods in Physics Research Section A: Accelerators, Spectrometers, Detectors and Associated Equipment* 597 (2008), 1–22.

[73] M. Ave, M. Bohacova, B. Buonomo, N. Busca, L. Cazon, S. Chemerisov, M. Conde, R. Crowell, P. Di Carlo, C. Di Giulio et al. Measurement of the pressure dependence of air fluorescence emission induced by electrons. *Astroparticle physics* 28 (2007), 41–57.

[74] F. Blanco and F. Arqueros. The role of secondary electrons in some experiments determining fluorescence emission from nitrogen $C^3\Pi_u$ levels. *Physics Letters A* 345 (2005), 355–361.

[75] J. Garcia-Guinea, V. Correcher, M. Lombardero and R. Gonzalez-Martin. Study of the ultraviolet emission of the electrode coatings of arc welding. *International journal of environmental health research* 14 (2004), 285–294.

[76] J. Sand. Alpha Radiation Detection via Radioluminescence of Air. PhD thesis. Tampere University of Technology: Tampere University of Technology, July 2016.

[77] S. Dondes, P. Harteck and C. Kunz. A spectroscopic study of alpha ray induced luminescence in gases: part I. *Radiation Research* 27 (1966), 174–210.

[78] A. Crompton, K. Gamage, S. Bell, A. Wilson, A. Jenkins and D. Trivedi. Gas Flow to Enhance the Detection of Alpha-Induced Air Radioluminescence Based on a UVTron Flame Sensor. *Sensors* 18 (2018), 1842.

[79] A. S. for Testing, M. C. G. on Weathering and Durability. *Standard tables for reference solar spectral irradiances: direct normal and hemispherical on* 37° *tilted surface*. ASTM international, 2003.

[80] R. W. Engstrom. Multiplier photo-tube characteristics: Application to low light levels. *JOSA* 37 (1947), 420–431.

[81] D. R. Williams. *Earth Fact sheet*. 2019. URL: `https://nssdc.gsfc.nasa.gov/planetary/factsheet/earthfact.html` (visited on 05/13/2019).

[82] T. Waldenmaier, J. Bluemer and H. Klages. Spectral resolved measurement of the nitrogen fluorescence emissions in air induced by electrons. *Astroparticle Physics* 29 (2008), 205–222.

[83] M. Born and R. Oppenheimer. Zur Quantentheorie der Moleküle. *Annalen der physik* 389 (1927), 457–484.

[84] A. Lofthus and P. H. Krupenie. The spectrum of molecular nitrogen. *Journal of physical and chemical reference Data* 6 (1977), 113–307.

[85] P. M. Morse. Diatomic molecules according to the wave mechanics. II. Vibrational levels. *Physical Review* 34 (1929), 57.

[86] A. D. S. Mesa, C. Quesne and Y. F. Smirnov. Generalized Morse potential: symmetry and satellite potentials. *Journal of Physics A: Mathematical and General* 31 (1998), 321.

[87] J. H. Moore Jr. Investigation of the Wigner spin rule in collisions of N^+ with He, Ne, Ar, N_2, and O_2. *Physical Review A* 8 (1973), 2359.

[88] A. N. Bunner. *Cosmic ray detection by atmospheric fluorescence*. Tech. rep. 1967.

[89] M. Fraga, L. Pereira, N. Castro, F. Veloso, F. Fraga, R. F. Marques, M. Pimenta and A. Policarpo. Temperature-dependent quenching of UV fluorescence of N_2. *Nuclear Instruments and Methods in Physics Research Section A: Accelerators, Spectrometers, Detectors and Associated Equipment* 597 (2008), 75–82.

[90] M. Zubek. Excitation of the $C^3\Pi_u$ state of N_2 by electron impact in the near-threshold region. *Journal of Physics B: Atomic, Molecular and Optical Physics* 27 (1994), 573.

[91] J. T. Fons, R. S. Schappe and C. C. Lin. Electron-impact excitation of the second positive band system ($C^3\Pi_u \rightarrow B^3\Pi_g$) and the $C^3\Pi_u$ electronic state of the nitrogen molecule. *Physical Review A* 53 (1996), 2239.

[92] G. Poparić, M. Vićić and D. Belić. Vibrational excitation of the $C^3\Pi_u$ state of N_2 by electron impact. *Chemical physics* 240 (1999), 283–289.

[93] Y. Itikawa. Cross sections for electron collisions with nitrogen molecules. *Journal of physical and chemical reference data* 35 (2006), 31–53.

[94] National Institute for Standards and Technology. *CODATA Value: bohr radius*. 2019. URL: `https://physics.nist.gov/cgi-bin/cuu/Value?bohrrada0` (visited on 05/22/2019).

[95] S. Chung and C. C. Lin. Excitation of the electronic states of the nitrogen molecule by electron impact. *Physical Review A* 6 (1972), 988.

[96] All Datasheets. *PerkinElmer Optoelectronics - MD1982 Datasheet*. 2019. URL: `https://www.alldatasheet.com/datasheet-pdf/pdf/14940/PERKINELMER/MD1982.html` (visited on 05/26/2019).

[97] Horiba Scientific. *IHR 550 Manual*. 2011.

[98] Thorlabs. *UV Coated Lens Transmittance*. 2019. URL: `https://www.thorlabs.com/newgrouppage9.cfm?objectgroup_id=3569&pn=LA4924-UV#3573` (visited on 08/26/2019).

[99] G. Hartmann and P. Johnson. Measurements of relative transition probabilities and the variation of the electronic transition moment for N_2 $C^3\Pi_u \rightarrow B^3\Pi_g$ second positive system. *Journal of Physics B: Atomic and Molecular Physics* 11 (1978), 1597.

[100] J.-F. Pineau and G. Imbard. *Remote αsource location device and method*. US Patent 6,281,502. Aug. 2001.

[101] C. Mahe, F. Lamadie and C. Le Goaller. Recent advances in low-level nuclear measurements at the CEA. (2009).

[102] C. Mahé and C. Chabal. Recent improvement of measurement instrumentation to supervise nuclear operations and to contribute input data to 3D simulation code. *Waste Management Conference, Phoenix, Arizona, USA*. 2013.

[103] T. Cousins and D. Haslip. Stand and deliver. *CBRNe World* (2006), 56–59.

[104] E. Inrig, V. Koslowsky, B. Andrews, M. Dick, P. Forget, H. Ing, R. Hugron and L. Wong. Development and testing of an air fluorescence imaging system for the detection of radiological contamination. *AIP Conference Proceedings*. Vol. 1412. AIP. 2011, 393–400.

[105] D. Chichester, S. Pozzi, E. Seabury, J. Dolan, M. Flaska, J. Johnson, S. Watson and J. Wharton. *FY09 Advanced instrumentation and active interrogation research for safeguards*. Tech. rep. Idaho National Laboratory (INL), 2009.

[106] J. S. Feener. Fluorescence Imaging for Nuclear Arms Control Verification. PhD thesis. 2014.

[107] J. Sand, S. Ihantola, K. Peräjärvi, H. Toivonen, A. Nicholl, E. Hrnecek and J. Toivonen. EMCCD imaging of strongly ionizing radioactive materials for safety and security. *International Quantum Electronics Conference*. Optical Society of America. 2013, JSII_P_1.

[108] European Nuclear Society. *Hot cell*. 2019. URL: `https://www.euronuclear.org/info/encyclopedia/h/hotcell.htm` (visited on 05/16/2019).

[109] J. S. STROUD and E. LELL. Optical absorption of lead in glass. *Journal of the American Ceramic Society* 54 (1971), 554–555.

[110] P. Limkitjaroenporn, J. Kaewkhao, P. Limsuwan and W. Chewpraditkul. Physical, optical, structural and gamma-ray shielding properties of lead sodium borate glasses. *Journal of Physics and Chemistry of Solids* 72.4 (2011), 245–251.

[111] H. A. Macleod and H. A. Macleod. *Thin-film optical filters*. CRC press, 2010.

[112] L. Elterman. *UV, visible, and IR attenuation for altitudes to 50 km, 1968*. Tech. rep. AIR FORCE CAMBRIDGE RESEARCH LABS HANSCOM AFB MA, 1968.

[113] J. Yao, J. Brenizer, R. Hui and S. Yin. Standoff alpha radiation detection via excited state absorption of air. *Applied Physics Letters* 102 (2013), 254101.

[114] S. Dondes, P. Harteck and C. Kunz. Production of the Oxygen 5577 Å Emission by Polonium-210 Alpha Radiation. *Zeitschrift für Natur-forschung A* 19 (1964), 6–12.

[115] A. Birot, H. Brunet, J. Galy, P. Millet and J. Teyssier. Continuous emissions of argon and krypton in the near ultraviolet. *The Journal of Chemical Physics* 63 (1975), 1469–1473.

[116] J. Brett, K. E. Koehler, M. Bischak, M. Famiano, J. Jenkins, L. Klankowski, P. Niraula, P. Pancella and R. Lakis. Spectral measurements of alpha-induced radioluminescence in various gases. *Nuclear Instruments and Methods in Physics Research Section A: Accelerators, Spectrometers, Detectors and Associated Equipment* 874 (2017), 88–93.

[117] T. Strickler and E. Arakawa. Optical emission from argon excited by alpha particles: Quenching studies. *The Journal of Chemical Physics* 41 (1964), 1783–1789.

[118] M. Tamura, P. A. Berg, J. E. Harrington, J. Luque, J. B. Jeffries, G. P. Smith and D. R. Crosley. Collisional quenching of CH (A), OH (A), and NO (A) in low pressure hydrocarbon flames. *Combustion and Flame* 114 (1998), 502–514.

[119] T. B. Settersten, B. D. Patterson and J. A. Gray. Temperature- and species-dependent quenching of NO $A^2\Sigma^+ (v' = 0)$ probed by two-photon laser induced fluorescence using a picosecond laser. *The Journal of chemical physics* 124 (2006), 234308.

[120] F. R. Gilmore, R. R. Laher and P. J. Espy. Franck–Condon factors, r-centroids, electronic transition moments, and Einstein coefficients for many nitrogen and oxygen band systems. *Journal of physical and chemical reference data* 21 (1992), 1005–1107.

[121] M. M. Osterhout. *Decontamination and decommissioning of nuclear facilities*. Springer Science & Business Media, 2012.

[122] P. Bachelor, D. Jordan, W. Harper, B. Cannon and E. Finn. Self-absorption effects on alpha-induced atmospheric nitrogen fluorescence yield. *Journal of radioanalytical and nuclear chemistry* 282 (2009), 873–876.

[123] K. Saito, H. Tawara, T. Sanami, E. Shibamura and S. Sasaki. Absolute number of scintillation photons emitted by alpha particles in rare gases. *IEEE Transactions on Nuclear Science* 49 (2002), 1674–1680.

[124] H. Morii, K. Mizouchi, T. Nomura, N. Sasao, T. Sumida, M. Kobayashi, Y. Murayama and R. Takashima. Quenching effects in nitrogen gas scintillation. *Nuclear Instruments and Methods in Physics Research Section A: Accelerators, Spectrometers, Detectors and Associated Equipment* 526 (2004), 399–408.

[125] J. Danielak, U. Domin, R. Ke, M. Rytel and M. Zachwieja. Reinvestigation of the Emission γ Band System ($A^2\Sigma^+ \rightarrow X^2\Pi$) of the NO Molecule. *Journal of Molecular Spectroscopy* 181 (1997), 394–402.

[126] P. Boyer. *By the bomb's early light: American thought and culture at the dawn of the atomic age*. Univ of North Carolina Press, 2005.

[127] Purity Gas. *Nitrogen Gas Applications*. 2019.

[128] T. Kerst and J. Toivonen. Alpha Radiation Induced Luminescence in Solar Blind Spectral Region. *CLEO: Applications and Technology*. Optical Society of America. 2018, ATh4O–8.

[129] G. Reiser, W. Habenicht, K. Müller-Dethlefs and E. W. Schlag. The ionization energy of nitric oxide. *Chemical physics letters* 152 (1988), 119–123.

[130] M. V. Beligni and L. Lamattina. Is nitric oxide toxic or protective?: *Trends in plant science* 4 (1999), 299–300.

[131] Y. Li and W. K. Hall. Catalytic decomposition of nitric oxide over Cu-zeolites. *Journal of Catalysis* 129 (1991), 202–215.

[132] J. Greaves and D. Garvin. Chemically Induced Molecular Excitation: Excitation Spectrum of the Nitric Oxide-Ozone System. *The Journal of Chemical Physics* 30 (1959), 348–349.

[133] A. Fontijn, A. J. Sabadell and R. J. Ronco. Homogeneous chemiluminescent measurement of nitric oxide with ozone. Implications for continuous selective monitoring of gaseous air pollutants. *Analytical chemistry* 42 (1970), 575–579.

[134] F. R. Gilmore. *Potential energy curves for* N_2, NO, O_2, *and corresponding ions*. Tech. rep. Rand Corp Santa Monica, CA, 1966.

[135] R. Gillette and E. H. Eyster. The fundamental rotation-vibration band of nitric oxide. *Physical review* 56 (1939), 1113.

[136] G. W. Bethke. Oscillator strengths in the far ultraviolet. I. Nitric oxide. *The Journal of Chemical Physics* 31 (1959), 662–668.

[137] J. I. Generosa and R. A. Harris. Effects of High Rotational Quantum Numbers on Rydberg–Klein–Rees Franck–Condon Factors: The Nitric Oxide (NO) Beta Band System. *The Journal of Chemical Physics* 53 (1970), 3147–3152.

[138] G. W. Robinson and R. Frosch. Electronic excitation transfer and relaxation. *The Journal of Chemical Physics* 38 (1963), 1187–1203.

[139] R. Schappe, R. Edgell and E. Urban. Electron-impact excitation of nitric oxide ($A^2\Sigma^+$ - $X^2\Pi$). *Physical Review A* 65 (2002), 042701.

[140] M. J. Brunger, L. Campbell, D. Cartwright, A. Middleton, B. Mojarrabi and P. Teubner. Electron-impact excitation of Rydberg and valence electronic states of nitric oxide: II. Integral cross sections. *Journal of Physics B: Atomic, Molecular and Optical Physics* 33 (2000), 809.

[141] L. Melton and W. Klemperer. Energy transfer in monochromatically excited nitric oxide: $A^2\Sigma^+$ and $B^2\Pi$. *The Journal of Chemical Physics* 59 (1973), 1099–1115.

[142] J. McNeely, G. Hurst, E. Wagner and M. Payne. Energy transfer from argon resonance states to nitrogen, hydrogen, and nitric oxide. *The Journal of Chemical Physics* 63 (1975), 2717–2723.

[143] L. G. Piper, L. M. Cowles and W. T. Rawlins. State-to-state excitation of NO ($A^2\Sigma^+(v'=0,1,2)$) by N_2 ($A^3\Sigma_u^+(v'=0,1,2)$. *The Journal of chemical physics* 85 (1986), 3369–3378.

[144] L. G. Piper. State-to-state $N_2(A^3\Sigma_u^+)$ energy pooling reactions. II. The formation and quenching of $N_2(B^3\Pi_g\, v'=1—12)$. *The Journal of chemical physics* 88 (1988), 6911–6921.

[145] W. Clark and D. Setser. Energy transfer reactions of N_2 ($A^3\Sigma_u^+$). 5. Quenching by hydrogen halides, methyl halides, and other molecules. *The Journal of Physical Chemistry* 84 (1980), 2225–2233.

[146] W. Rawlins, M. Fraser and S. Miller. Rovibrational excitation of nitric oxide in the reaction of oxygen with metastable atomic nitrogen. *The Journal of Physical Chemistry* 93 (1989), 1097–1107.

[147] J. Brzozowski, N. Elander and P. Erman. Direct measurements of lifetimes of low-lying excited electronic states in nitric oxide. *Physica Scripta* 9 (1974), 99.

[148] J. Luque and D. R. Crosley. Transition probabilities and electronic transition moments of the $A^2\Sigma^+ \rightarrow X^2\Pi$ and $D^2\Sigma^+ \rightarrow X^2\Pi$ systems of nitric oxide. *The Journal of chemical physics* 111 (1999), 7405–7415.

[149] B. R. Munson, T. H. Okiishi, W. W. Huebsch and A. P. Rothmayer. *Fluid mechanics*. Wiley Singapore, 2013.

[150] Y.-c. Fung. *Biomechanics: circulation*. Springer Science & Business Media, 2013.

[151] Andor. *iStar 320 T Manual*. 2019.

[152] C. Arroyave and M. Morcillo. The effect of nitrogen oxides in atmospheric corrosion of metals. *Corrosion Science* 37 (1995), 293–305.

[153] IPCS Inchem. *Nitric Oxide Material Safety Data Sheet*. 2015. URL: `http://www.inchem.org/documents/icsc/icsc/eics1311.htm` (visited on 08/23/2019).

[154] Hamamatsu Photonics KK. *Photon Counting Head H11870 Series*. 2018.

[155] Semrock. *2016/16 Brightline single-band bandpass filter*. 2019.

[156] S. Kharitonov, D. Yates, R. Robbins, P. Barnes, R. Logan-Sinclair and E. Shinebourne. Increased nitric oxide in exhaled air of asthmatic patients. *The Lancet* 343 (1994), 133–135.

[157] M. S. Matheson. The formation and detection of intermediates in water radiolysis. *Radiation Research Supplement* 4 (1964), 1–23.

[158] S. Yamamoto, M. Komori, S. Koyama and T. Toshito. Luminescence imaging of water during alpha particle irradiation. *Nuclear Instruments and Methods in Physics Research Section A: Accelerators, Spectrometers, Detectors and Associated Equipment* 819 (2016), 6–13.

[159] S. Yamamoto, T. Akagi, T. Yamashita, J. Toivonen, M. Yamaguchi, M. Komori and N. Kawachi. Source of luminescence of water lower energy than the Cerenkov-light threshold during irradiation of carbon-ion. *Journal of Physics Communications* 2 (2018), 065010.

[160] Lumatec. *Liquid Lightguide Manual*. 2019.

[161] Hellma Analytics. *Optische Komponenten für UV/VIS/NIR Spektroskopie*. 2018.

[162] O. B. Egorov, R. S. Addleman, M. J. O'Hara, T. Marks and J. W. Grate. Direct measurement of alpha emitters in liquids using passivated ion implanted planar silicon (PIPS) diode detectors. *Nuclear Instruments and Methods in Physics Research Section A: Accelerators, Spectrometers, Detectors and Associated Equipment* 537 (2005), 600–609.

[163] D. J. Segelstein. The complex refractive index of water. PhD thesis. University of Missouri–Kansas City, 1981.

[164] J. D. Jackson. *Classical electrodynamics*. 1999.

[165] National Institute for Standards and Technology. *CODATA Value: finestructure constant*. 2019. URL: `https://physics.nist.gov/cgi-bin/cuu/Value?alph%7Csearch_for=fine+structure` (visited on 05/28/2019).

[166] N. Ackerman and E. Graves. The potential for Cerenkov luminescence imaging of alpha-emitting radionuclides. *Physics in Medicine & Biology* 57.3 (2012), 771.

[167] Z. Francis, S. Incerti, M. Karamitros, H. Tran and C. Villagrasa. Stopping power and ranges of electrons, protons and alpha particles in liquid water using the Geant4-DNA package. *Nuclear Instruments and Methods in Physics Research Section B: Beam Interactions with Materials and Atoms* 269 (2011), 2307–2311.

[168] Plexigla by Arkema. *Acryl-Resins: Optical and Weaterhing Properties*. 2019.

[169] Sico GmbH & Co. KG. *SQ1, SQ2: Transmissionskurve*. 2019.

[170] H. Christensen and S. Sunder. Current state of knowledge of water radiolysis effects on spent nuclear fuel corrosion. *Nuclear Technology* 131 (2000), 102–123.

[171] Oak Ridge National Laboratory. Graphite Reactor. (2013).

[172] J. Fleming. A technique for the absolute measurement of activity using a gamma camera and computer. *Physics in Medicine & Biology* 24 (1979), 176.

PUBLICATIONS

PUBLICATION

I

Standoff Alpha Radiation Detection for Hot Cell Imaging and Crime Scene Investigation

T. Kerst, J. Sand, S. Ihantola, K. Peräjärvi, A. Nicholl, E. Hrnecek, H. Toivonen and J. Toivonen

Optical Review 25.(2018), 429–436

Standoff alpha radiation detection for hot cell imaging and crime scene investigation

Thomas Kerst[1,2], Johan Sand[1], Sakari Ihantola[3], Kari Peräjärvi[3], Adrian Nicholl[4], Erich Hrnecek[4], Harri Toivonen[3], Juha Toivonen[1]

1 Laboratory of Photonics, Tampere University of Technology, Korkeakoulunkatu 3, 33720 Tampere, Finland

2 Helsinki Institute of Physics, Gustaf Hällströmin katu 2, 00014 Helsinki, Finland

3 STUK – Radiation and Nuclear Safety Authority, Laippatie 4, 00880 Helsinki, Finland

4 European Commission, Joint Research Centre (JRC), Directorate G – Nuclear Safety & Security, Nuclear Safeguard and Forensics, P.O. Box 2340, 76125 Karlsruhe, Germany

Phone: +358 50 300 5968

Email: thomas.kerst@tut.fi

Abstract: This paper presents the remote detection of alpha contamination in a nuclear facility. Alpha-active material in a shielded nuclear radiation containment chamber has been localized by optical means. Further, sources of radiation danger have been identified in a staged crime scene setting. For this purpose, an electron-multiplying charge-coupled device camera was used to capture photons generated by alpha-induced air scintillation (radioluminescence). The detected radioluminescence was superimposed with a regular photograph to reveal the origin of the light and thereby the alpha radioactive material. The experimental results show that standoff detection of alpha contamination is a viable tool in radiation threat detection. Further, the radioluminescence spectrum in air is spectrally analyzed. Possibilities of camera-based alpha threat detection under various background lighting conditions are discussed.

keywords: radioluminescence, remote detection, alpha radiation, solar blind

1 Introduction

Standoff detection of alpha contamination for nuclear safety, security and safeguard has proven to be a challenging task. Compared to beta and gamma radiation, alpha particles have a very short range in air (roughly 4 cm), effectively

limiting the detection range of techniques depending on direct interaction. This range limitation can be overcome by utilizing the radioluminescent light that alpha particles induce in air. Radioluminescence has been first discovered in 1905 [1], yet it took more than a century before advances in technology made it possible to utilize it as a means to detect alpha contamination [2, 3, 4, 5, 6]. In principal, detection of radioluminescence is a technique well-suited to optically detect all ionizing radiation. However, it is particularly useful for alpha particles given the limitations on measurement by direct interaction. Standoff alpha detection technology responds to an increasing demand in the field, e.g. in detection of radioactive materials at crime scenes and decommissioning of nuclear facilities [7].

Radioluminescence in air is created when highly energetic, charged particles traveling through air cause the creation of secondary free electrons. Those electrons lose energy by inelastic collisions with air molecules. A small fraction of the deposited energy is reemitted as luminescence, while most of it disperses as heat due to collisional quenching processes [8, 9].

Air luminescence, for the most part, originates from N_2 and N_2^+ molecules, which emit light in the spectral range of $280 - 430$ nm. Measurements that quantify the number of photons that a single alpha particle induces are sparse. While Duquesne and Kaplan [10] found a value of 60 photons per one 4.6 MeV particle, Baschenko [3] concluded that a single alpha particle produces 30 UV photons. In a study from 2011, it has been concluded by Chichester and Watson [5] that the photon yield per $4 - 5$ MeV is somewhere between 20 and 200. Recent investigation from Sand et al. [11] found that an alpha particle with an energy that falls within the range of $0.3 - 5.1$ MeV produces an amount of UV photons that is described by the linear relation 19 ± 3 photons per one MeV of energy released under typical indoor conditions.

These studies show that the light yield of even strong alpha sources with high activities is so low that remote optical detection of alpha contamination has to happen at the single photon level. Often, the actual usable amount of light from air

radioluminescence is a fraction of all the light produced, considering that for standoff detection at a distance r from the source the intensity of the radioluminescence drops by a factor r^{-2}. Given these circumstances, it is easy to see that background lighting containing UV light easily supersedes the amount of light from the alpha source and thus potentially makes alpha contamination localization by means of a UV light detection difficult.

The presence of an alpha particle source causes the surrounding air to scintillate. Hence, an image taken in total darkness will reveal point emitters as small scintillating hemispheres, whereas surface activity will appear as a more evenly illumination on the image. For this reason, alpha contamination in an environment, which can be made completely dark, is detectable by superimposing a conventional image taken under normal lighting conditions and another UV image taken in complete darkness [4]. The conventional image provides information relating image coordinate to the location of physical objects whereas the UV image provides information about the contamination as a function of the image coordinates. The intensities recorded on the UV image are proportional to the alpha activities at the specified location [11]. Accurate quantitative measurements require exact knowledge of the background lighting level, and thus, the method is only well suited for a situation where the background lighting levels are sufficiently low.

The idea of directly imaging radioluminescence has been around since the early 2000s [2]. Significant advancements in camera technology and rigorous development of the technique made radioluminescence imaging a viable approach to alpha radiation detection and finally led to successful applications in nuclear facilities, the characterization of glove boxes and nuclear safeguards [2, 3, 4, 13, 14]. A study carried out in 2015 conducted a side-by-side comparison of two of the most promising camera technologies in a field environment [12]. There the authors successfully demonstrated that existing camera technology is up to the task of rapidly imaging and localizing alpha emitters at a nuclear facility. As long as a dark environment is ensured, off-the-shelf intensified charge-coupled device

(ICCD) and electron-multiplying charge-coupled device (EMCCD) cameras proved to be a way to remotely detect alpha contamination.

This work presents the measurement of the air radioluminescence spectrum and the imaging of alpha particle emitters by virtue of the radioluminescence they induce in air. The spectrum is measured with a resolution of 0.5 nm. Alpha imaging is applied to detect contamination in a staged crime scene scenario. Thereby we demonstrate that standoff detection of radioluminescence is able to rapidly localize hazardous alpha radiation in a potentially dangerous environment without the need of entering the scene itself. Further, we apply a similar principle to locate sources in a shielded nuclear radiation containment chamber (hot cell). The hot cell contains various objects with unknown, yet high, ionizing radiation levels and we show that the alpha radiating ones can be identified by collecting air and potentially other radioluminescence through a lead glass window that commonly serves as a viewport into the cell. Thereby we demonstrate that standoff detection of radioluminescence is able to operate in such a way that the confinement of the hot cell does not need to be accessed, thus saving costs and time.

All radioluminescence images presented in this work were captured during two measurement campaigns at the JRC-Karlsruhe, Germany. Complete darkness could not always be assured, since background lighting from warning- and exit signs could not be avoided. In addition, radioluminescence imaging under different background lighting conditions and the requirements for detection systems resulting form it are discussed.

2 Experiments

2.1 Spectrum of radioluminescence in air

The measurement of the radioluminescence spectrum in air was carried out by placing a 13 MBq alpha active ^{241}Am in a quartz tube (Robson scientific, outer diameter = 30 mm, wall thickness = 1.5 mm) which has access to open air. The parts of the tube close to the source were surrounded by a 21 mm thick steel

mantle intended to protect personnel and equipment from gamma radiation. A cone-shaped hole with the f-number $f/1.378$ in the steel mantle allowed radioluminescent light to be collected. The light was guided via a Keplerian telescope (Thorlabs LA4052-UV, $f = 35.0$ mm and LA4924-UV, $f = 175.0$ mm) to a computer-controlled monochromator (Horiba iHR 550). The telescope was matched to both f-numbers of the steel mantle opening and the input of the monochromator to guarantee optimal light collection efficiency. The focus of the imaging optics is located at the center of the quartz tube, which makes scintillation light from the quartz glass tube, if it arises, unlikely to enter the monochromator. The monochromator selected a wavelength and guided it to a photon counting photomultiplier tube (PMT, Perkin-Elmer MP-1982). A schematic illustration of the setup is shown in Fig. 1. The entrance slit of the monochromator was adjusted such that it operates with a spectral resolution of 0.5 nm. It was scanned in 0.5 nm steps from 200.0 nm to 500.0 nm. The integration time per data point in the so recorded spectrum was 60 s. Each data point has been corrected for the PMT's dark count.

2.2 Imaging of crime scene scenario and nuclear hot cell

Camera technology

The camera selected for the both the crime scene investigation and the localization of hidden sources was an EMCCD camera (iXon X3 897 with UV coating from Andor). The quantum efficiency of the EMCCD is over 30 % at the whole wavelength range from 250 nm to 450 nm [12]. The noise contribution of the dark current was minimized by cooling the EMCCD sensor to -85°C. The laboratory in which the EMCCD camera was operated was at room temperature. The camera was operated with an UV quartz objective lens (UV1228CM, Kogaku) that has a focal length of 12 mm, an f-number of f/2.8, and transmission over 75 % at the spectral band of 250 nm - 450 nm [15]. By placing an interference-filter (FF01-334/40-25, Semrock) with a single, narrow transmission band around 334 nm in front of the objective lens the influence of hard-to-avoid stray light from surrounding fluorescent light sources was mitigated.

Experiment preparation

A crime scene scenario was staged by placing two ^{241}Am sources (35.9 ± 0.9 MBq and 12.8 ± 0.3 MBq) under a fume hood among typical laboratory equipment. The ^{241}Am sources were prepared by evaporation of ^{241}Am solution on stainless steel planchettes that were then placed into quartz petri dishes among the other objects in the setting. The laboratory containing the crime scene was made completely dark by turning off any fluorescent light generation and by preventing any light from entering the laboratory. Given the expectedly small radioluminescence signal, a thorough approach to the light shielding required to seal the door cracks to prevent even small amounts of light from leaking through. A schematic illustration of the scenario is shown in Fig. 2.

The EMCCD camera was further used for the purpose of detecting alpha contamination in a hot cell. The hot cell was separated from the rest of laboratory and only a thick lead windows allowed to view the insides of the containment chamber. The hot cell was believed to contain a mix of various types of ionizing radiation, where the precise location and strength of alpha radiating material was unknown. It was known, though, that alpha contamination was present in significant levels. The contents of the hot cell were imaged with the camera through the lead glass, which allows for remote alpha radiation detection without breaching the confinement of the hot cell [4, 19].

Glasses containing lead usually absorb ultraviolet light [20]. Though the precise transmittance for each lead glass window varies with material and thickness, we consider it safe to assume that most of the radioluminescent light with wavelengths shorter than about 400 nm will be strongly attenuated by the lead glass window. Thus, only a small fraction of the radioluminescence of air can reach the EMCCD camera. Scintillation other than this of nitrogen, if it arises, can also be used for the detection of radioluminescence, provided that is able to pass the lead glass window. We removed the interference filter from the camera to collect also the long wavelength part of the radioluminescence spectrum of air (390 nm – 440 nm) and all other possible scintillation light originating from inside the hot cell.

The camera was shielded from light originating from within the laboratory using black rubberized fabric (Thorlabs, BK5). To minimize leaks in the shielding, at least two layers of fabric were required to sufficiently suppress light from penetrating the fabric. A schematic illustration is shown in Fig. 3.

Image acquisition

A single UV image was acquired by exposing the sensor for 60 s to the radioluminescent light. A single image with an exposure time as long as this will accumulate a lot of saturated pixels, which is due to the fact that gamma radiation from the source will hit the camera sensor and cause maximal activation of this particular pixel. Removing saturated pixels in a post-processing of the images will result in an incomplete intensity map of the contamination. Carrying out the experiment multiple times, processing every single image, and then summing up the pixel values across the images was used to avoid this problem. With this procedure, the total image acquisition time for the crime scence scenario was 10 min, for the hot cell imaging it was 1 h.

In the image processing, the pixels in the UV image saturated by gamma and cosmic rays are detected with local standard deviation analysis and their value is replaced by a local mean of the nearest neighbors. Then, a Gaussian blur ($r = 7$ px, $\sigma = 5$) is applied to smoothen the image. In the last stage, low intensity fluctuations are discarded with a threshold to produce an adequate intensity map. This step of the image processing is meant only for displaying the contamination and it is not applied when performing the signal-to-noise ratio (SNR) calculations. The processed UV image is superimposed on a grayscale photograph that was taken under normal lighting condition. The photograph provides information about the location of the detected radioluminescence.

The SNR calculation is done with a method similar to the one outlined by Lamadie et al. [4]. In the initial step the camera baseline is removed the image is manually divided up into signal and no-signal areas. The signal in a particular signal area is measured straightforwardly as a mean of all pixel intensities within

this area. The noise figure is extracted from the image in a two-step process. First, the high frequency pixel variations are isolated by subtracting a Gaussian-filtered ($\sigma = 5$) image from it. Afterwards, the standard deviations pixel in the no-signal areas was decided to be the noise figure. The ratio of these numbers defines the SNR.

3 Results

Air radioluminescence spectrum

The recorded spectrum of the air radioluminescence is shown in Fig. 4. There an emission spectrum in the range of $280 - 430$ nm appears, where most of the light is contained within the wavelength regime of $300 - 400$ nm. The lines in the so called solar blind (SB) spectral region below 300 nm are faint, yet visible. Visible light above 400 nm makes up a small fraction of the entire spectrum.
The recorded lines coincide with the emissions bands from both N_2 and N_2^+ molecules [18].

Crime scene investigation

The processed image of the crime scene scenario are shown in Fig. 5. After the total exposure time of 600 s the radioluminescence stemming from the alpha radiation sources is visible, resolved and can be easily located. The accumulated UV signal is made visible as a colored overlay on an otherwise grayscale background image. The bright dots indicate an increased production of UV light in their respective areas and thus reveal the location of alpha active material. The UV light is supposed to mainly originate from the radioluminescence of air, as several luminescence lines of nitrogen coincide with the spectral detection band of the experiment. The camera is equipped with the narrowband optical filter allowing only the spectral band of 314 nm – 354 nm to pass to the sensor, heavily attenuating the other wavelengths. Further, alpha particles can directly interact only with the steel substrate and air, ruling out other possible scintillation sources.

The locations of the detected alpha active material perfectly coincide with the locations where the steel planchettes with ^{241}Am have actually been put, thus showing the radioluminescence imaging is capable of resolving the positions of alpha emitters. The measured radioluminescence intensity of the source of the left side is about three times as large as this of the source on the right side. This is congruent with the activity level of the sources, which are 35.9 MBq and 12.8 MBq, respectively.

Hot cell imaging through lead glass

The photograph from the inside of the hot cell taken through its lead glass window is shown in Fig. 6. It shows an assortment of objects, all of which are believed to exhibit various forms of radioactivity. The lead glass window is opaque to light of wavelengths shorter than 400 nm, thus, only the visible part of air radioluminescence originating from within the hot cell can leave it through the window and reach the camera sensor.

Through standoff detection a few objects have been identified to cause the emission of large amounts of UV light. A bottle in the right hand side and an object in the center of the image reveal being alpha contaminated, causing the generation of UV light in their vicinity.

Though it is difficult to gain information about the precise levels of radioactivity inside a hot cell, the image can be consulted to give a rough estimate of the levels one might encounter in this particular scenario. The camera settings and conditions under which this image was produced was similar to those at the crime scene investigation. Assuming that all radioluminescent light was originating from molecular nitrogen and less than 10 % of this light has a wavelength longer than 400 nm, the activity levels can be estimated to be larger than 1 GBq.

3.1 Discussion

The results show that remote detection of alpha radiation by means of air radioluminescence imaging is a technique, which finds applications in nuclear

threat detection scenarios. The method is capable of rapidly detecting alpha emitters from a distance, without exposing devices or personnel to the radiation itself. This offers a multitude of possibilities for decommissioning tasks. In addition, if the background lighting conditions allow for it, this method gives security officials and first responders a tool to identify potential threats at a crime scene or a site of accident. Standoff detection of alpha radiation offers a complementary tool to the detection of gamma radiation.

Air radioluminescence imaging can be a convenient tool of alpha threat detection during hot cell decommissioning. Most decommissioning procedures rely on breaking the hot cell's confinement, making a swipe-test to identify type and location of radiation sources and then removing one of the contaminated items. Even though this procedure has been, by in large, automatized and personnel can be kept at a safe distance with the use of remote-controlled robots [21], the need to break the confinement and expose equipment to the radiation remains. Opening a hot cell comes with a large cost for the decommissioning facility and any equipment used during this process will become radioactively contaminated itself. The presented imaging technique provides a viable work-around to these problems.

Air radioluminescence imaging requires very low background lighting for it to properly work and thus powerful light shielding of the site under investigation is mandatory. In many field environments this is likely to impose limitations on the use of the imaging techniques. In nuclear facilities, where background lighting can be sufficiently diminished, standoff detection by alpha induced air radioluminescence provides a viable alternative to contemporary approaches.

3.2 Operation in illuminated environments

If a completely dark environment cannot be guaranteed, then background illumination imposes strict limitations on to which extent air radioluminescence imaging can be utilized. Under these conditions, the detection system can be modified to account for the change in lighting levels, such that its effect on the measurement can be mitigated or alleviated. Depending on the spectrum of the

background lighting three different scenarios can be identified: either there is no background lighting, there is only visible light or there is natural light. Table 1 contains a summary of these scenarios and the requirements they impose on the detector system.

The detector system does not require any modifications if complete darkness can be guaranteed. The presence of illumination with visible light complicates the discrimination of radioluminescent light. Light with wavelengths longer than 400 nm has to be kept from reaching the detector. This is can be achieved by installing a filter system in front of the detector that prevents light of those wavelengths from reaching the detector – UV light will still be able to reach the detector with good efficiency. In [22] the authors demonstrate such a system modification by replacing the camera with a photomultiplier tube and equipping it with interference filters to block out visible light.

Filtering the incoming light only works to a limited extent in an environment where natural light is present. Natural light contains UV components with wavelengths shorter than 400 nm. Fig. 7 illustrates this by contrasting the solar spectrum reaching the earth's surface with the emission lines of molecular nitrogen in the UV region. This shows that even small amounts of daylight in the background illumination are capable of superseding the radioluminescent light, making standoff alpha detection difficult. However, it can also be seen that the solar spectral irradiance for wavelengths shorter 300 nm (the solar blind spectral region) rapidly decreases, which is due to absorption of these wavelengths in the upper atmosphere by ozone [17]. Preventing any light with wavelengths larger than 300 nm from reaching the detector negates any background signal natural light would cause in a standoff detection system. Such a change in the limit of detection reduces the radioluminescence that can be used for standoff detection to wavelengths that lie in the solar blind spectral region. Air radioluminescence is for the most part composed of light with wavelengths longer than 300 nm. Only small amounts of its spectrum are located in the solar blind spectral region, with the strongest emission lines being at 296 nm and 282 nm. Standoff detection under daylight conditions may be possible, given that proper wavelength

discrimination of the incoming light is possible and that the detector is able to record light with wavelengths shorter than 300 nm. However, this comes at the cost of losing the most of the radioluminescent light at the discrimination stage, which effectively results a two orders of magnitude larger limit of detection for alpha active sources.

5 Conclusion

We presented the application of standoff detection of alpha radiation via air radioluminescence imaging in two practical scenarios. For this we spectrally analyzed the air scintillation induced by alpha particles with a monochromator and chose an electron-multiplying charge-coupled device camera for imaging purposes. The technique has been applied to localize alpha-active material in a crime scene scenario. Further, radioluminescence imaging has been utilized to identify alpha contamination in a hot cell via imaging through a lead glass window. In the process, that cell's confinement has not been broken. Finally, techniques to overcome the limitations imposed by different background lighting conditions have been discussed. The acquired results show that imaging of air radioluminescence is a way to rapidly locate alpha contamination without exposing personnel or equipment to the radiation itself.

Acknowledgements

This work is supported by Tekes (The Finnish Funding agency for Innovation) through their project "Novel Instrumentation for Nuclear Safety, Security and Safeguard" (NINS3). In addition, the work was supported by GIFT CBRN project (EU FP7 grant agreement no: 608100) in part. The authors acknowledge IAEA task JNT A 1628 MSSP Umbrella Task (Support for Novel Technologies) and for the camera used in this work. Special thanks are extended to the people at ITU for their support with the measurements. On behalf of all authors, the corresponding author states that there is no conflict of interest.

References

[1] Huggins, W., Huggins, L.: On the spectrum of the spontaneous luminous radiation of radium at ordinary temperatures. Proc. R. Soc. Lond., Vol. 72, No. 512, 488-492 (1903)

[2] Pineau, J.-F., Imbard, G.: Remote α source location device and method. US Patent 6,281,502 (2001)

[3] Baschenko, S.M.: Remote optical detection of alpha particle sources. J. Rad. Prot. Vol. 24, No. 1, 75-82 (2004)

[4] Lamadie, F., Delmas, F., Mahe, C., Gironès, P., Le Goaller, C., Costes, J. R.: Remote Alpha Imaging in Nuclear Installations: New Results and Prospects. IEEE Transactions on Nuclear Science, Vol. 52, No. 6, 3035 – 3039 (2005)

[5] Chichester, D.L., Watson, S.M.: Multispectral UV-Visual Imaging as a Tool for Locating and Assessing Ionizing Radiation in Air. IEEE Nuclear and Plasma Sciences Society, Vol. 58, No. 5, 2512-2518 (2011)

[6] Feener, J.S., Charlton, W.S.: Preliminary results of nuclear fluorescence imaging of alpha and beta emitting sources. Advancements in Nuclear Instrumentation Measurement Methods and their Applications 3rd Conference, Marseille, France, 23-27 June (2013). doi: 10.1109/ANIMMA.2013.6728086

[7] McFee, R.B., Leikin, J.B.: Death by polonium-210: Lessons learned from the murder of former Soviet spy Alexander Litvinenko. Seminars in Diagnostic Pathology. Vol 26, No. 1, 61-67 (2009)

[8] Arqueros, F., Blanco, F., Rosado, J.: Analysis of the fluorescence emission from atmospheric nitrogen by electron excitation and its application to fluorescence telescopes. New Journal of Physics, No. 11 (2009), doi: 10.1088/1367-2630/11/6/065011

[9] Collins, P, Chukanov, A., Grebenyuk, V., Naumov, D., Nédélec, P., Nefedov, Y., Onofre, A., Porokhovoi, S., Sabirov, B., Tkatchev, L.: Measurement of air and nitrogen fluorescence light yields induced by electron beam for UHECR experiments. Astroparticle Physics, No. 27, 317-325 (2007)

[10] Duquesne, M., Kaplan, I.: Mesure de la luminescence induite par le rayonnement α du ^{210}Po dans l'air et dans l'eau. J. Physique et le Radium, No. 21, 708-716 (1960)

[11] Sand, J., Ihantola, S., Peräjärvi, K., Toivonen, H., Toivonen, J.: Radioluminescence yield of alpha particles in air. New Journal of Physics, No. 16 (2014), doi: 10.1088/1367-2630/16/5/053022

[12] Sand J., Ihantola, S., Peräjärvi, K., Nicholl, A., Hrnecek, E., Toivonen, H., Toivonen, J.: Imaging of alpha emitters in a field environment. Nuclear Instruments and Methods in Physics Research A, NO. 782, 13-19 (2015)

[13] Mahé, C.: Alpha imaging: recent achievements and glove box characterization. Decommissioning, Decontamination and Reutilization Topical Meeting, Idaho Falls, Idaho, USA, 29. August – 2. September (2010)

[14] Chichester, D.L., Pozzi, S.A., Seabury, E.H., Dolan, J.L., Flaska, M., Johnson, J.T., Watson, S.M., Wharton, J.: FY09 Advanced Instrumentation and Active Interrogation Research for Safeguards, Technical Report, Idaho National Laboratory (2000) doi: 10.2172/974754

[15] Kogaku: UV1228CM transmission curve. http://www.universeoptics.com/wp-content/uploads/uv1228cm_trans_curve.pdf, Accessed 22 January 2018

[16] National Renewable Energy Laboratory: Direct and Global 37 Deg Tilt: ASTM G-173. http://rredc.nrel.gov/solar/spectra/am1.5/ASTMG173.html, Accessed 4 October 2017

[17] Hudson, R.D.: Critical review of ultraviolet photoabsorption cross sections for molecules of astrophysical and aeronomic interest. Review of Geophysics, Vol. 9, No. 2, 305-406 (1971) doi: 10.1029/RG009i002p00305
[18] Lofthus, A. Krupenie, P.H.: The spectrum of molecular nitrogen. J. Phys, Chem. Ref. Data, Vol. 6, No. 1, 113-307 (1977)
[19] Ihantola S. Sand, J., Peräjärvi, K., Toivonen J., Toivonen H.: Fluorescence assisted gamma spectrometry for surface contamination analysis. IEEE Transactions on Nuclear Science, Vol. 60, No. 1, 305 – 309 (2013)
[20] Stroud, J. S., Lell, E.: Optical absorption of lead in glass. Journal of the American Ceramic Society, Vol. 54, No. 11, 554 – 555 (1971)
[21] Kim, K-H., Park, J.-J., Yang, M.-S., Park, H.S.: Remote-controlled mobile cleaning apparatus for removal and collection of high radioactive waste debris in hot cells. US Patent 6,625,843 (2003)
[22] Sand, J., Nicholl, A., Hrnecek, E., Toivonen, H., Toivonen, J., Peräjärvi, K.: Standoff radioluminescence mapping of alpha emitters under bright lighting. IEEE Transactions on Nuclear Science, Vol. 63, No. 3, 1777-1783 (2016)

FIGURES

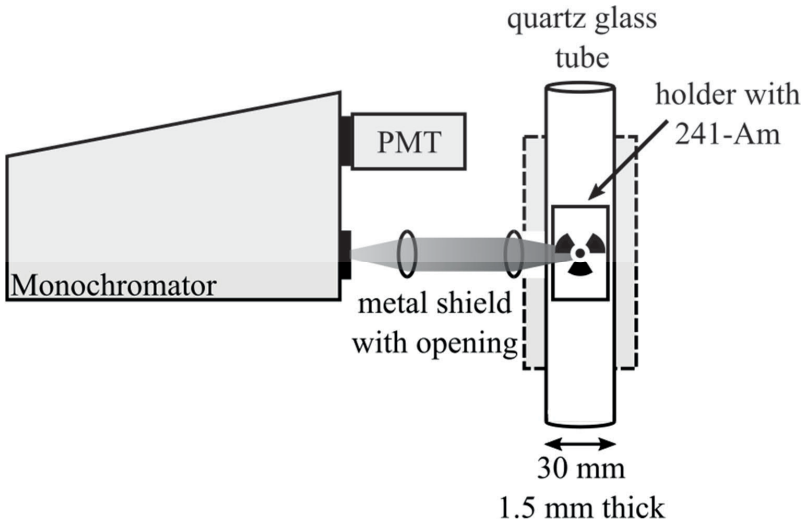

Fig 1 Setup to measure the radioluminescence of nitrogen in air. A 13 MBq alpha source was placed in a quartz tube with access to laboratory air. The quartz tube was partially surrounded by a thick tube of metal to shield the personnel from γ-radiation. A Keplerian telescope guides the light into a monochromator where selected wavelengths are guided to a PMT. Both the PMT and the monochromator are computer-controlled.

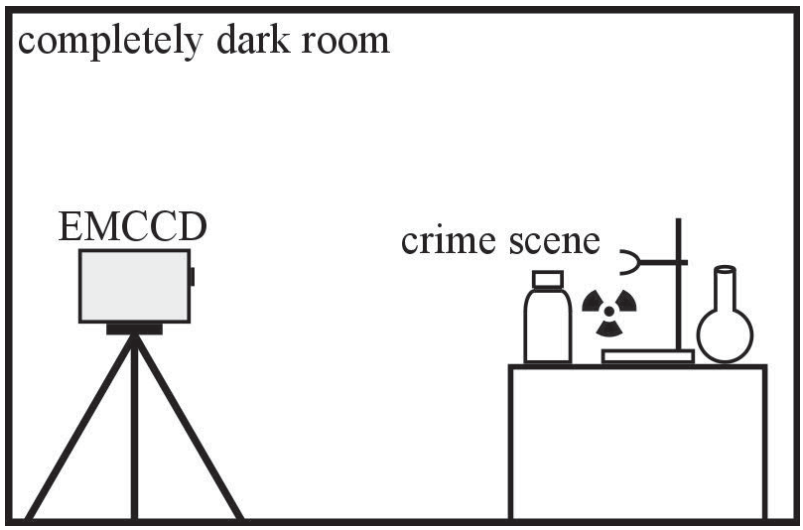

Fig 2 Staging of the crime scene scenario. Radioactive material is placed in the midst of laboratory equipment. An EMCCD camera is placed a meter away from the arrangement and the room is made completely dark.

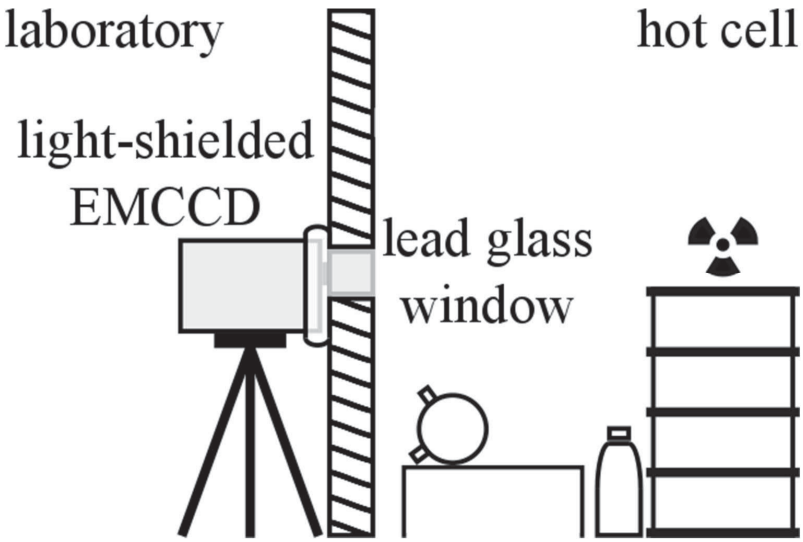

Fig 3 Setup to localize sources of alpha radiation in a hot cell. An EMCCD camera is attached to the thick lead glass window of a hot cell. It's sensor is shielded from background lighting with layers of black cloth. Air radioluminescence originating from inside the cell reaches the camera through the window.

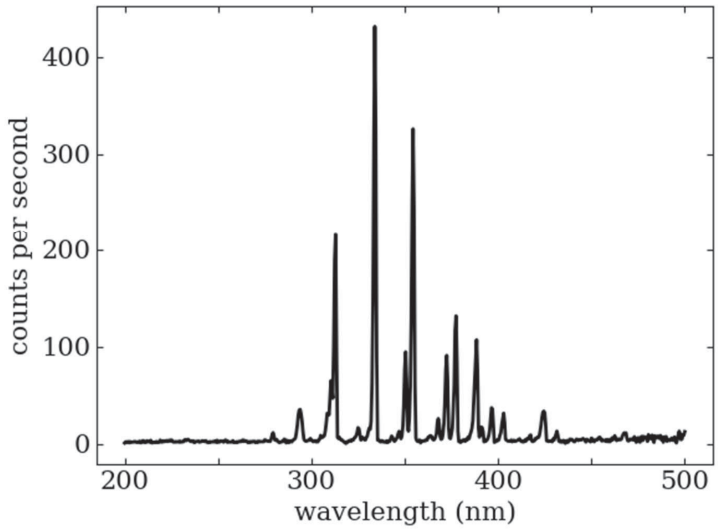

Fig 4 Measurement of the radioluminescence spectrum of alpha particles in air. The recorded emissions lines appear between $280 - 430\text{nm}$. The lines coincides with the 2+ spectrum of molecular nitrogen [18].

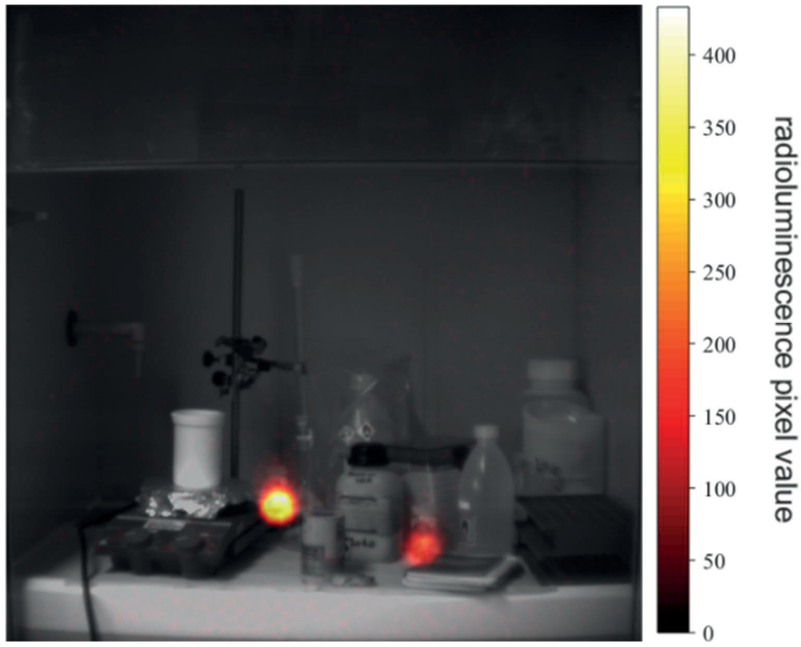

Fig. 5 Detection of alpha emitting sources in a crime scene scenario. The grayscale image shows the scenario from where radioluminescent light is detected. Accumulated UV light is displayed as a colored intensity distribution and is superimposed on the image. The intensity bar on the right hand side translates intensities into detected radioluminescence pixel values. The collected UV light identifies the presence of two distinct alpha radioactive sources.

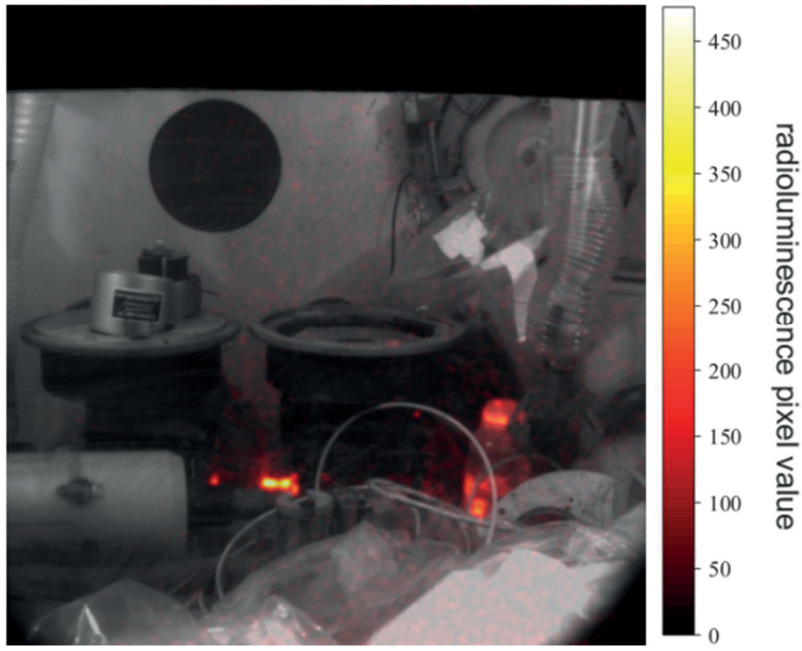

Fig. 6 View into the inside of a hot cell. The grayscale image displays the content of the hot cell, the colored overlay the detected levels of scintillation. A scale that translates the overlay into radioluminescence pixel values is displayed next to the picture on the right. Among many different objects few stand out by causing the creation of large amounts of photons. The bottle-shaped object on the right side of the picture can be safely identified as highly contaminated. In the center of the picture, an intense radiation source has been localized. The emission intensity remained constant over the period of one hour which shows that the light is induced by radiation effects.

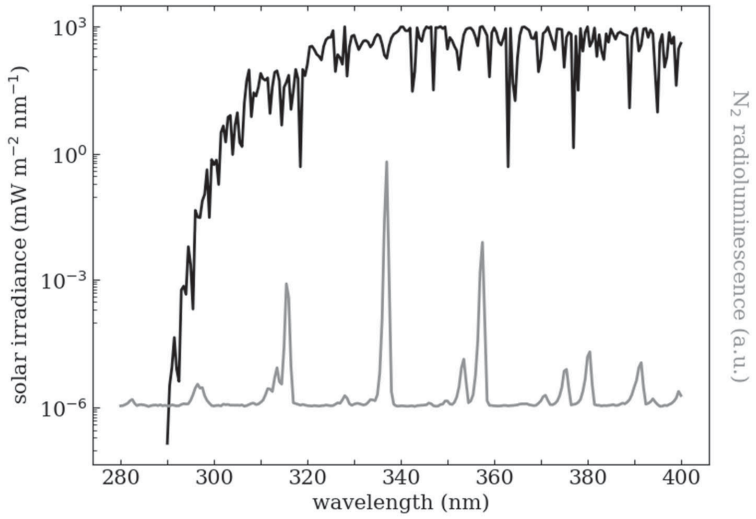

Fig. 7 The spectrum of the sunlight reaching the earth's surface on a logarithmic scale (AM1.5 Global tilt, data taken from [16]). The spectrum of the radioactively induced N_2 emission is displayed in arbitrary units and in linear scale for comparison. The irradiance of the sun starkly overlaps with the strong emission lines of the molecular nitrogen. At around 290 nm the intensity of the background lighting of the sun decreases by nine order of magnitudes, compared to its intensity at the strongest N_2 emission line at 337.13 nm.

TABLES

Table 1 Requirements for air radioluminescence detection systems under different lighting conditions.

Illumination	Detection
Darkness	No spectral discrimination required
Visible ($400 - 700$ nm)	Visible blind detection
Natural light ($300 - 800$ nm)	Solar blind detection

PUBLICATION

II

Intense Radioluminescence of NO/N_2-mixture in Solar Blind Spectral Region

T. Kerst and J. Toivonen

Optics express 26.(2018), 33764–33771

Research Article | Vol. 26, No. 26 | 24 Dec 2018 | OPTICS EXPRESS 33764
Optics EXPRESS

Intense radioluminescence of NO/N_2-mixture in solar blind spectral region

THOMAS KERST[1,2,*] AND JUHA TOIVONEN[1]

[1]*Laboratory of Photonics, Tampere University of Technology, P.O. Box 692 33101 Tampere, Finland*
[2]*Helsinki Institute of Physics, Helsinki University, P.O. Box 64 00014 Helsinki, Finland*
[*]*thomas.kerst@tut.fi*

Abstract: Luminescence in air induced by alpha particle emitters can be used to optically detect radioactive contamination from distances that surpass the range of the alpha radiation itself. Alpha particles excite nitrogen molecules in air and the relaxation creates a faint light emission. When the composition of the gases surrounding the alpha particle emitter is altered then the luminescence spectrum changes. In this work, we report the creation of an intense light emission in the wavelength regime below 300 nm originating from alpha particle excited nitric oxide (NO). The light yield has been investigated as a function of the NO concentration in an N_2 atmosphere. Unlike the emission from molecular nitrogen, NO emits at wavelengths shorter than 300 nm, where solar background and artificial lighting are negligible, thus enabling optical detection of alpha radiation even under bright lighting conditions. We show that the radioactively induced NO emission reaches its maximum intensity at a concentration of 50 ppm of NO diluted in N_2. At this concentration, the strongest emission line of NO is about 25 times more intense than the most intense line of N_2 radioluminescence. Lastly, we discuss potential applications and limitations of the technique.

1. Introduction

Radioluminescence light is created when molecules excited by ionizing radiation relax radiatively to lower energy states and emit photons. The molecular excitations are caused mainly by numerous ionizing radiation induced secondary electrons, while they collide with the surrounding gas molecules [1]. The excited molecules relax either by non-radiative inelastic collisions with other molecules or by spontaneous radiative decay. The photon emitted in the latter process is said to be radioluminescent light and is indicative of the presence of ionizing radiation. Alpha radiation causes the most localized radioluminescence source as alpha particles lose their energy in about 4 cm in air, whereas beta and gamma radiation ionize air in the range of about 1 m and 50 m, respectively. The range of the induced light greatly surpasses the range of the alpha particles themselves, making alpha induced radioluminescence well suited for remote detection of radioactive sources [2].

The radioluminescence in air is generated mostly by emission of molecular nitrogen. The most intense N_2 emission lines are generated when a N_2 molecule radiatively decays from the $C^3\Pi_u$ state to an energetically lower $B^3\Pi_g$ state, and thereby emits an ultraviolet (UV) photon. Similarly, ionized nitrogen N_2^+ emits at the same wavelength band. Together, the N_2 molecules and ions compose narrow emission lines in the spectral range from 280 nm to 430 nm [3]. Also other molecules in air can produce a faint radioluminescence. However, the emission of nitrogen is utilized in all the recent applications that aim to detect alpha radiation from a distance [2,4–7].

Molecular nitrogen that surrounds an alpha emitter is effectively turned into a light source that emits on UV wavelengths. The spectrum of this light source is indicative of the presence of a nearby radioactive source, and for locating the source, it is thus sufficient to detect the origin of the UV light at the area under investigation. A single alpha particle causes the generation of about 100 UV photons in normal air and about 600 UV photons in a nitrogen

#344807 https://doi.org/10.1364/OE.26.033764
Journal © 2018 Received 31 Aug 2018; revised 15 Nov 2018; accepted 18 Nov 2018; published 12 Dec 2018

Optics EXPRESS

atmosphere [8]. As a consequence, even a strong alpha emitter generates a light emission that is much weaker than the light emission from light bulbs or even dimly-lit exit signs. An obvious way to overcome this obstacle is to filter the measured light and discriminate the UV light from visible light. Wavelengths of light that are associated with nitrogen emission are transmitted while everything else is rejected. This approach works well for environments in which no UV light from other sources than the radioluminescence is present [3,9,10].

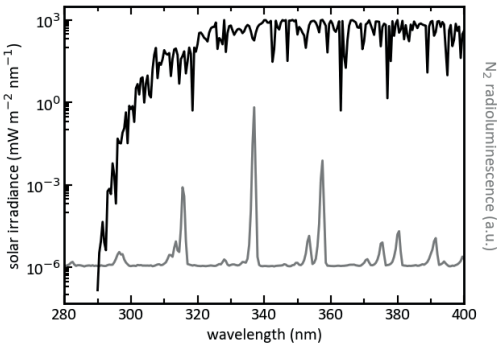

Fig. 1. Spectrum of sunlight reaching the earth's surface (black) contrasted with the radioluminescence of N_2 (gray) in the wavelength range 280 nm – 400 nm. The solar irradiance (AM1.5 Global tilt [11]) is displayed on a logarithmic scale, while the N_2 emissions are shown on a linear scale. At wavelengths longer than 290 nm the solar irradiance spectrally overlaps with the radioluminescence of N_2.

The spectral filtering is of limited use in normal lighting conditions. The spectrum of sunlight reaching the earth contains UV components that overlap with the nitrogen radioluminescence spectrum, and similarly, the most of typical artificial lighting solutions contain UV wavelengths. Consequently, the radioluminescence cannot be discriminated from the background lighting. Figure 1 shows the spectrum of the solar radiation reaching the earth's surface together with the nitrogen emission spectrum. It can be seen that the solar irradiance for wavelengths shorter than 300 nm is drastically diminished, which is due to the absorption of these wavelengths in the atmosphere by ozone [12]. This is region is called a solar blind (SB) spectral region, which is so deep in the UV that it is free of artificial lighting, too, and optical measurements can be conducted without an interference from the lighting conditions. A small fraction of the nitrogen emission is at the wavelengths shorter than 290 nm. Thus, standoff detection of alpha radiation is possible even under bright lighting by measuring this small fraction of the radioluminescence with solar blind UV photodetection [7].

A different approach to overcome the problem with interfering background lighting is to utilize the luminescence of molecules other than nitrogen. Nitric oxide (NO) is known to emit light in the solar blind spectral region. This light originates from a radiative transition from the $A^2\Sigma^+$ state to the ground state $X^2\Pi$ of NO emitting a photon with a wavelength between 220 nm and 305 nm. The spectrum formed by this emission is called the NO γ-band [13]. The intensity of the NO emission is critically dependent on the content of the surrounding gas, as many colliding molecules are capable of quenching the excited state, thereby eliminating its possibility for the radiative transition. Even in small amounts, molecular oxygen causes most of the NO excitations to decay without emitting a UV photon.

In this work, we present a spectrum of nitric oxide radioluminescence and show that its intensity can exceed that of nitrogen. We investigate the intensity of the NO radioluminescence as a function of the NO concentration in an N_2 atmosphere and show that

Optics EXPRESS

the most intense radioluminescence is achieved at a concentration of about 50 ppm. The radioluminescence spectrum of the NO/N_2-mixture is recorded at the wavelength range from 200 nm to 400 nm. It shows that the strong NO radioluminescence is indeed in the solar blind spectral region. With this approach, we overcome two major limitations of the standoff detection of alpha radiation conducted under normal lighting conditions. First, the radioluminescence signal is free from interference caused by the background lighting. Second, under proper conditions, nitric oxide radioluminescence photons are substantially more numerous than those of nitrogen radioluminescence. Under ideal conditions, the strongest NO peak is about 25 more intense the strongest N_2 radioluminescence peak. Compared to the amount of photons generated from N_2 radioluminescence is normal air, the NO radioluminescence is about 150 times more intense. This can be utilized to either lower the detection limit or for remote detection from larger distances.

2. Experiments and methods

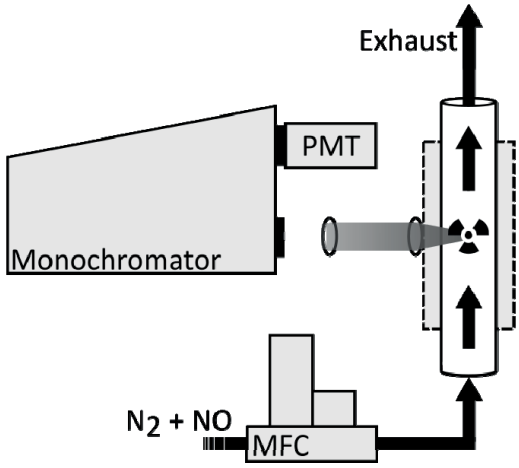

Fig. 2. Schematic illustration of the experimental setup. An alpha radiating source is located within a flow tube made of quartz glass. The tube is constantly flushed with a mixture of N_2 and NO. A monochromator and a PMT are used to record the radioluminescence intensity at a specified wavelength.

Figure 2 shows a schematic illustration of the experimental setup used in this work. All measurements were carried out by placing a 32 MBq alpha active AM-241 source in a 25-mm-diameter quartz tube (Robson scientific). A 21-mm-thick steel mantle, protecting personnel and equipment from gamma radiation of the source, surrounded the parts of the tube close to source. A cone shaped hole with the f-number f/1.378 in the steel mantle allowed light originating in the quartz tube to escape. The light was guided via a Keplerian telescope (Thorlabs LA4052-UV, 35 mm and LA4924-UV, 175 mm) to a computer controlled monochromator (Horiba iHR 550). The telescope was matched to both f-numbers of the steel mantle opening and the monochromator entrance to guarantee optimal light collection efficiency. The monochromator selected a wavelength and guided it to a photon counting photomultiplier tube (PMT, Perkin-Elmer MP-1082). The monochromator was operated with slits of 0.5 mm in width resulting a spectral resolution of 0.45 nm. The gas in the quartz tube was controlled with two mass flow controllers (Bronkhorst High-Tech, 18BRF-201CV-1K0 and 18BRF-201CV-20K). The first controller was attached to a gas bottle filled with 1500 ppm of NO in type 5.0 N_2 (AGA). The latter one was connected to a

Optics EXPRESS

bottle filled with type 6.0 N_2 (AGA). The end of the quartz tube not attached to the controllers was connected to an exhaust. All tubing was kept as short as possible to prevent the formation of large dead volumes.

The intensity of the γ-band emission as a function of the NO concentration in N_2 was measured by constantly flushing the tube with 3 SLPM of a mix consisting of N_2 and varying the concentration of NO. The concentration of the mixture was controlled with the mass flow controllers. The NO concentration was increased in 2 min intervals, starting from 25 ppm and ranging to 300 ppm with a total of 18 different concentrations. After each change in concentration, we waited for 60 s to let the gas mixture become a homogeneous mix. Then we recorded the photons with an associated wavelength of 236 nm travelling through the monochromator with the PMT using an integration time of 60 s.

The radioluminescence spectrum was recorded by scanning the monochromator in 0.5 nm steps from 200 nm to 400 nm. At each step, the number of photons reaching the PMT was recorded for a total of 60 s. During the entire spectrum scan, the atmosphere inside the glass tube consisted of 50 ppm of NO dissolved in N_2.

3. Results and discussion

The radioluminescence intensity of NO was recorded at 236 nm as a function of the NO concentration in constantly flowing N_2 carrier gas. Figure 3 shows the intensity of the radioluminescence as counts per second of the recording photon counting PMT detector. Recording of the intensity only at one of the NO lines at 236 nm is considered well representative measurement for the relative NO radioluminescence intensity as all the NO emission lines originates from the same γ-band transition. It can be seen that the NO radioluminescence intensity increases with the increasing NO concentration. This holds true up to a concentration of 50 ppm, after which the intensity decreases.

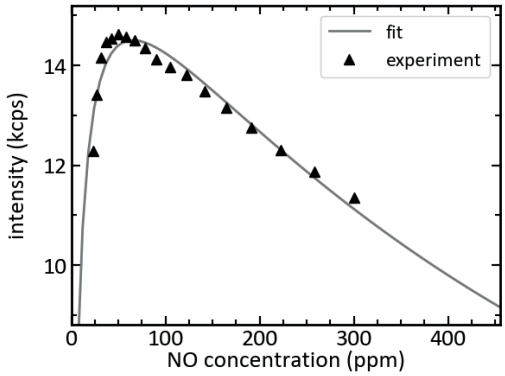

Fig. 3. Intensity of NO emissions recorded at 236 nm as a function of the NO concentration in an N_2 atmosphere. The intensity is recorded with a photon counting PMT and presented in thousands of counts per seconds (kcps). The concentration sweep has been made from low to high NO concentrations. The maximum in the intensity is reached at the NO concentration of about 50 ppm. The gray line, based on Eqs. (1), (2) and (3) is a fit to the data having a coefficient of determination of $R^2 = 0.93$.

The recorded curve suggests that the mechanism by which the nitric oxide radioluminescence is produced is different than that of N_2 radioluminescence. When N_2 radioluminescence is created, the nitrogen gets electronically excited mainly due to free electrons created by the alpha particle. The radiative decay of this excitation then gives rise to radioluminescence. If a similar direct excitation would be assumed to be the cause for NO

Optics EXPRESS

radioluminescence, then the shape of the curve showing the radioluminescence intensity as a function of the NO in concentration would be a linear increase until affected by NO self-quenching. Using the quenching coefficients from Settersten et al. [14] this point of maximum concentration can be estimated to be about 5000 ppm. This is in contrast to our observation and we can therefore conclude that the radioluminescence mechanism in the case of the NO/ N_2- mixture is different from the one observed with nitrogen radioluminescence.

Excitation of NO by excitation transfer via interaction with N_2 molecules appears to be able to explain our data. In this process, molecular nitrogen in the long-lived N_2 $A^3\Sigma_u^+$ state excites ground state nitric oxide to the NO $A^2\Sigma^+$ state, while the N_2 molecule loses its excitation and decays to the ground state [21]. If this excitation mechanism is assumed to be the predominant excitation mechanism of NO, then the dynamics of the system can be described by the following rate equations

$$\frac{\mathrm{d}}{\mathrm{d}t}c_{\mathrm{N}_2^X} = \alpha c_{\mathrm{N}_2^X} - \frac{c_{\mathrm{N}_2^A}}{\tau_{\mathrm{N}_2}} - k_{et}c_{\mathrm{N}_2^A}c_{\mathrm{NO}^X} \tag{1}$$

$$\frac{\mathrm{d}}{\mathrm{d}t}c_{\mathrm{NO}^A} = k_{et}c_{\mathrm{N}_2^A}c_{\mathrm{NO}^X} - \frac{c_{\mathrm{NO}^A}}{\tau_{\mathrm{NO}}} - q_{\mathrm{N}_2}pc_{\mathrm{NO}^A}c_{\mathrm{N}_2^X} - q_{\mathrm{NO}}pc_{\mathrm{NO}^A}c_{\mathrm{NO}^X}, \tag{2}$$

where $c_{\mathrm{N}_2^X}$ / $c_{\mathrm{N}_2^A}$ is the concentration of nitrogen in the excited state / ground state. The sum of both number concentration is assumed to be constant at all times. Likewise, c_{NO^X} / c_{NO^A} is the concentration of nitric oxide in the exited state / ground state. Further, we assume that the gas is only made up of these four components, thus the sum of all four concentrations equals to 1. τ_{N_2} and τ_{NO} are the radiative lifetimes of the excited state of molecular nitrogen and nitric oxide, respectively. q_{N_2} and q_{NO} are the quenching coefficients describing the quenching of excited NO by the presence of ground state nitrogen and ground state nitric oxide, respectively. We do not take into consideration the quenching effects by other molecules, since ground state nitrogen and nitric oxide ideally make up the entire gas mixture. p = 760 Torr is the pressure of the gas. α describes the excitation of ground state N_2 by the presence of the radioactive source. We assume α to be a small value larger than 0. As long as α is not too large, it's numerical value hardly matters, since it does not influence the dynamics of the system but solely determines the magnitude of the observed radioluminescence. k_{et} is the excitation transfer rate and in our model the only mechanism effectively populating the excited state of NO.

We retrieve the values for $c_{\mathrm{N}_2^A}$ and c_{NO^A} from Eqs. (1) and (2) for a given concentration of nitric oxide using numerical evaluation. The system is assumed to be in equilibrium at the time of measurement, which allows us to set the both Eqs. (1) and (2) to 0. We solve them numerically by computing the eigenvalues of the associated matrices using the linear algebra package NumPy with Python 3.6. The eigenvalue problem has to be solved separately for each nitric oxide concentrations. This gives us the equilibrium concentration of NO in excited state c_{NO^A} as a function of k_{et} and the ground state NO concentration in the system c_{NO^X}. We still need to evaluate how many photons these excited states of NO emit, before fitting to the recorded radioluminescence curve in Fig. 3 can be made.

Solving the number of NO emitted photons per unit of time requires evaluation of the excited nitric oxide fraction that decays radiatively, i.e. the quantum efficiency QE for the luminescence. The QE can be evaluated by comparing the radiative decay rate to the sum of all possible decay rates from Eq. (2), resulting in

Optics EXPRESS

$$\mathrm{QE} = \frac{c_{\mathrm{NO}}\tau_{\mathrm{NO}}^{-1}}{c_{\mathrm{NO}}\tau_{\mathrm{NO}}^{-1} + q_{\mathrm{N_2}}pc_{\mathrm{NO}^A}c_{\mathrm{N_2}^X} + q_{\mathrm{NO}}pc_{\mathrm{NO}^A}c_{\mathrm{NO}^X}}, \tag{3}$$

where the denominator term includes the radiative decay, nitrogen quenching and nitric oxide self-quenching. The total number of photons reaching the detector per unit of time is found by weighing the concentration of excited nitric oxide with the quantum efficiency. This number is multiplied with a free scaling constant C accounting for the alpha activity and for the geometry of our detection scheme, yielding to total number of detected photons

$$\Phi = C \cdot \mathrm{QE} \cdot c_{\mathrm{NO}^A} = \frac{c_{\mathrm{NO}^A}}{1 + \tau_{\mathrm{NO}}p\left(q_{\mathrm{N_2}}c_{\mathrm{N_2}^X} + q_{\mathrm{NO}}c_{\mathrm{NO}^X}\right)}. \tag{4}$$

The number of photons detected as a function of the nitric oxide concentration c_{NO^X} is mainly determined by the excitation transfer rate k_{et}, affecting c_{NO^A}, and the nitric oxide self-quenching rate q_{NO}. Therefore, we treated them, along with the scaling constant C, as free parameters in the fitting, while assigning fixed values to all other parameters from literature [3,14,15].

The solution fits the data with a coefficient of determination $R^2 = 0.93$. Our fitted value for k_{et} is 63 kHz. This deviates by roughly 30% from the value of 89 kHz predicted by Piper et al. [16] for NO concentration of 50 ppm. Likewise, our fitted value is about 20% - 30% lower than other published values [17–19], which might relate to a slightly slower excitation transfer rate in our system or be a result of measurement uncertainty of the experimental setup. The fitted value for q_{NO} is $8.5 \cdot 10^6$ Hz Torr^{-1}. This is within the predictions of $8.17 \cdot 10^6$ Hz Torr^{-1} by Settersten et al. [14], $8.9 \cdot 10^6$ Hz Torr^{-1} by Paul et al. [20], and $8.9 \cdot 10^6$ Hz Torr^{-1} by Tamura et al. [21] indicating that the decrease in radioluminescence intensity with an increasing concentration of NO is fully determined by the self-quenching. Overall, the model fits to our data very well, and we can conclude that the excitation transfer from nitrogen to nitric oxide does play a dominant role in the occurrence and characteristics of NO radioluminescence.

In Fig. 4 we present the radioluminescence spectrum of the NO/N_2-mixture having NO concentration of 50 ppm. The NO γ-band emission lines dominate the recorded radioluminescence spectrum at wavelengths between 200 nm and 300 nm. Radioluminescence of nitrogen lines at wavelengths longer than 300 nm remain about at the same intensity than with pure nitrogen atmosphere. Thus, the amount of total energy emitted as radioluminescence significantly increases in comparison to the gas atmosphere of air or pure nitrogen. In Table 1 we present a side-by-side comparison of the radioluminescence yield and the energy conversion efficiencies when an alpha particle is stopped in different gases. Our demonstrated 50 ppm of NO in N_2 generates a radioluminescence photon count rate that is 25 times larger than that of nitrogen radioluminescence, and thus about 150 times larger compared to the radioluminescence in air using values reported by Sand et al. [8]. In energy conversion efficiency from kinetic energy of an alpha particle to radioluminescence photon energy this yields to 200 times larger conversion efficiency in the NO/N_2-mixture than in air due the difference in emitted photon energies. The resulted energy conversion efficiency of 2% is already a remarkably large value enabling enhanced detection limits in optical detection of radiation.

Optics EXPRESS

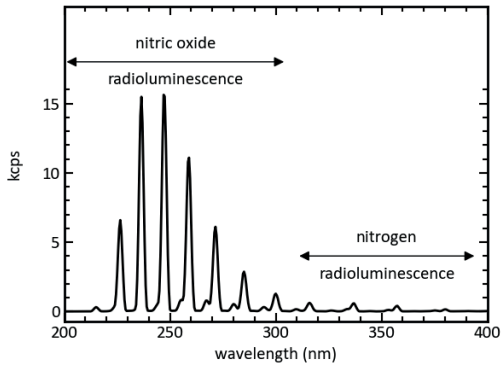

Fig. 4. Radioluminescence spectrum of gas a gas mixture containing 50 ppm of NO diluted in N_2. The nitric oxide emission is about 25 times stronger than N_2 emission and most of the NO emission lines are located in the solar blind spectral region.

Table 1. The intensity of radioluminescence between 200 nm – 400 nm for three different gas environments. The intensity is expressed in relation to the intensity found in normal air, highlighting the improvement in photon yield by changing gases. The energy conversion efficiency shows how much of the energy deposited in air by an alpha particle is emitted as light.

Gas environment	Radioluminescence intensity	Energy conversion Efficiency	Reference
Air	1	$1{\cdot}10^{-4}$	Ref. 8
Nitrogen	6	$6{\cdot}10^{-4}$	Ref. 8
50 ppm of NO/N_2	150	$2{\cdot}10^{-2}$	This work

Using nitric oxide radioluminescence is especially helpful when working under bright lighting conditions. NO emission spectrum does not overlap with sunlight or artificial lighting, thus enabling the use of background-free solar blind optical detection. A detection system being solar blind means that it is insensitive to light at wavelengths longer than 300 nm, while being sensitive to wavelengths shorter than 300 nm. Sand et al. [7] reported about a stand-off solar blind radioluminescence scanner that was able to map locations of alpha radiation sources at the distance of 1 m. The resulted limit of detection in air atmosphere was 800 kBq due to very low amount of nitrogen luminescence at the wavelengths shorter than 300 nm. That is too high activity level for many safety applications. However, radioactive materials are often handled in closed gloveboxes were the gas atmosphere can be controlled. In typical nitrogen atmosphere Sand et al. [7] achieved already more reasonable 6 kBq limit of detection that was attributed to minor NO impurities in the system. Comparing that with our results indicate that introducing 50 ppm of NO in the nitrogen atmosphere would enhance the limit of detection down to 16 Bq. That would be a remarkable enhancement in the performance and still possible to operate under normal lighting. However, introducing 50 ppm of NO is not viable in many cases due to safety and corrosion reasons. We estimated from our model that already 1 ppm trace amount of NO would increase the radioluminescence remarkably at the solar blind spectral region up to the level of pure nitrogen luminescence at longer wavelengths yielding about 400 Bq limit of detection in presented solar blind application by Sand et al. [7]. That is more than 10 times better performance than under nitrogen atmosphere and worth to consider in applications were the gas atmosphere can be controlled.

Optics EXPRESS

4. Conclusions

We presented the creation of intense radioluminescence in the solar blind spectral region using nitric oxide. By monitoring the NO radioluminescence intensity as a function of the amount of NO that is diluted in N_2 we demonstrated that the excitation mechanism for NO is different from that of N_2 radioluminescence. We showed that an excitation transfer from radiatively excited N_2 is the main mechanism for NO excitation, which yields to a maximum energy conversion efficiency of 2% from kinetic energy of alpha particle to optical photons at NO concentration of 50 ppm. At this concentration NO radioluminescence is 25 times more intense than that of pure nitrogen. Our results indicate that adding a trace amounts of nitric oxide into nitrogen atmosphere is a potential method for optical alpha radiation detection in under bright lighting conditions.

Funding

Business Finland, Finland Distinguished Professors (FiDiPro), Project: Novel Instrumentation for Nuclear Safety, Security and Safeguard (NINS3)

References

1. F. Arqueros, F. Blanco, and J. Rosado, "Analysis of the fluorescence emission from atmospheric nitrogen by electron excitation, and its application to fluorescence telescopses," New J. Phys. **11**(6), 065011 (2009).
2. S. M. Baschenko, "Remote optical detection of alpha particle sources," J. Radiol. Prot. **24**(1), 75–82 (2004).
3. A. Lofthus and P. H. Krupenie, "The spectrum of molecular nitrogen," J. Radiol. Prot. **24**(1), 75–82 (1977).
4. F. Lamadie, F. Delmas, C. Mahe, P. Gironès, C. Le Goaller, and J. R. Costes, "Remote alpha imaging in nuclear installations: new results and prospects," IEEE Trans. Nucl. Sci. **52**(6), 3035–3039 (2005).
5. J. Sand, S. Ihantola, K. Peräjärvi, A. Nicholl, E. Hrnecek, H. Toivonen, and J. Toivonen, "Imaging of alpha emitters in a field environment," Nucl Instrum. Meth. A **782**, 13–19 (2015).
6. D. S. Haslip, T. Cousins, V. Koslowsky, and H. Ing, H. R. Andrews, E. T. H. Clifford, and D. Locklin, "Standoff radiation imaging detector," U.S. patent US7317191B1 (8. Jan. 2008).
7. J. Sand, A. Nicholl, E. Hrnecek, H. Toivonen, J. Toivonen, and K. Peräjärvi, "Stand-off radioluminescence mapping of alpha emitters under bright lighting," IEEE Trans. Nucl. Sci. **63**(3), 1777–1783 (2016).
8. J. Sand, S. Ihantola, K. Peräjärvi, H. Toivonen, and J. Toivonen, "Radioluminescence yield of alpha particles in air," New J. Phys. **16**(5), 053022 (2014).
9. P. Colin, A. Chukanov, V. Grebenyuk, D. Naumov, P. Nédélec, Y. Nefedov, A. Onofre, S. Porokhovoi, B. Sabirov, and L. Tkatechev, "Measurement of air and nitrogen fluorescence light yields induced by electron beam for UHECR experiments," Astropart. Phys. **27**(5), 317–325 (2007).
10. J.-F. Pineau and G. Imbard, "Remote alpha source location device and method," US Patent 6281502B1 (2001).
11. National Renewable Energy Laboratory, "Direct and Global 37 Deg Tilt: ASTM G-173," *http://rredc.nrel.gov/solar/spectra/am1.5/ASTMG173.html*, Accessed 4 October 2017.
12. R. D. Hudson, "Critical review of ultraviolet photabsorption cross sections for molecules of astrophysical and aeronomic interest," Rev. Geophys. **9**(2), 305–406 (1971).
13. J. Danielak, U. Domin, R. Kepa, M. Rytel, and M. Zachwieja, "Reinvestigation of the emission gamma band (A2S+-X2P) system of the NO molecule," J. Mol. Spectrosc. **181**, 394–402 (1997).
14. T. B. Settersten, B. D. Patterson, and J. A. Gray, "Temperature- and species-dependent quenching of NO A 2Sigma+(v′=0) probed by two-photon laser-induced fluorescence using a picosecond laser," J. Chem. Phys. **124**(23), 234308 (2006).
15. A. B. Callear and M. J. Pilling, "Fluorescence of nitric oxide. Part7.—quenching rates of NO C 2 P (v=0), its rate of radiation to NO A 2 S+, energy transfer efficiencies, and mechanisms of predissociation," Trans. Faraday Soc. **66**(0), 1618–1634 (1970).
16. L. G. Piper, L. M. Cowles, and W. T. Rawlins, "Einstein coefficients and transition moment variation for the NO (A^2S+-X2P) transition," J. Chem. Phys. **85**, 3369–3378 (1986).
17. J. W. Dreyer, D. Perner, and C. R. Roy, "Rate constants for the quenching of N_2 (A3Su$^+$, va=0-8) by CO, CO_2, NH_3, NO, and O_2," J. Chem. Phys. **61**(8), 3164–3169 (1974).
18. W. G. Clark and D. W. Setser, "Energy transfer reactions of N2 (A3. SIGMA. u+). 5. Quenching by hydrogen haildes, methyl haildes, and other molecules," J. Phys. Chem.-US **84**(18), 2225–2233 (1980).
19. R. A. Young and G. A. St. John, "Experiments on N2(A3Su+). Ii. Excitation of NO," J. Chem. Phys. **48**(2), 898–900 (1968).
20. P. H. Paul, J. Gray, J. L. Durant, and J. W. Thomann, "Collisional quenching corrections for laser-induced fluorescence measurement of NO A2S+," AIAA J. **32**(8), 1670–1675 (1994).
21. M. Tamura, P. A. Berg, J. E. Harrington, J. Luque, J. B. Jeffries, G. P. Smith, and D. R. Crosley, "Collisional quenching of CH(A), OH(A), and NO(A) in low pressure hydrocarbon flames," Combust. Flame **114**(3), 502–514 (1998).

PUBLICATION

III

Alpha Radiation-Induced Luminescence by Am-241 in Aqueous Nitric Acid Solution

T. Kerst, R. Malmbeck, N. l. Banik and J. Toivonen

Sensors 19.(2019), 1602

sensors

MDPI

Article

Alpha Radiation-Induced Luminescence by Am-241 in Aqueous Nitric Acid Solution

Thomas Kerst [1,2,*], Rikard Malmbeck [3], Nidhu lal Banik [3] and Juha Toivonen [1]

[1] Photonics Laboratory, Physics Unit, Tampere University, P.O. Box 692, 33101 Tampere, Finland; juha.toivonen@tuni.fi
[2] Helsinki Institute of Physics, Helsinki University, P.O. Box 64, 00014 Helsinki, Finland
[3] European Commission, Joint Research Centre (JRC), Directorate G–Nuclear Safety and Security, Advanced Nuclear Knowledge, 76125 Karlsruhe, Germany; rikard.malmbeck@ec.europa.eu (R.M.); nidhu.banik@ec.europa.eu (N.B.)
* Correspondence: thomas.kerst@tuni.fi; Tel.: +358-50-300-5968

Received: 13 February 2019; Accepted: 28 March 2019; Published: 2 April 2019

Abstract: When exposed to air, alpha particles cause the production of light by exciting the molecules surrounding them. This light, the radioluminescence, is indicative of the presence of alpha radiation, thus allowing for the optical sensing of alpha radiation from distances larger than the few centimeters an alpha particle can travel in air. While the mechanics of radioluminescence in air and other gas compositions is relatively well understood, the same cannot be said about the radioluminescence properties of liquids. Better understanding of the radioluminescence properties of liquids is essential to design methods for the detection of radioactively contaminated liquids by optical means. In this article, we provide radioluminescence images of Am-241 dissolved in aqueous nitric acid (HNO_3) solution and present the recorded radioluminescence spectrum with a maximum between 350 nm and 400 nm, and a steep decrease at the short wavelength side of the maximum. The shape of the spectrum resembles a luminescence process rather than Cerenkov light, bremsstrahlung, or other mechanisms with broadband emission. We show that the amount of light produced is about 150 times smaller compared to that of the same amount of Am-241 in air. The light production in the liquid is evenly distributed throughout the sample volume with a slight increase on the surface of the liquid. The radioluminescence intensity is shown to scale linearly with the Am-241 concentration and not be affected by the HNO_3 concentration.

Keywords: alpha radiation; radioluminescence; liquid phase luminescence; americium

1. Introduction

Radioluminescence describes the spontaneous emission of light as a consequence of interaction of luminescent material with ionizing radiation. The ionizing particle typically originates from, but is not limited to, a form of radioactive decay. In the process of creating radioluminescence, the ionizing particle or an induced secondary electron collides with a luminescent material, resulting in the elevation of an orbital electron [1]. The excited electron then has a chance to radiatively decay, thereby emitting a photon of light. Photons created this way are said to be radioluminescence, since the presence of ionizing radiation ultimately lead to its production. Thus, the presence of radioluminescence is to be taken as an indicator for the presence of ionizing radiation itself.

Radioluminescence induced by alpha particles allows for their remote detection by optical means. In air, alpha particles come to a halt after having travelled for about 4 cm, losing almost all their kinetic energy in the process [2]. In contrast, beta and gamma radiation travel a few meters and tens of meters in air, respectively [3], making alpha radiation a comparably short ranged type of nuclear radiation. This makes it rather easy to avoid exposure to a known alpha source by keeping distance, while at

the same time making it difficult to detect unknown alpha sources with methods that rely on direct interaction with the particles. Alpha induced radioluminescence is not limited to a travel distance of a few cm, thus making it possible to remotely detect alpha radiation by collecting radioluminescent light. [4].

How little alpha radiation can reliably be detected by collecting radioluminescence depends on the conditions surrounding the source. To understand the reasons for this, it is necessary to recognize that even high-activity alpha sources create amounts of photons that can be considered almost negligible in comparison to the number of photons a typical ambient light source, such as the sunlight on earth or a fluorescent door sign, emits. A single alpha particle being stopped in air leads to the production of about 100 photons [5,6], each of which is isotropically radiated away from the location of the alpha source. Thus, photon counting devices must be employed to make radioluminescence detectable. In a recent study, Sand et al. [7] thoroughly investigated the question of how small an alpha contamination can one detect by optical means alone, given that one can use state-of-the art equipment to detect single UV photons and the site of contamination is exposed to normal air. Under ideal conditions, e.g., the only present light source being radioluminescence, they were able to detect sources with an alpha activity of 4 kBq or surface contamination with an activity of 300 Bq cm^{-2}, respectively, by using an UV sensitive low-noise PMT at a distance of about 1 m with a measurement time of about 10 s.

Once background lighting must be taken into account, a straightforward approach of collecting light is no longer feasible. The spectral patterns of both the air radioluminescence, being mostly made up of N_2 emissions [1], and of the background lighting must be considered. Furthermore, the optical design must be optimized to mitigate the effects of the typically high ambient light levels [7–11]. Another way of overcoming the problem of background lighting is by only collecting photons with wavelengths that are in the UVC wavelength range at wavelengths shorter than 280 nm. Daylight, one of the most common source background lighting containing UV parts, does not extend into the UVC [12]. Thus, choosing equipment that is both sensitive to those wavelengths and able to detect single photons can be used for remote detection of alpha radiation. Ivanov et al. [13,14] are one of the first reporting on such an approach using cameras, whereas Crompton et al. [15] pioneered the field with using a detector that uses the photoelectric effect and gas multiplication to detect individual UVC photons. However, restricting the detection to the UVC limits the sensitivity of the optical detection as UVC range contains only a small fraction of the radioluminescence [16]. One way to overcome this impediment is by relying, when possible, on an artificial atmosphere that allows for enhanced yield of radioluminescence [17–19].

The ability of liquids to exhibit luminescence upon irradiation with ionizing particles has not been as thoroughly studied as it has been done for gases. Even though there have been a few studies reaching back into the 60s [20], renewed interest into the topic has been partly sparked by the observations of Yamamoto and colleagues [21]. They showed that faint radioluminescence is produced by placing an Am-241 source in water. In a later study, it was estimated using long-pass filters that the spectrum is a very broad one with increasing intensity towards shorter wavelengths [22]. However, a fully resolved spectrum was not presented.

In this paper, we present radioluminescence images originating from a liquid with Am-241 dissolved in an aqueous solution of nitric acid (HNO_3). The imaging reveals equal distribution of light production throughout the sample volume with a slight increase at the surface of the liquid interfacing with air. We present a fully resolved radioluminescence spectrum in the spectral range between 280 nm and 550 nm. Lastly, we investigate the intensity of the radioluminescence as a function of the amount of Am-241 and the HNO_3 concentration, and discuss about the possible mechanisms producing the observed radioluminescence.

In section 2 we describe our experimental arrangements and give detailed information on how data was obtained. We also given detailed information about the image processing involved and how the reader can reproduce the algorithms and methods used in the digital post-processing. The results

are presented and discussed in section 3. Section 4 concludes this work and summarizes the main findings.

2. Materials and Methods

All experiments have been carried out in the laboratories and premises of the Joint Research Centre (JRC) in Karlsruhe, Germany, during two measurement campaigns. For safety reasons, all radioactive material used was kept and handled in a plexiglass glovebox while most of the other equipment remained outside. The only modifications to the glovebox were a replacement of one glove with a quartz window (Sico Technology GmbH, SQ1, Austria) and the insertion of another quartz glass window into the plexiglass ceiling of the box. The chosen quartz glass has a flat transmission spectrum down to 180 nm wavelength and is thus well suited for this experiment [23].

The box has been shielded from ambient light with black rubberized fabric (Thorlabs, BK5, Newton, NJ, USA). A very thorough shielding with multiple layers was required to block all ambient light, especially given that the laboratory could not be made totally dark. We made sure that radioluminescence was the only significant source of light during the data acquisition by recording a control image without the alpha source prior to actual data recording with different radioactive samples.

The radioactive samples used during the measurements included a planchet with a thin layer of Pu-239 evaporated onto it (from now on referred to as: the solid sample) and several liquids containing Am-241 (from now on referred to as: the liquid samples). The surface activity of the solid sample was verified by alpha spectroscopy to be 5.6 MBq. We prepared the liquid samples by evaporating a pure Am-241 solution to dryness and then adding nitric acid (HNO_3) solution to it. Depending on the sample, we used 1 M, 3 M or 7 M, with the solvent having been deionized water. M is the molar concentration, i.e., mols per liter. We prepared each liquid sample to measure a volume of 2 mL. We denote the concentration of Am-241 dissolved in each sample by dividing the amount of μg of Am-241 with the number of grams of the liquid sample. Thus, the concentration is defined by mass, and throughout the paper we express it with the unit ppm. We prepared a total of 7 liquid samples divided on 2 distinct sets. The first set comprised a total of 3 different solutions each containing 150 ppm of Am-241, but with varying HNO_3 concentrations of 1 M, 3 M and 7 M. The second set comprised a total of 4 different solutions each with a HNO_3 concentration of 3 M, but with varying Am-241 concentrations being 50 ppm, 75 ppm, 150 ppm and 750 ppm. Using the specific activity of Am-241 [24], the liquid samples have activities of roughly 13 MBq, 19 MBq, 38 MBq and 190 MBq, respectively. When using a liquid sample in an experiment, we filled it into a standard quartz glass fluorescence cuvette that transmits light at the wavelength range of 200 nm - 2 500 nm (12.5 mm length and width, 45 mm height, 10 mm light path length, Hellma analytics GmbH & Co. KG, type: 101-QS, material: QS).

2.1. Radioluminescence Imaging

We imaged the radioluminescence by placing a sample on a holder close to the quartz window and an EMCCD camera (Andor iXon3 897) on the other side of the window. Sample holder and camera objective were kept at a constant distance of about 30 cm throughout all experiments. The camera sensor was internally cooled down to $-80^{\circ}C$ to reduce thermal noise. We placed the sample and the holder insight a light-tight PVC tube and wrapped the camera in black fabric to further improve the ambient light shielding. The imaging lens was a UV-objective (Universe Kogaku, UV1228CM) with a focal length of 12 mm and a light collection efficiency of f/2.8. A schematic illustration of the arrangement is shown in Figure 1.

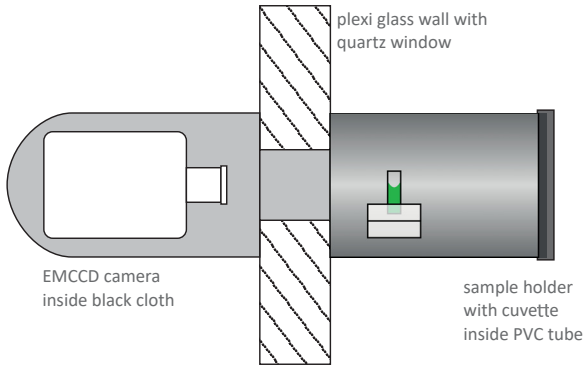

Figure 1. Schematic of the arrangement designed to image radioluminescence: A liquid or solid alpha active sample (green) resides on a holder placed inside black and light-tight PVC tube. The tube is placed around a glove port of box which is holding a quartz glass window instead of a glove. Light exiting the glove box through the window form an image on the sensor of an EMCCD camera. Multiple layers of black fabric wrapped around the camera and the glove port prevent stray light form entering the setup.

For each sample we took one background image in normal laboratory lighting conditions and then darkened the setup to obtain images of the radioluminescence. For each liquid sample we took 30 images with an exposure time of 60 s each, resulting in a total integration of 30 min. For the solid sample, a single exposure of 100 s length proofed sufficient to acquire image material with good enough signal-to-noise ratio. The individual images accumulated numerous hot pixels, e.g., pixels with maximum value, which likely occurs due to exposure of the sensor to gamma radiation predominantly from the 59.6 keV line of Am-241.

All image material has been post-processed by taking the pixel-wise median of the 30 consecutive images. The so-constructed median image is largely free of hot pixels all the while leaving the features and resolution of the image unaffected. The procedure is illustrated in Figure 2 with data from the experiments serving as example. For image processing we used python 3.6.3 as programming language and made use of the libraries OpenCV 3.3.1, matplotlib 2.1.0 and NumPy 1.13.3.

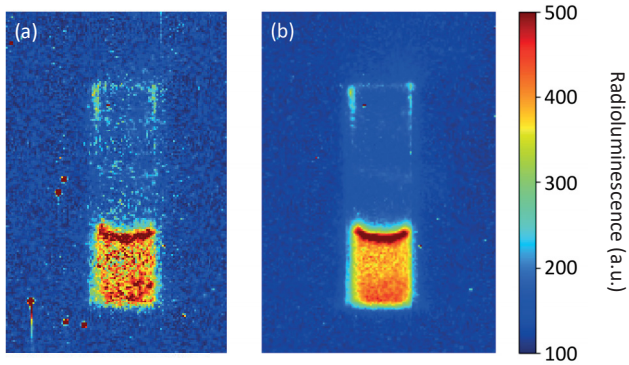

Figure 2. Demonstration of the post-processing using 30 images with exposure times of 60 s each. (**a**) A single capture, raw data. The cuvette and the liquid are clearly visible, hot pixels appear as red dots. (**b**) The pixel-wise median over a total of 30 images. The z-scale shows raw pixel values.

2.2. Spectral Measurement

The radioluminescence spectrum was measured by transporting light with a system of liquid light guides outside the glove box, where it was analyzed. A schematic illustration of the arrangement is presented in Figure 3. The sample was placed on a height-adjustable pedestal inside the glovebox. The liquid light guide (Lumatec GmbH, Series 300, 8mm core diameter) was installed next to the pedestal to collect the light emanating from the sample. The fiber was put as close as possible to the sample to eliminate the need for collimating optics. When the liquid sample was spectrally analyzed, the fiber was installed as close as possible to the sample holder to make sure that only radioluminescence from the bulk of the liquid reaches the detector. From there the light was guided to a 10 mm thick quartz window in the ceiling of the glove box. Another liquid light guide at the other side of the window then picked up the light and further transported it to a motorized monochromator (Horiba Scientific Inc., iHR 550), where it was spectrally dispersed. Light of only one selected wavelength leaves the monochromator at a time. The monochromator was operated with a UV sensitive grating (model 51050, 300 gr mm^{-1}, 250 nm blaze) and an entrance slit width of 2 mm, resulting in a spectral resolution of about 6 nm. The light passing the monochromator was measured with a low-noise photon counting PMT (Perkin Elmer GmbH, MP-1982, $<$ 1 cps DC) and read out via computer.

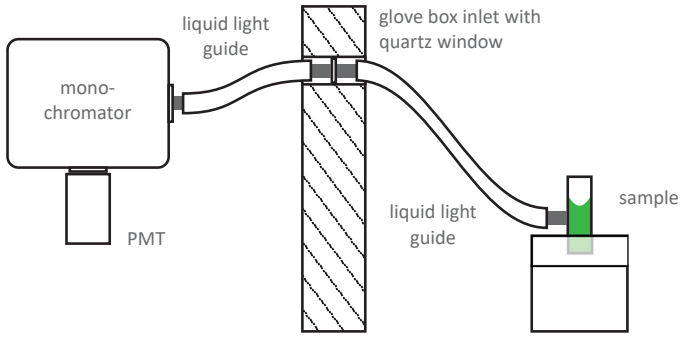

Figure 3. Schematic of the setup designed to measure the radioluminescence spectrum. A liquid or solid alpha active sample (green) resides on a holder inside holder in the glove box. A system of liquid light guides transports radioluminescent light to a monochromator, where it is spectrally separated and detected by a PMT.

A spectrum was obtained by counting the photons with the PMT at each individual wavelength and then arranging the so-measured counts according to their associated wavelength. The monochromator scanned from 280 nm to 550 nm in 3 nm steps, integrating for a total of 10 s at each step. The scan was repeated multiple times both to improve the signal-to-noise ratio by having more data points available and to compensate for drifts of the PMT. A drift of the PMT could not have been counteracted against if the measurement consisted of one long single scan.

During post-processing, the spectral data we accounted for effects that alter the measured spectrum. The cuvette, the light guide, and the PMT have a flat response. They can change the intensity of the light they respond to, but they cannot alter the shape of the spectrum of this light. The reflectance of the grating has been calibrated to give a flat spectral response. A 10 mm thick water column has a negligible absorption in the measurement wavelength range [25], thus it has no effect on the measured spectral shape.

3. Results and Discussion

3.1. Imaging

Radioluminescence of 750 ppm Am-241 which has been dissolved in 3 M HNO_3 was imaged with the EMCCD camera in darkness. In addition, we took a photograph image under normal lighting conditions for a reference. We repeated the procedure for the Pu-239 solid sample planchet, where we expected radioluminescence of air to occur above it. That served as an intensity calibration regarding to previously published results [26]. The recorded images are shown in Figure 4.

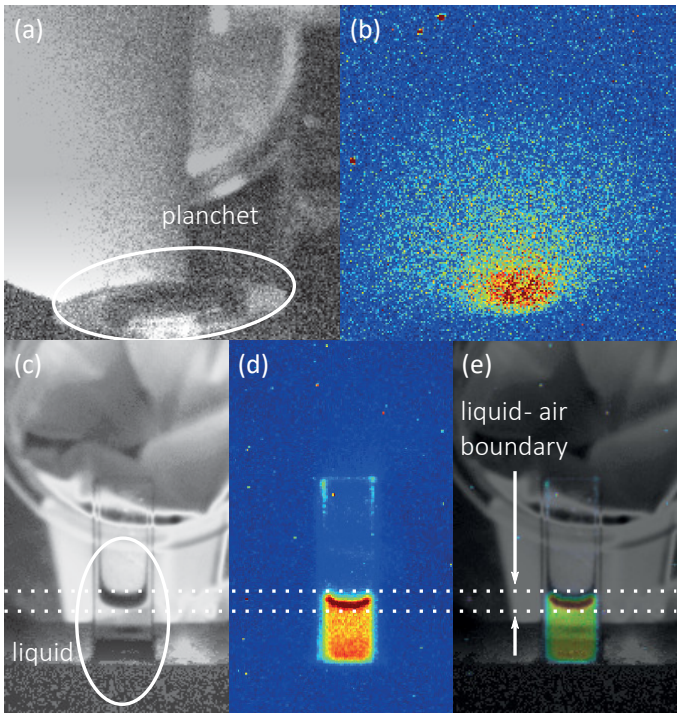

Figure 4. Images of radioluminescence and the locations where they occur. The gray scale images each show a single 0.1 s capture of the samples under normal lighting conditions. The colorful images next to them show the same scenes in darkness using much longer exposure times. Dotted lines throughout the images (**c**–**e**) frame the area of the images where the surface of the liquid with air is displayed. The z-scale used in the images is the same as the one used in Figure 2. (**a**) Image of the Pu-239 coated planchet under normal lighting conditions. (**b**) Radioluminescence image of the Pu-239 coated planchet. (**c**) Image of the sample holder and the cuvette which resides in it taken under normal lighting conditions. The camera is slightly tilted and reveals part of the sample holder behind the cuvette. The cuvette holds the transparent liquid, the camera tilt makes it possible to see the boundary of the liquid with the air. (**d**) Radioluminescence image of the cuvette containing 750 ppm of Am-241 in 3 M HNO_3 solution. (**e**) Overlay of the cuvette radioluminescence image (**d**) on the image of the cuvette (**c**).

The image of the solid planchet radioluminescence in Figure 4b shows radioluminescence emanating from the surface of the planchet, in a fashion similar to what has been found and described in greater detail by Sand et al. in an experiment under similar conditions [26]. The imaging of radioluminescence emanating from the liquid was performed with a total integration time of 1800 s,

whereas the imaging the solid sample was performed in 100 s. This is due to the much lower light yield of the liquid, even though the overall alpha activity is higher. We estimated the light yield per alpha particle in the liquid by integrating the pixel intensities of the background-corrected planchet image and dividing with activity and exposure time. A similar procedure has been used for to the central parts of liquid radioluminescence image, and the resulting light yield was further scaled to take into account the total liquid area in the cuvette. The energies of alpha particles emitted by Pu-239 are 5.157 MeV and by Am-241 are 5.486 MeV, respectively[27], thus the two samples are quite similar from an alpha radiation point of view. From this analysis, we find that the light yield of an alpha particle in the liquid is roughly 150 times lower than in air. A similar effect has been noticed by Yamamoto et al. in their research on liquid radioluminescence [21], where they observe a decreased light yield with a factor of about 100.

The pixel intensities at the liquid-air boundary in Figure 4d are higher compared to the pixel intensities further down the water column. The shape of this area is coincidental with the shape of the liquid-air boundary in Figure 4c, which can be even better seen in the overlay image in Figure 4e. The camera is slightly tilted towards the cuvette, which makes it possible to look on top of the interface of the liquid-air boundary. The increase in the intensity might be due to an optical effect or an increased light production at the surface. The optical refraction at the liquid-air boundary can redirect more radioluminescent light towards the camera. Also, it is known that alpha particles are emitted out from the liquid[28], and thus can create radioluminescence in air [5]. The radioluminescence yield in air was previously shown to be approximately 150 times more efficient, which can result in the increased intensity at the surface in Figure 4d.

It can also be seen there is an area of slightly increased pixel intensities at the lower end of the cuvette. The camera looks with a slightly tilted angle at the cuvette, making a part of the cuvette which is surrounded by the holder visible to the camera. It is those parts of the image that show increased pixel intensities. In the overlay image in Figure 4e this becomes even clearer. Thus, it is very likely that the increased intensity in the radioluminescence image in this particular area is not created by an increased radioluminescence production but rather by reflection of radioluminescence photons from the sample holder towards the camera.

Vertical and horizontal cross sections of the radioluminescence image of the cuvette are shown in Figure 5 for detailed analysis of the intensity distribution. In the horizontal cross section in Figure 5a it can be seen that the radioluminescence is evenly distributed throughout the liquid. We notice that the glass walls have no influence on the light production. In the vertical cross section in Figure 5b the differences in radioluminescence intensity as a function of height become clearly visible. The rightmost peak corresponds to the slightly increased intensity seen at the point where the cuvette is submerged in the holder. The maximum in the vertical cross section shows the increased light production at the surface of the liquid. Dotted lines indicate the position where the interface of the liquid-air boundary faces the camera. They correspond to the same dotted lines shown in Figure 4. Between these two peaks, the radioluminescence intensity is notably evenly distributed.

The local maxima to the left in Figure 5b correspond to the increased radioluminescence observed at the top end of the cuvette. This is very likely radioluminescence from dried liquid. The same cuvette was used to hold all liquid samples. Changing the sample made it necessary to empty and refill the cuvette. During refilling contact of the liquid with the walls was difficult to avoid, thus contaminating it. Even careful cleaning rarely removed all contamination, and it were the edges of the cuvette that proved most difficult to clean. It is this contamination that is seen in the radioluminescence image. Though the radioluminescence from contamination of the cuvette walls is somewhat of a nuisance for this particular work, it shows once again that radioluminescence imaging is a very efficient method to find alpha contamination in difficult to access areas.

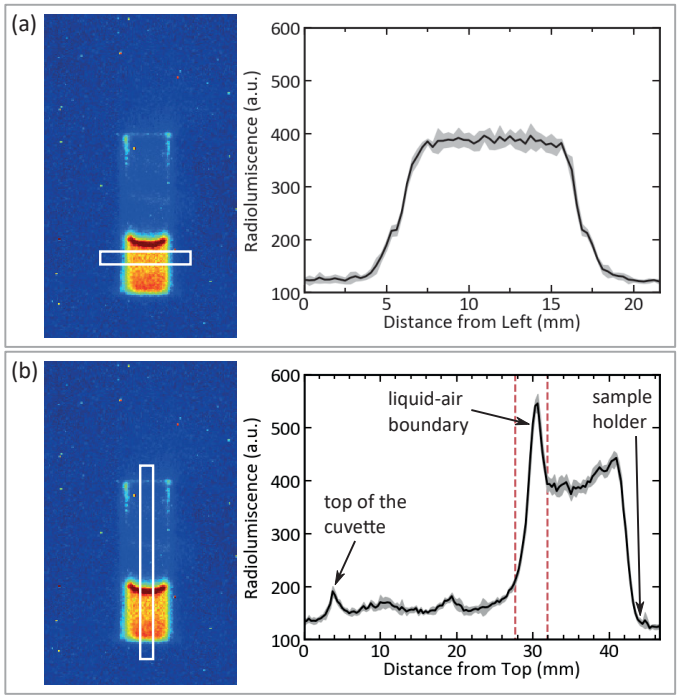

Figure 5. Cross sections of parts of the radioluminescence image of 750 ppm Am-241 in 3 M HNO_3. (**a**) Horizontal cross section across the cuvette. The uncertainty displayed in gray is identical to the standard deviation of the pixel values in vertical direction. (**b**) Vertical cross section across the cuvette. The uncertainty displayed is identical to the standard deviation of the pixel values in the horizontal direction. Labels point to notable features and name the position where they occur.

3.2. Influence of Am Concentration and Acidity

A dependency of the radioluminescence intensity on alpha active Am-241 and nitric acid concentrations was studied, since it is not clear what exactly causes the light emission. The role of nitric acid was tested with samples, where the activity was held constant by having 150 ppm of Am-241 while the nitric acid concentration was varied. The effect of Am-241 was studied with samples, where the HNO_3 concentration was held constant at 3 M while the americium concentration was varied. In all the experiments, the post-processing of the radioluminescence images was done as outlined in section 2. The radioluminescence signal level was calculated as an average of pixels corresponding the liquid volume of the cuvette. Then this average was corrected for the background level of the image. The resulting data is presented in Figure 6. The radioluminescence shows little or no dependency on the nitric acid concentration. However, the data shows that the radioluminescence is linearly dependent on the Am-241 concentration. Thus, we can exclude nitric acid from potential luminescent species in the solutions. We can further reduce the number of possible sources of radioluminescence by comparing our results with experiments by using an ion beam as an ionizing source [22]. In that work, a water phantom was irradiated with a carbon-ion beam producing radioluminescence with properties similar to what we found. This leads us to conclude that Am-241 is unlikely linked to the luminescent properties in other ways than as a source of the ionizing radiation.

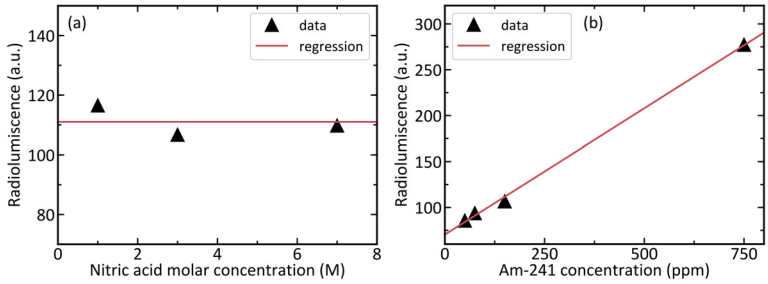

Figure 6. Dependence of the measured radioluminescence intensity on the nitric acid concentration and the americium concentration. The pixel values displayed as radioluminescence have been corrected for the image background. (**a**) Change of the radioluminescence with a varying nitric acid concentration. A constant has been fitted to the data. (**b**) Change of the radioluminescence with varying Am-241 concentration. A linear function has been fitted to the data.

3.3. Radioluminescence Spectrum

Radioluminescence properties of the both solid and liquid samples were further studied by measuring the spectra of the luminescence using a monochromator and a photomultiplier tube. The measurements of the solid and liquid samples were otherwise performed in very similar way, except the liquid sample was with an extra quartz glass wall of the cuvette in the optical path and different spectral scanning parameters were used. For the solid sample, only a single scan from 280 nm to 500 nm in 0.5 nm steps was used and the integration time at each step was set to 30 s. To record spectrally narrow nitrogen radioluminescence lines in air over the solid sample, we used the grating model 53020 with a groove density of 1800 gr mm^{-1} blazed at 250 nm yielding to 1 nm spectral resolution. These modifications allowed us to record the well-known radioluminescence spectrum of air, shown in Figure 7a, in less than four hours. For the liquid sample, the procedure followed the steps described in section 2. The spectral resolution for a liquid sample was 6 nm and the scanning was performed from 280 nm to 550 nm in 3 nm steps, integrating for 10 s at each step. The spectral scan was repeated overnight for 88 times to achieve reasonable signal-to-noise ratio for the weak liquid radioluminescence resulting total recording time of 22 hours. Figure 7b shows the resulted spectrum of the aqueous solution under ionizing radiation. The correct spectral shape of the well-known radioluminescence of air in Figure 7a verifies that the calibration of spectral response has been successful and that the spectral shape of the liquid radioluminescence in Figure 7b can be trusted. The only additional elements in the optical path are the quartz cuvette and the water column, which both have negligible absorption at the measured wavelength range from 280 nm to 550 nm.

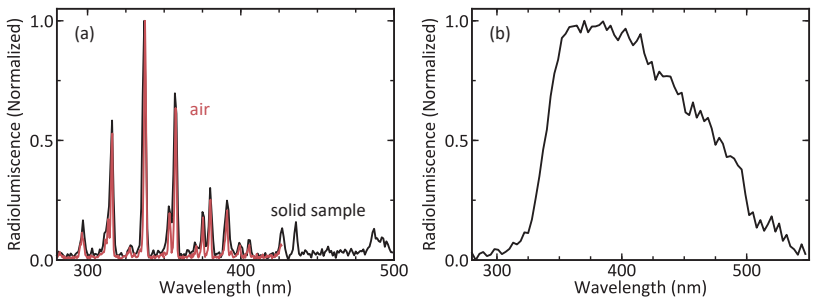

Figure 7. The normalized radioluminescence spectra of (**a**) light created by the solid sample (black) contrasted with this of air (red, data from [19]) (**b**) 750 ppm Am-241 in 3 M HNO_3 solution.

The normalized spectrum of the light produced by the solid sample in Figure 7a shows the N_2 lines [16], which is commonly associated with radioluminescence in air. This is congruent with other works investigating air radioluminescence [1,7,29]. To demonstrate the validity of the measurement, the spectrum has been superimposed with the normalized spectrum of radioluminescence in air which has been measured at a higher spectral resolution [19]. Contrary to the radioluminescence of air, the spectrum of aqueous solution under ionizing radiation has not been fully resolved earlier apart from a rough estimation using several long-pass filters [22]. Thus, the spectrum of the radioluminescence of aqueous solution in Figure 7b is, to the best of our knowledge, reported here for the first time. The radioluminescence is weak and spectrally broad, which makes it difficult to record. The spectrum shows a broad maximum between 350 nm and 400 nm with a gradual decrease until 550 nm at the longer wavelength side. On the other hand, the spectrum exhibits a pronounced decrease at shorter wavelength side reaching down to the background level already at 300 nm. This steep decreasing slope at shorter wavelength side contrasts with the earlier study done with long-pass filters [22], where they estimated a continuous increase towards the shorter wavelengths resembling the spectral shape of the Cerenkov light. Cerenkov light has a spectrum that is proportional to λ^{-2}, where λ is the wavelength of the emitted light [30]. The data in Figure 7 (b) clearly shows this is not the case with the radioluminescence of aqueous solutions, as there is the steep decrease at short wavelength side of the spectrum. Furthermore, alpha particles are not capable of producing Cerenkov light directly or through secondary mechanisms [31] and therefore we conclude that the measured radioluminescence must have an origin other than Cerenkov radiation. The spectral response of the measurement system is compensated in the results and the air radioluminescence spectrum with the same setup demonstrates the correct spectral shape down to 300 nm, thus validating the spectral response of the measurements. The only optical difference between the measurement arrangements is the quartz cuvette, which has a flat spectral transmittance over the whole measurement range and therefore no effect on the results. The steep decrease at the short wavelength side of the spectrum makes it uncharacteristic for broadband emissions such as Cerenkov light and bremsstrahlung emission. We rather speculate that some of the radiolysis products [32] of water, such as H_2O_2, OH or H_2, might be responsible for the recorded luminescence of water under the ionizing radiation.

4. Conclusions

We studied the radioluminescence produced by alpha active Am-241 dissolved into an aqueous solution of nitric acid. We showed that the amount of light created is about 150 times smaller than what is produced with same alpha activity by the radioluminescence of air. The low amounts of light made it necessary to use photon counting devices and intensified cameras to record the data. We analyzed the spatial distribution of the radioluminescence showing a very evenly distributed light emission. Furthermore, we showed for the first time the aqueous radioluminescence spectrum in the wavelength range between 280 nm and 550 nm, where we found a broad spectrum between 330 nm and 500 nm. The demonstrated radioluminescence is potentially useful in applications where visible background light can be avoided by light shielding, such as in radioactive liquid monitoring in closed chambers. We concluded that Cerenkov light, bremsstrahlung or other mechanisms producing broadband emission cannot be the source of the observed radioluminescence due to steep decrease at the short wavelength side of the recorded spectrum, which leaves intrinsic processes of water and its radiolysis products as strong candidates for the luminescence.

Acknowledgments: The authors wish to thank Business Finland, Finland Distinguished Professors (FiDiPro), Project Novel Instrumentation for Nuclear Safety, Security and Safeguard (NINS3), for the funding that made this project possible. The authors also wish to acknowledge the Actinide User Laboratory (AUL) in Karlsruhe, for providing access to their laboratories, sources, and infrastructure. The authors wish to especially thank Adrian Nicholl for his constant support before, during, and after the experiments.

Author Contributions: T.K.participated in designing the experiments, was part of execution of the experiments and handled the optics referred to in this study. R.M. and N.B. participated in designing the experiment, were

part in execution of the experiments and handled all the chemistry and radioactive sources referred to in this study. R.M. and J.T. planned, guided, and oversaw the collaboration leading to the conception of the experiments.

Conflicts of Interest: The authors declare no conflict of interest.

References

1. Arqueros, F.; Blanco, F.; Rosado, J. Analysis of the fluorescence emission from atmospheric nitrogen by electron excitation, and its application to fluorescence telescopes. *New J. Phys.* **2009**, *11*, 065011. [CrossRef]
2. Brown, A.; Suit, H. The centenary of the discovery of the Bragg peak. *Radiother. Oncol.* **2004**, *73*, 265–268. [CrossRef]
3. Williams, W.S.C. Nuclear Instability. In *Nuclear and Particle Physics*; Oxford University Press: Oxford, UK, 1991; pp. 66–80.
4. Baschenko, S.M. Remote optical detection of alpha particle sources. *J. Radiol. Prot.* **2004**, *24*, 27–92. [CrossRef]
5. Sand, J.; Ihantola, S.; Peräjärvi, K.; Toivonen, H.; Toivonen, J. Radioluminescence yield of alpha particles in air. *New J. Phys.* **2014**, *16*, 053022. [CrossRef]
6. Colin, P.; Chukanov, A.; Grebenyuk, V.; Naumo, D.; Nédélec,P.; Nefedov, Y.; Onofre,A.; Porokhovoi, S.; Sabirov, B.; Tkatchev, L; et al. Measurement of air and nitrogen fluorescence light yields induced by electron beam for UHECR experiment. *Astropart. Phys.* **2007**, *27*, 317–325. [CrossRef]
7. Sand, J.; Nicholl, A.; Hrnecek, E.; Toivonen, H.; Toivonen, J.; Peräjärvi, K. Stand-Off Radioluminescence Mapping of Alpha Emitters under Bright Lighting. *IEEE Trans. Nucl. Sci.* **2016**, *63*, 1777–1783. [CrossRef]
8. Pineau, J.F.; Imbard, G. Remote αsource location device and method, US Patent 6281502B1, 2001.
9. Lamadie, F.; Delmas, F.; Mahe, C.; Gironès, P.; Goaller, C.L.; Coestes, J.R. Remote Alpha Imaging in Nuclear Installations: New Results and Prospects. *IEEE Trans. Nucl. Sci.* **2005**, *52*, 3035–3039. [CrossRef]
10. Chichester, D.L.; Watson, S.M. Multispectral UV-Visual Imaging as a Tool for Locating and Assessing Ionizing Radiation in Air. *IEEE Trans. Nucl. Sci.* **2011**, *58*, 2512–2518. [CrossRef]
11. Feener, J.S.; Charlton, W.S. Preliminary results of nuclear fluorescence imaging of alpha and beta emitting souces. In Proceedings of the 2013 3rd International Conference on Advancements in Nuclear Instrumentation, Measurement Methods and their Applications (ANIMMA), Marseille, France, 23–27 June 2013.
12. National Renewable Energy Laboratory: Direct and Global 37 Deg Tilt: ASTM G-173. Available online https://www.astm.org/Standards/G173.html. (accessed on 27 February 2019).
13. Ivanov, O.; Danilovich, A.; Stepanov, V.; Smirnov, S.; Volkovich, A. Visualization of Radioactive Sources without Gamma-Radiation with UV Imaging Systems. In Proceedings of the 12th International Conference on Environmental Remediation and Radioactive Waste Management, Liverpool, UK, 11–15 October 2009; pp. 321–325.
14. Ivanov, O.P.; Stepanov, V.E.; Smirnov, S.V.; Volkovich, A.G. Development of method for detection of alpha contamination with using UV-camera "DayCor" by OFIL. In Proceedings of the 2011 IEEE Nuclear Science Symposium Conference Record. Valencia, Spain, October 23–29, 2011, pp. 2192–2194.
15. Crompton, A.; Gamage, K.; Bell, S.; Wilson, A.; Jenkins, A.; Trivedi, D. First Results of Using a UVTron Flame Sensor to Detect Alpha-Induced Air Fluorescence in the UVC Wavelength Range. *Sensors* **2017**, *17*, 2756. [CrossRef]
16. Lofthus, A.; Krupenie, P.H. The spectrum of molecular nitrogen. *J. Phys. Chem* **1977**, *6*, 113–307. [CrossRef]
17. Crompton, A.; Gamage, K.; Bell, S.; Wilson, A.; Jenkins, A.; Trivedi, D. Gas Flow to Enhance the Detection of Alpha-Induced Air Radioluminescence Based on a UVTron Flame Sensor. *Sensors* **2018**, *18*, 1842. [CrossRef]
18. Dondes, S.; Harteck, P.; Kunz, C. A Spectroscopic Study of Alpha-Ray-Induced Luminescence in Gases: Part I. *Radiat. Res.* **1966**, *27*, 174–210. [CrossRef]
19. Kerst, T.; Toivonen, J. Intense radioluminescence of NO/N2-mixture in solar blind spectral region. *Opt. Express* **2018**, *26*, 33764–33771. [CrossRef] [PubMed]
20. Duquesne, M.; Kaplan, I. Mesure de la luminescence induite par le rayonnement α du 210Po dans l'air et dans l'eau. *J. Phys. Radium* **1960**, *21*, 708–716. [CrossRef]
21. Yamamoto, S.; Komori, M.; Koyama, S.; Toshito, T. Luminescence imaging of water during alpha particle irradiation. *Nucl. Instrum. Meth. A* **2016**, *819*, 6–13. [CrossRef]

22. Yamamoto, S.; Akagi, T.; Yamashita, T.; Toivonen, J.; Yamaguchi, M.; Komori, M.; Kawachi, N. Source of luminescence of water lower energy than the Cerenkov-light threshold during irradiation of carbon-ion. *J. Phys. Commun.* **2018**, *2*, 065010. [CrossRef]
23. Sico GmBH: Transmission of Synthetic Quartz Glass (SQ) and Silu. Available online http://www.sico.at/assets/files/transmission.pdf. (accessed on 6 March 2019).
24. Live Chart of Nuclides. Available online https://www-nds.iaea.org/relnsd/vcharthtml/VChartHTML.html. (accessed on 22 January 2019).
25. Segelstein, D.J. The Complex Refractive Index of Water; Ph.D. Thesis, University of Missouri, Kansas City, MO, USA, 1981.
26. Sand, J.; Ihantola, S.; Peräjärvi, K.; Nicholl, A.; Hrnecek, E.; Toivonen, H.; Toivonen, J. Imaging of alpha emitters in a field environment. *Nucl. Instrum. Meth. A* **2015**, *782*, 13–19. [CrossRef]
27. Radioactive elements: Table of nucleids. Available online: http://www.kayelaby.npl.co.uk/atomic_and_nuclear_physics/4_6/4_6_1_part09_090_099.html. (accessed on 18 March 2019).
28. Egorov, O.B.; Addleman, R.S.; O'Hara, M.J.; Marks, T.; Grate, J.W. Direct measurement of alpha emitters in liquids using passivated ion implanted planar silicon (PIPS) diode detectors. *Nucl. Instrum. Methods Phys. Res. Sect. A* **2005**, *537*, 600–609. [CrossRef]
29. Waldenmaier, T. Spectral Resolved Measurement of the Nitrogen Fluorescence Yield in air Induced by Electrons. *Astropart. Phys.* **2008**, *29*, *205–222* [CrossRef]
30. Jelley, J. Cerenkov radiation and its applications. *Br. J. Appl. Phys.* **1955**, *6*, 227. [CrossRef]
31. Ackerman, N.; Graves, E. The potential for Cerenkov luminescence imaging of alpha-emitting radionuclides. *Phys. Med. Biol.* **2012**, *57*, 771. [CrossRef]
32. Christensen, H.; Sunder, S. Current State of Knowledge of Water Radiolysis Effects on Spent Nuclear Fuel Corrosion. *Nucl. Technol.* **2000**, *131*, 102–123. [CrossRef]

PUBLICATION

IV

Dynamic Enhancement of Nitric Oxide Radioluminescence with Nitrogen Purge

T. Kerst and J. Toivonen

accepted for publication in 'Scientific Reports' (2019)

Dynamic Enhancement of Nitric Oxide Radioluminescence with Nitrogen Purge

Thomas Kerst[1,2,*] **and Juha Toivonen**[1]

[1]Photonics Laboratory, Physics Unit, Tampere University, Tampere, Finland
[2]Helsinki Institute of Physics, Helsinki University, Helsinki, Finland
[*]thomas.kerst@tuni.fi

ABSTRACT

Remote detection of alpha radiation is commonly realised by collecting the light, the radioluminescence, that is produced when alpha particles are stopped in air. Radioluminescence of nitric oxide (NO) is primarily emitted between $200\,\mathrm{nm}$ and $300\,\mathrm{nm}$, which makes it possible to use it for remote detection under daylight conditions. Quenching by ambient oxygen and water vapour, however, makes it generally difficult to effectively create NO radioluminescence. We present the detection of intense NO radioluminescence in ambient air under standard indoor lighting conditions using a nitrogen purge. The nitrogen contained NO impurities that were intrinsic to the gas and had not explicitly been added. We study the mechanisms that govern the NO radioluminescence production and introduce a model to describe the dynamics of the process. The level of NO contained in the gas was found to determine how successful a purge can be. We conclude by discussing possible applications of the technique in nitrogen-flushed gloveboxes at nuclear facilities where NO concentration of $100\,\mathrm{ppb} - 1\,\mathrm{ppm}$ would be sufficient for efficient optical alpha radiation detection in standard lighting conditions.

Introduction

An alpha particle that is being stopped in air causes the production of light. Upon decay, an atomic nucleus loses energy by emitting a combination of alpha particles, beta particles, and gamma radiation. All three forms of radiation are ionising, which means that they can detach electrons from atoms or molecules. Electrons freed through ionisation deposit their energy into the matter they interact with, which can cause it to become electronically excited.[1,2] When this excitation is lost in a radiative process, then the generated light is called radioluminescence rather than fluorescence. The radioactive decay had to occur for the photon to be generated, and the name highlights this fact.

Radioluminescence is a useful indicator for the presence of alpha radiation. Unlike other forms of nuclear radiation, alpha radiation is very localised. Alpha particles do not travel further than about 4 cm in air, whereas beta and gamma radiation can reach distances of about 1 m and 50 m, respectively.[3] All ionising radiation can create radioluminescence. However, alpha radioluminescence is special in that it travels much farther than the alpha particles themselves. This gives any alpha radiation detection scheme based on radioluminescence two key advantages over those based on direct interaction. The scheme works at much larger distances, and equipment does not need to be exposed to the particles themselves, which present a particularly large hazard to both personnel and equipment.[4,5] In short, it enables the remote detection of alpha radiation from a safe distance. In the rest of this article, we focus exclusively on alpha radiation-induced radioluminescence and address it by the shorthand "radioluminescence".

In ambient air, nitrogen (N_2) radioluminescence is a reliable indicator for the presence of alpha radiation. Alpha particles create free electrons which then electronically excite nitrogen molecules.[1] Those excitations that radiatively decay over the $C^3\Pi_u \rightarrow B^3\Pi_g$ transition cause the emission of photons whose spectral pattern is commonly referred to as 'Second Positive System' (or '2+' in short), which primarily consists of ultraviolet light emitted between 320 and 400 nm and a notably strong peak around 337 nm.[3,6,7] A small fraction of the N_2 radioluminescence is emitted in the deep ultraviolet regime, where it reaches wavelengths as short as 260 nm.[8] In principle, the 2+ comprises light with even shorter wavelengths, however the shortest wavelengths used so far to remotely detect alpha radiation have been around 260 nm.[6,8] The spectral pattern of N_2 radioluminescence is very characteristic, and it is generally accepted that under normal circumstances detecting light emitted on the 2+ system is a good indicator for the presence of alpha radiation.

Radioluminescence in air is very weak compared to other light sources, such as the sun. A single alpha particle stopped in air produces of a small amount of roughly 100 UV photons which are isotropically radiated away.[3,7] Consequently, even strong alpha sources provide few photons that can be used for remote detection at reasonable distances. For this reason, radioluminescence detection schemes generally rely on technology capable of detecting individual photons.[5] For instance,

detecting N_2 radioluminescence with a photomultiplier tube (PMT) in a UV-background lighting free environment is generally possible. In a recent contribution, a PMT equipped with optimised light collection optics was able to resolve sources with surface activities as low as 300 Bq mm^{-2} at 1 m distance.[8] Some cameras, too, are sufficiently sensitive to detect radioluminescence. In recent years a sizable body of works has accumulated reporting on the successful imaging of alpha radiation using various types of specialised cameras like ICCD and EMCCD.[4,9–11]. Both types of collecting radioluminescence have made it possible to detect alpha radiation in difficult-to-access areas like gloveboxes and hot-cells from a safe distance.[10,12,13]

The presence of UV background light makes N_2 based remote detection difficult. By in large, the remote detection schemes demonstrated so far rely on the assumption that the presence of UV light is an indicator good enough to potentially reveal the presence of alpha radiation. If, however, any other UV light source other than radioluminescence is present, this assumption no longer holds. Some of the presented technologies tackle this problem by tailoring the detection optics to only transmit light of wavelengths around 337 nm while rejecting all others.[8] However, a UV background at just those wavelengths can supersede the faint radioluminescence. Sunlight reaching the surface of the earth is such a light source.[14] It is for this reason that remote detection of alpha radiation with sunlight present is a much more challenging task than without it.[8,15]

One way to make N_2 radioluminescence detection operable in daylight is by making the detection optics solar blind. Sunlight that is emitted between 100 to 280 nm is absorbed by ozone in the upper atmosphere and does not reach the earth's surface.[14,16] This part of the electromagnetic spectrum is called the UVC region and its essential characteristic is the absence of sunlight that reaches the earth surface. Making the optics unresponsive to photons of wavelengths longer than 280 nm, that is to make it solar blind, while leaving it responsive to the UVC adequately addresses the issue. Sand et al. successfully built and demonstrated such a system in a field environment using a caesium-telluride PMT and a set of bandpass filters centred around 260 nm.[8] Another successful demonstration of an optical system with a tailored response was by Ivanov et al. who imaged N_2 radioluminescence using a UVC-sensitive camera that at the same time was insensitive to sunlight.[17] However, all those approaches suffer from the fact that only a small portion of N_2 radioluminescence is located in the UVC region.[18] Restricting the optical response of the detection system to the UVC limits its ability to detect weaker alpha sources. By using solar blind optics, the detection system gains the ability to operate under daylight conditions but at the same time severely reduces its sensitivity.

Another way to address a daylight background is to use radioluminescence from molecules other than N_2. A wide variety of species have been shown to produce radioluminescence, where OH, CN, NH, CO_2, N_2^+, He_2, O^- are only a few of them.[19–21] Most of them, however, are generally irrelevant for detecting alpha particle radiation since they are commonly not present where remote detection would be required. In most cases, alpha contamination is surrounded by air, which typically limits the useful species to N_2. It is the only species that both is sufficiently abundant and at the same time produces radioluminescence that it is not as strongly affected by O_2 and H_2O quenching like radioluminescence from most other species is.[18,22–25] If, however, one can alter the atmosphere around an alpha emitter, then one is no longer limited to relying on N_2 as luminescent species. In a recent study, Crompton and colleagues tested a few known radioluminescent species for their aptitude to be used in remote detection of alpha radiation.[15] Among others, they found that xenon is a strong candidate that could potentially be used to address the daylight issue.

Another molecule that is potentially useful as luminescent species is nitric oxide (NO). NO can produce radioluminescence that is almost exclusively located in the UVC by forming the so-called NO γ-band between 200 nm and 300 nm.[26] Its advantageous spectrum combined with its ability to quickly re-excite after a radiative decay by interaction with N_2 makes NO a strong candidate.[27] A nitrogen molecule that has been excited by the presence of an alpha source transfer its excitation to a nitric oxide molecule, where it radiatively decays as radioluminescence. This process is very efficient and thus introducing some nitric oxide to an otherwise pure nitrogen atmosphere leads to the production of large amounts of UVC radioluminescence. Adding as little as 50 ppm of NO alpha emitter can increase the overall radioluminescence yield 25-fold, where almost all of the so-created radioluminescence is located in the UVC.[28] The conditions under which this can be achieved have to be very controlled and potent quenchers like O_2 and H_2O have to be absent.[22,23,28] In ambient air, where NO is present in concentrations ranging between tens of ppt and tens of ppb,[29] those quenchers are very abundant which renders nitric oxide radioluminescence generally unpractical. However, if conditions can be created that favour its production, nitric oxide radioluminescence is a viable option to generate intense radioluminescence in the UVC.

In this paper, we present radioluminescence emanating from nitric oxide impurities in otherwise pure nitrogen and study the conditions under which it arises. We demonstrate that higher levels of impurities not only increase the overall intensity of the radioluminescence but also speed up the process that maximises its production rate. We show that the predictions made by the model of NO radioluminescence production based on excitation transfer match with the predictions made by more established theories. We provide further evidence for the plausibility of the model by showing that a simulation which is based on a description with excitation transfer can replicate experimental findings. We experimentally demonstrate that a nitrogen purge with adequate levels of impurities can produce large amounts of UVC photons around an alpha emitter placed in ambient air. We conclude our work by discussing the usefulness of a nitrogen purge in nuclear research facilities.

Methods

All experiments were carried out in one of two distinct arrangements which are sketched in Fig. 1. With Arrangement A, we studied the dynamics of NO radioluminescence production by placing an alpha emitter in a glass tube where we precisely controlled the gas atmosphere. With arrangement B, we studied how efficiently UVC radioluminescence can be generated in ambient air by placing the same emitter in ambient air and applying a nitrogen purge. In both arrangements, we used the same 32 MBq alpha active Am-241 source. The active area of the source was 50 mm in length and 12.5 mm in width. In both arrangements, we used nitrogen gas to modify the radioluminescence production (AGA, Product Codes: Instrument Nitrogen 5.0 and Scientific Nitrogen 6.0). Instrument Nitrogen 5.0 contained impurities up to a total volume concentration of 10 ppm and a NO volume concentration of 5 ppb, to which we refer by using the shorthand N_2 (NO: 5 ppb). Scientific Nitrogen 6.0 contained impurities up to a total volume concentration of 1 ppm and a NO volume concentration of 50 ppb, to which we refer by using the shorthand N_2 (NO: 50 ppb). The NO concentrations had been verified using a chemiluminescence analyser[30] which we calibrated using a N_2 gas sample containing a known NO concentration.

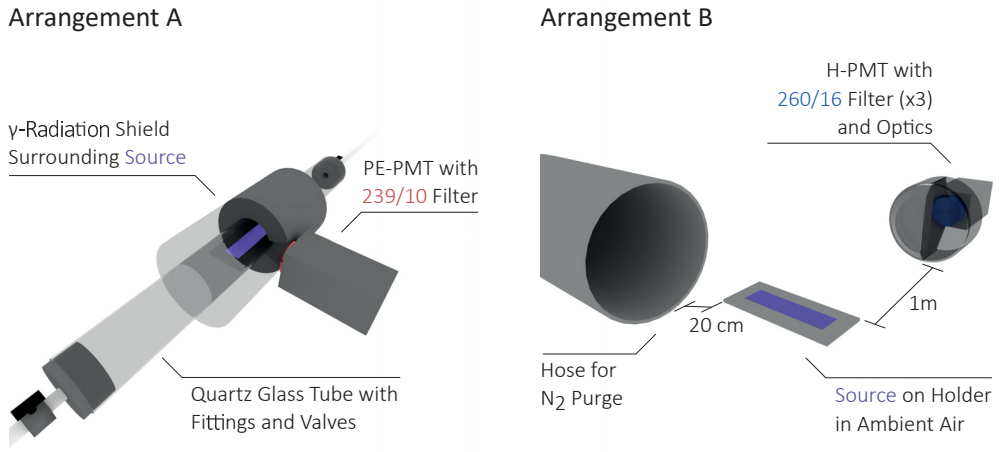

Figure 1. The experimental arrangements used in this work. In **Arrangement A** we placed a 32 MBq alpha source on glass holder resting inside a quartz glass tube. A UVC-sensitive PMT equipped with a 239/10 optical bandpass filter picked up radioluminescence emanating inside it. A metal shield around the tube protected both personnel and equipment from γ radiation. The glass tube was connected to a system of mass flow controllers that allowed to flush with either a N_2 (NO: 5 ppb) or N_2 (NO: 50 ppb) at different flow rates. Valves allowed to prevent gas exchange with the laboratory air. In **Arrangement B**, we placed the same alpha source in ambient air and installed a large diameter hose in 20 cm distance to it. The hose provided a purge with either N_2 (NO: 5 ppb) or N_2 (NO: 50 ppb). A UVC-sensitive PMT equipped with a stack of three 260/16 optical bandpass filters and an adequate objective was placed at a distance of about 1 m and picked up light emanating from the source.

Radioluminescence Dynamics

With arrangement A, we studied the dynamics of radioluminescence production by placing the source in a quartz glass tube and controlled the atmosphere inside with a set of mass flow controllers and valves. The quartz glass tube was 1 m long, had an outer diameter of 30 mm and 1.5 mm thick walls (Robson Scientific, Product Code: RQT 30). The source rested on a rectangular sample holder made of glass at the centre of the tube. A 21 mm thick steel mantle surrounded the glass tube, protecting personnel and equipment from gamma radiation. A cone-shaped hole with the f-number $f/1.378$ in the steel mantle allowed light originating close to the source to escape the tube and be collected by a UV-sensitive photomultiplier tube (PMT, Perkin-Elmer, Product Code: MP-1082, Dark Count: < 1 cps). An optical bandpass filter between PMT and tube only transmitted light around the wavelength 239 nm with a FWHM of 10 nm (Edmund Optics, Product Code: 67805, transmittance shown in Fig. 2 in red).[31] By using a filter with a transmittance spectrum deep in the UVC, we made sure that we only studied the dynamics of NO radioluminescence. Some of the NO radioluminescence could pass the filter and reach the detector, while radioluminescence of N_2 was prevented from doing so. We controlled the atmosphere inside the tube with two mass flow controllers (MFC, Bronkhorst High-Tech, Product Codes: 18BRF-201CV-10K and 18BRF-201CV-20K), where each controller

had access to either type of used nitrogen. We sealed the tube with custom fittings to shield the atmosphere inside the tube from laboratory air and made sure that the tube was only connected to the MFCs, and a gas exhaust and mechanical valves (Swagelok, Product Code: SS-6P4T-MM-BK). All tubings were kept as short as possible to prevent the formation of large dead volumes.

We studied the dynamics of radioluminescence production by monitoring the changes in radioluminescence intensity when a flow of nitrogen that had been applied for 30 min was suddenly stopped. In each experiment we flushed the laboratory air-filled tube with either 1 SLPM, 2 SLPM or 4 SLPM of either N_2 (NO: 5 ppb) or N_2 (NO: 50 ppb). Then we stopped the flow, closed the valves and continued to monitor the radioluminescence intensity for another 10 min. Before experimenting, we removed the glass tube from the setup and exposed it to normal laboratory air for at least 2 hours. This way we made sure that all flow experiments were carried out with identical initial conditions: The initial atmosphere inside the tube was always ambient laboratory air, and the initial amount of water present at the inside tube walls was always the same. We took those measures to address the problem of changing water concentrations during our experiments. Water forms a thin film on glass surfaces[32], and it was challenging to remove this film to the degree that would be required to make radioluminescence quenching negligible.[23] At the same time, it was difficult to keep the water concentration constant during the experiment, such that water quenching would reduce the overall NO radioluminescence but not change the observed dynamics that we intended to study. Flushing slowly but gradually removed water from the walls, making it impossible to keep the water concentration constant. Thus it was sensible to address the issue by considering the influence of water when post-processing the data and making sure that each experiment was carried out with identical initial conditions.

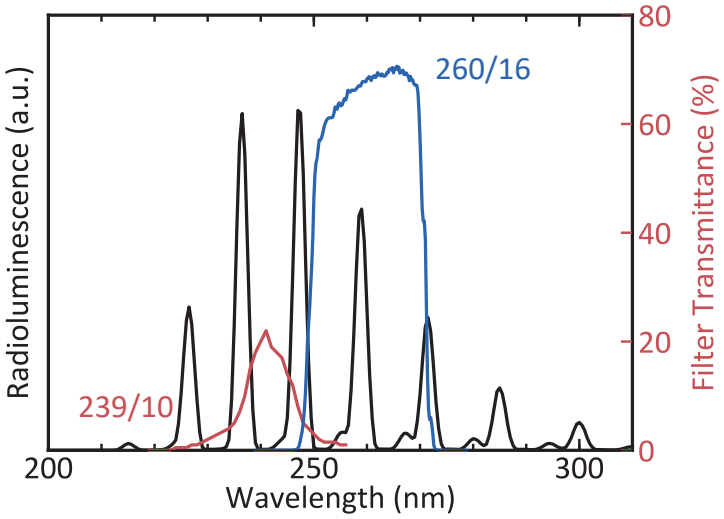

Figure 2. The spectrum of NO radioluminescence and the transmittance of the bandpass filters used in this work. NO produces radioluminescence (black, taken from Kerst et al.[28]) that appears in distinct spectral lines between 200 nm and 320 nm.[26] The optical filters used for either setup only transmitted parts of the spectrum. Arrangement A used a filter (red) that transmitted light around 239 nm with a FWHM of 10 nm and a peak transmittance of about 20 %.[31] Arrangement B used a stack of three filters (blue), each of which transmitted light around 260 nm with a FWHM of 16 nm and a peak transmittance of about 70 %.[33] The stack of all three of these filters had a peak transmittance of about 30 %.

Remote Detection

With arrangement B we studied how useful of a nitrogen flush can be in producing NO radioluminescence in otherwise ambient air. For this experiment, we placed the source in ambient air under normal lighting conditions. We placed a hose with 10 cm diameter in 20 cm distance to it which was able to provide a purge using either type of nitrogen. In 1 m distance we placed a caesium-telluride photocathode PMT (Hamamatsu, Product Code: H11870-09) and equipped it with an objective made of standard UV fused silica lenses as described in Sand et al.[8] a stack of three identical bandpass filters that transmitted light around 260 nm with an FWHM of 16 nm (Semrock, Product Code: FF01-260/16-25, transmittance of a single filter shown in

Fig. 2 in blue).[33] The filters chosen for this arrangement had peak transmittances superior to this in arrangement A and were better suited to detect increases in radioluminescence production in ambient air. We carried out an experiment by applying a purge of about 100 SLPM of either N_2 (NO: 5 ppb) or N_2 (NO: 50 ppb) for about 5 seconds. At all times, we measured the UVC light emanating from the source.

Results and Discussion

Radioluminescence Dynamics

Radioluminescence Dynamics

Fig. 3 shows the dynamics of the radioluminescence we observed upon stopping the nitrogen flow. Flushing with N_2 (NO: 50 ppb) produced significantly more radioluminescence than flushing with N_2 (NO: 5 ppb) and flushing with more litres per minute produced more radioluminescence than flushing with fewer. After stopping the flow, the radioluminescence intensity jump-like increased for N_2 (NO: 5 ppb) but not for N_2 (NO: 50 ppb). For both gases, however, the intensity gradually decreased after the flow had been stopped. We hypothesise this decrease to be caused by quenching by water vapour, which diffused into the optical volume. In the absence of a nitrogen flow, water vapour no longer got flushed out and could concentrate in the optical volume. A concentration of water vapour could also explain the observation that a larger mass flow resulted in more radioluminescence production since a larger mass flow provided more nitrogen in which water vapour could be diluted into, thus reducing the effects of quenching. Water quenches nitric oxide radioluminescence very efficiently, and even ppm-levels of water vapour have a significant effect on the radioluminescence intensity.[22,23]

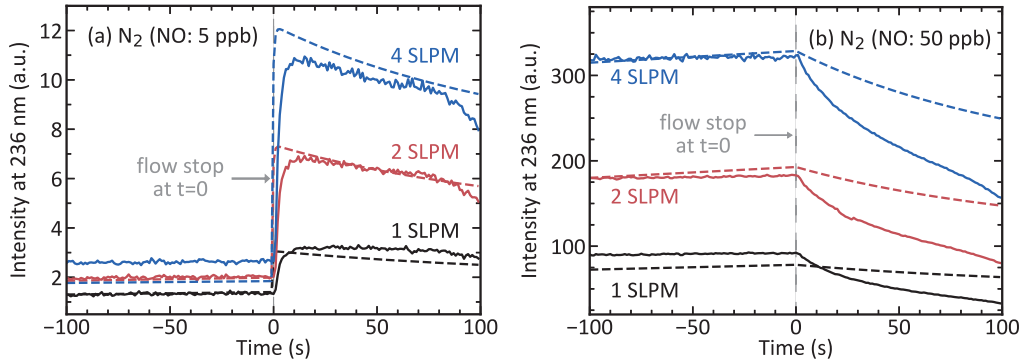

Figure 3. The dynamics of NO radioluminescence in the tube once a previously applied nitrogen flow had been stopped. A 30 min lasting nitrogen mass flow of 1, 2 or 4 SLPM of either **(a)** N_2 (NO: 5 ppb) or **(b)** N_2 (NO: 50 ppb) had been stopped and the valves closed at $t = 0$. For N_2 (NO: 5 ppb) gas, stopping the flow caused an immediate jump-like increase in the radioluminescence, whereas for N_2 (NO: 50 ppb) gas it did not. For both gases, radioluminescence gradually decreased afterwards. Solid lines show the measured data and dashed lines the best fit of the simulation to it.

The more intense radioluminescence produced by a N_2 (NO: 50 ppb) flush can not be explained with a higher amount of nitric oxide alone. N_2 (NO: 50 ppb) contained 10 times more nitric oxide than N_2 (NO: 5 ppb). Thus, it is sensible to assume that under equilibrium conditions N_2 (NO: 50 ppb) produces significantly more radioluminescence, given that nitric oxide with concentrations that small exhibits negligible self-quenching.[23] However, the data reveals that the increase in radioluminescence production is different whether the flow had been stopped or not. Before stopping, the radioluminescence was about 100 times and after stopping about 30 times more intense, irrespective of whether the intensities for a mass flow of 1, 2 or 4 SLPM are compared. We, therefore, conclude that before the flow had been stopped, radioluminescence produced by N_2 (NO: 5 ppb) had not fully developed, and it can not be assumed that the system was in equilibrium.

More careful consideration of the processes that lead to the production of nitric oxide radioluminescence offers a better explanation. NO radioluminescence is produced as the last step in a chain of three consecutive events: first alpha radiation excites surrounding molecular nitrogen into the long-lived $A^3\Sigma_u^+$ state, then this excitation is transferred to ground state nitric oxide where it causes the $A^2\Sigma^+$ state to be populated and lastly this excitation radiatively decays by emitting a photon.[26,28] Nitric oxide decays with a natural lifetime of approximately 200 ns,[34] which is considerably shortened in the presence of potent quenchers like water vapour and molecular oxygen.[22,23] Thus, the mechanism that limits the speed by which NO

radioluminescence is produced is the speed by which the excitations are transferred. The rate equation[28]

$$\frac{\mathrm{d}}{\mathrm{d}t}[\mathrm{N}_2^{\mathrm{A}}] = \alpha[\mathrm{N}_2^{\mathrm{X}}] - k_{\mathrm{f}}[\mathrm{N}_2^{\mathrm{A}}] - k_{\mathrm{et}}[\mathrm{NO}^{\mathrm{X}}][\mathrm{N}_2^{\mathrm{A}}] \tag{1}$$

describes this transfer, where $[\mathrm{N}_2^{\mathrm{X}}]$, $[\mathrm{N}_2^{\mathrm{A}}]$ and $[\mathrm{NO}^{\mathrm{X}}]$ are the concentrations of ground state nitrogen, excited state nitrogen and ground state nitric oxide, respectively. α is the rate by which the alpha radiation excites nitrogen and $k_{\mathrm{et}}[\mathrm{NO}^{\mathrm{X}}]$ the rate by which those excitations are transferred to ground state nitric oxide. Nitrogen fluorescence is with a rate of $k_{\mathrm{f}} \approx 0.4\,\mathrm{Hz}$[6] very slow compared to excitation transfer and thus negligible. Further, the short lifetime of excited nitric oxide makes it that most of the nitric oxide is present in the ground state, i.e. one can approximate $[\mathrm{NO}^{\mathrm{X}}] \approx [\mathrm{NO}]$, where $[\mathrm{NO}]$ the total nitric oxide concentration. Such an approximation allows to express the excited state nitrogen concentration $[\mathrm{N}_2^{\mathrm{A}}]$ after a time t after first exposure to the alpha source with a simple exponential function

$$[\mathrm{N}_2^{\mathrm{A}}](t) = [\mathrm{N}_2^{\mathrm{A}}]_\infty \left(1 - e^{-\gamma t}\right), \tag{2}$$

where $[\mathrm{N}_2^{\mathrm{A}}]_\infty$ is the equilibrium concentration and $\gamma = k_{\mathrm{et}}[\mathrm{NO}]$ the speed by which this equilibrium is approached. In this model the rate of excitation transfer limits the rate by which radioluminescence is produced, thus the radioluminescence intensity $I(t)$ is proportional to the excited state nitrogen concentration $[\mathrm{N}_2^{\mathrm{A}}](t)$. With this model, the jump-like behaviour of N_2 (NO: 5 ppb) induced radioluminescence can be understood as a result of the excited state nitrogen not having reached equilibrium concentration during the short amount of time it was exposed to the source during flushing. For a NO concentration of 5 ppb the model estimates a rise-time of roughly 90 ms for the radioluminescence to reach half its maximum intensity and 600 ms to reach 99 %. With flows in the range of litres per minute, the time the gas is exposed to the source is a few hundreds of milliseconds or less, which does not allow the gas to reach maximum radioluminescence production. After stopping the flow, however, it had sufficient time and eventually reached maximum intensity. According to the model, this happens in less than a second, which is in agreement with the measured data. N_2 (NO: 50 ppb) contained much more nitric oxide and, according to the model, approached the equilibrium much faster. Thus stopping the flow and exposing it longer to the source did not have as much of an effect as it had for N_2 (NO: 5 ppb).

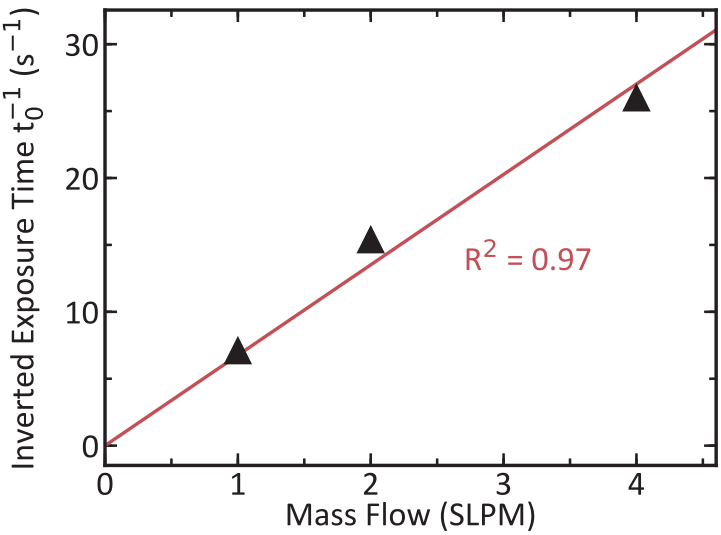

Figure 4. The estimated time the N_2 (NO: 5 ppb) is exposed to the source displayed inverted against the mass flow. The estimates (black) have been calculated by numerically solving Eq. (3) using data from Fig. 3 (a). A linear fit crossing the coordinate origin (red) with goodness of fit $\mathrm{R}^2 = 0.97$ shows that the exposure time is inversely proportional to the mass flow.

Our interpretation of the data based on excitation transfer makes predictions about the experiment that match those made by more established theories. In Eq. (2), our model links the radioluminescence intensity of a partially evolved system to this of a fully evolved one using the excitation transfer rate and the time t_0 the gas is exposed to the source. By applying this to the stop-flow behaviour of the radioluminescence of N_2 (NO: 5 ppb), the exposure time as a function of the mass flow can be estimated. The relation between mass flow and exposure time can be tested for its compliance with the fundamental principles of fluid dynamics. To properly apply the model to the measured data, it has to be adjusted to include the fact that the PMT picked up light emanating from all parts of the source. Radioluminescence produced at the start of the source is less intense than this produced at the end of it. By approximating all parts to equally contribute to the total intensity, irrespective of their actual distance to the PMT, the intensity measured by the PMT can be expressed by calculating the simple average and a multiplying with a geometry-specific scaling constant C, which is to say

$$I_{\mathrm{PMT}}(t_0) = C \cdot \frac{1}{t_0} \int_0^{t_0} I(t)\,\mathrm{d}t = C \cdot I_\infty \left(1 - \frac{1 - e^{-\gamma t_0}}{\gamma t_0}\right). \tag{3}$$

We numerically solved this equation for the exposure time t_0 for all three mass flows Q. For $I_{\mathrm{PMT}}(t_0)$ we used radioluminescence values from Fig. 3 (a) at $t < 0$ and for $C \cdot I_\infty$ values at $t > 0$. We picked values around $t = 0$ to ensure that the amount of water in the tube at both points in time was similar. The so-calculated inverted exposure times are plotted against the mass flow in Fig. 4. There it can be noticed that exposure time and mass flow are inversely proportional to each other, which we highlighted by adding a linear regression with zero offset and quality of fit $R^2 = 0.97$. This inverse relationship is congruent with the predictions of fluid dynamics. Nitrogen gas is a Newtonian fluid and as such travels over the length of the source in a time $t_0 \sim Q^{-1}$, if the flow is laminar.[35] In our system, the Reynolds numbers for all flows were well below the values for which transitions to turbulent flows might start to occur.[36]

We further tested how well our model can replicate the dynamics of the stop-flow behaviour by fitting a simulation of the experiment to the measured data. The simulation is based on the model of NO radioluminescence production described by Kerst et al.[28] This description consists of a set of rate equations which we amended by a second set of rate equations that modelled the changing water concentration in the tube. We solved the first set of equations using an ODE solver[37] where we simplified the calculation by assuming that all layers of the gas over the source moved at identical speed and were equally exposed to alpha radiation, much as it has been done in Eq. (3). All rate equations had been amended to account for quenching by water using known quenching constants.[22,23,38] The geometry of the system, filter transmittance and PMT quantum efficiency have been included using a global scaling constant. We modelled the water dynamics as simple as possible but still able to include diffusion and effects of flushing. For that, we approximated the water to be present in one of two distinct reservoirs. Reservoir I represented the optical volume, and water present here quenched the radioluminescence. When a mass flow was present, the water concentration lowered and quenching reduced. Reservoir II represented the parts of the system that were unaffected by flushing, like glass walls and other adhesive surfaces. We modelled it to exchange water with reservoir I using ordinary linear differential equations of the form

$$\frac{\mathrm{d}}{\mathrm{d}t}[\mathrm{H_2O}]_{\mathrm{wall}} = -k_{\mathrm{diff.}}[\mathrm{H_2O}]_{\mathrm{wall}} + k_{\mathrm{adh.}}[\mathrm{H_2O}]_{\mathrm{vol.}} \tag{4}$$

$$\frac{\mathrm{d}}{\mathrm{d}t}[\mathrm{H_2O}]_{\mathrm{vol.}} = k_{\mathrm{diff.}}[\mathrm{H_2O}]_{\mathrm{wall}} - k_{\mathrm{adh.}}[\mathrm{H_2O}]_{\mathrm{vol.}} - k_{\mathrm{flow}}\Phi[\mathrm{H_2O}]_{\mathrm{vol.}}, \tag{5}$$

where Φ is the mass flow in SLPM. All parameters introduced with this simple model were free for the optimiser to tune.

We optimised the parameters such that the simulation best fits all six measured curves all at once,[39] which means that all simulated curves used identical parameters and only differed in nitric oxide concentration and mass flow. The simulated curves were superimposed on the measured data and are shown in Fig. 3. The curves correctly replicate key features of the measured data. They show that N_2 (NO: 5 ppb) induced radioluminescence is much less intense than this of N_2 (NO: 50 ppb). They also show that only N_2 (NO: 5 ppb) features a jump-like behaviour upon stopping. The gradual diminishing of the radioluminescence after stopping is replicated by the simulation, too. None of the simulated curves fits the corresponding data perfectly well, however. The imperfect fit is likely due to our very simplified model of the water dynamics. The key concept of the model, however, is well captured. The simulation clearly shows that differences in radioluminescence intensity and stop-flow behaviour can be explained with the dynamics of excitation transfer.

Remote Detection

In Fig. 5 we show that a nitrogen purge can make an alpha emitter produce large amounts of UVC radioluminescence. The source was placed in ambient air, which allowed oxygen and water to quench both a significant fraction of the nitrogen[38] and

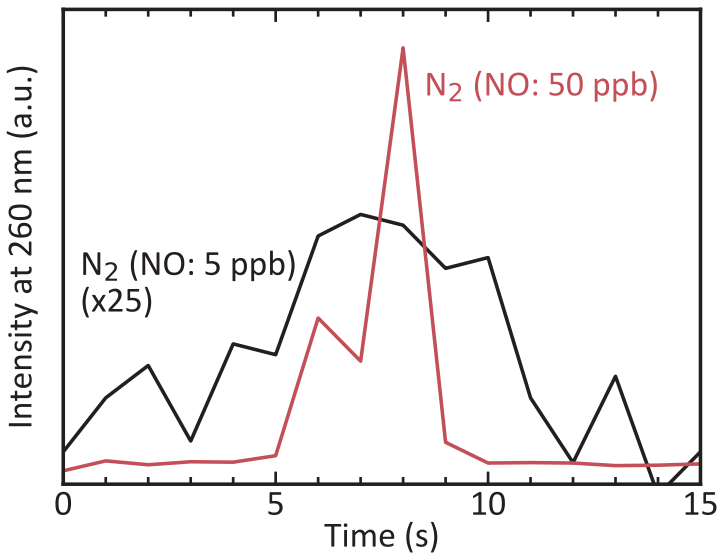

Figure 5. Radioluminescence at 260 nm measured in broad daylight and ambient air. The alpha source has been exposed to a brief but intense nitrogen purge of either N_2 (NO: 5 ppb) (black, 25 times magnified) or N_2 (NO: 50 ppb) (red). For both types of gas, the purge temporarily increased the detected radioluminescence. N_2 (NO: 50 ppb) was about 50 times more effective in doing so.

almost all of nitric oxide radioluminescence[22,23]. However, by applying a few seconds long lasting nitrogen purge, we created a brief period of increased radioluminescence production. The likely explanation for this behaviour is a reduced influence of quenchers. The purge temporarily replaced the atmosphere around the alpha emitter with NO impurity containing nitrogen, thereby creating an atmosphere similar to this in the tube. Under these conditions, quenchers are absent, and radioluminescence is created more efficiently. When the purge ends, atmospheric conditions turn unfavourable again, and radioluminescence production declines.

The additional radioluminescence produced during the purge consists mostly of contributions from nitric oxide. The stack of interference filters used in this experiment transmitted light around 260 nm[33] and thus allowed both nitrogen and nitric oxide radioluminescence to reach the PMT. However, nitric oxide is likely to make up the bulk of it, which can be inferred from the observation that a purge with N_2 (NO: 50 ppb) lead to a more than a hundred-fold increase in intensity. In a pure nitrogen atmosphere nitrogen radioluminescence can only be about six times more intense than in air.[7,8,15] Thus, the increase in intensity is likely caused by a vastly increased nitric oxide radioluminescence production.

Purging with nitrogen that contains slightly elevated levels of NO concentration is beneficial for enhancing UVC radioluminescence. The direct comparison of the radioluminescence increase in Fig. 5 shows that N_2 (NO: 50 ppb) is disproportionally more effective than N_2 (NO: 5 ppb) in amplifying the light production, when compared to the respective gases' nitric oxide content. This disproportionally weak radioluminescence produced by a N_2 (NO: 5 ppb) purge can be explained the same way the low light production of the N_2 (NO: 5 ppb) flow in the tube has been. In Eq. (2) we concluded that nitric oxide radioluminescence approaches maximum light production in an exponential manner with a speed $\gamma = k_{et}[\mathrm{NO}]$. The higher the NO concentration, the faster the radioluminescence production maximises. In the flow experiment, the radioluminescence from N_2 (NO: 5 ppb) did not fully develop because its NO content was too small for the production to maximise during the brief amount of time the gas was exposed to the source. During a purge, the time the gas remains over the source is even shorter and hence it is to be expected that radioluminescence will not maximise. N_2 (NO: 50 ppb) with a ten times higher concentration of NO did not have those problems and thus showed a disproportionally increased radioluminescence production. This reasoning makes a slightly elevated amount of NO not only beneficial for the additional UVC production, but it also puts less strict requirements on the time the gas needs to be in the active area for purge-induced NO radioluminescence production to be effective.

Conclusions

In this paper, we demonstrated the production of NO radioluminescence in ambient air. We did so by applying a N_2 purge that contained NO impurities, which were intrinsic to the gas. It was argued that for such a purge to create NO radioluminescence, the N_2 gas needs to contain an amount of NO that is dependent on the time the gas remains in the active area. The shorter this time, the more NO is needed. Using N_2 with elevated levels of NO is generally a good option compared to N_2 with lower levels of NO. This rule holds as long as self-quenching does not significantly affect the radioluminescence production, which is the case for NO concentrations up to about 50 ppm.[28]

We have shown that NO radioluminescence can be detected in standard indoor lighting conditions using an N_2 purge that contains NO impurities in concentrations as small as 5 ppb and 50 ppb. The intensity of the produced radioluminescence differs whether the gas is flown over the alpha source or whether it stays static. Under flow conditions, the NO radioluminescence intensity is reduced by the flow due to a limited rate of the energy transfer process. The model explains this behaviour very well, and it can predict the levels of NO that are required in an otherwise pure N_2 flow to produce intense NO radioluminescence. The model can be used to tailor the application-specific gas atmosphere around an alpha emitter under flow conditions. Concentrations higher than 1 ppm can be harmful for life,[40] so in practice, suitable NO concentrations would be in the range of 100 ppb − 1 ppm for safety reasons. The technique can be directly utilised in nitrogen-flushed gloveboxes at nuclear facilities for efficient optical alpha radiation detection in standard lighting conditions.

Data Availability

The datasets generated during and/or analysed during the current study are available from the corresponding author on reasonable request.

References

1. Arqueros, F., Blanco, F. & Rosado, J. Analysis of the fluorescence emission from atmospheric nitrogen by electron excitation, and its application to fluorescence telescopes. *New J. Phys.* **11**, 065011, DOI: 10.1088/1367-2630/11/6/065011 (2009).
2. Brocklehurst, B. & Downing, F. Mechanisms of excitation of luminescence in nitrogen gas by fast electrons. *The J. Chem. Phys.* **46**, 2976–2991 (1967).
3. Baschenko, S. M. Remote optical detection of alpha particle sources. *J. Radiol. Prot.* **24**, 75–82, DOI: 10.1088/0952-4746/24/1/006 (2004).
4. Lamadie, F. *et al.* Remote alpha imaging in nuclear installations: new results and prospects. *IEEE Transactions on Nucl. Sci.* **52**, 3035–3039, DOI: 10.1109/TNS.2005.862911 (2005).
5. Haslip, D. S. *et al.* Standoff radiation imaging detector (2006). US Patent 7,317,191 B1.
6. Lofthus, A. & Krupenie, P. H. The spectrum of molecular nitrogen. *J. Phys. Chem. Ref. Data* **6**, 113–307, DOI: 10.1063/1.555546 (1977).
7. Sand, J., Ihantola, S., Toivonen, H. & Toivonen, J. Radioluminescence yield of alpha particles in air. *New J. Phys.* **16**, 053022, DOI: 10.1088/1367-2630/16/5/053022 (2014).
8. Sand, J. *et al.* Stand-off radioluminescence mapping of alpha emitters under bright lighting. *IEEE Transactions on Nucl. Sci.* **63**, 1777–1783, DOI: 10.1109/TNS.2016.2562359 (2016).
9. Sand, J. *et al.* Imaging of alpha emitters in a field environment. *Nucl. Instruments Methods Phys. Res. A* **782**, 13–19, DOI: 10.1016/j.nima.2015.01.087 (2015).
10. Feener, J. S. & Carlton, W. S. Prelminary results of nuclear fluorescence imaging of alpha and beta emitting sources. In *2013 3rd International Conference on Advancements in Nuclear Instrumentation, Measurement Methods and their Applications (ANIMMA)*, DOI: 10.1109/ANIMMA.2013.6728086 (2013).
11. Ivanov, O., Danilovich, A., Stepanov, V., Smirnov, S. & Volkovich, A. Visualization of radioactive sources without gamma-radiation with uv imaging systems. In *ASME 2009 12th International Conference on Environmental Remediation and Radioactive Waste Management*, 321–325 (American Society of Mechanical Engineers, 2009).
12. Mahé, C. Alpha imaging: recent achievements and glove box characterization. *Proccedings DD&R* **10** (2010).
13. Kerst, T. *et al.* Standoff alpha radiation detection for hot cell imaging and crime scene investigation. *Opt. Rev.* **25**, 429–436 (2018).

14. Laboratory, N. R. E. Direct and global 37 deg tilt: Astm g-173. https://www.astm.org/Standards/G173.html. Last accessed: 2019-02-27.

15. Crompton, A., Gamage, K., Jenkins, A. & Taylor, C. Alpha particle detection using alpha-induced air radioluminescence: a review and future prospects for preliminary radiological characterisation for nuclear facilities decommissioning. *Sensors* **18**, 1015 (2018).

16. Elterman, L. UV, visible, and IR attenuation for altitudes to 50 km. Tech. Rep., AIR FORCE CAMBRIDGE RESEARCH LABS HANSCOM AFB MA (1968).

17. Ivanov, O. P., Stepanov, V. E., Smirnov, S. V. & Volkovich, A. G. Development of method for detection of alpha contamination with using uv-camera "daycor" by ofil. In *2011 IEEE Nuclear Science Symposium Conference Record*, 2192–2194 (IEEE, 2011).

18. Waldenmaier, T. Spectral resolved measurement of the nitrogen fluorescence yield in air induced by electrons. Tech. Rep. (2006).

19. Dondes, S., Harteck, P. & Kunz, C. Production of the oxygen 5577 å emission by polonium-210 alpha radiation. *Zeitschrift für Naturforschung A* **19**, 6–12 (1964).

20. Dondes, S., Harteck, P. & Kunz, C. A spectroscopic study of alpha-ray-induced luminescence in gases: part i. *Radiat. Res.* **27**, 174–210 (1966).

21. Crompton, A. *et al.* Gas flow to enhance the detection of alpha-induced air radioluminescence based on a uvtron flame sensor. *Sensors* **18**, 1842 (2018).

22. Tamura, M. *et al.* Collisional quenching of CH (A), OH (A), and NO (A) in low pressure hydrocarbon flames. *Combust. Flame* **114**, 502–514 (1998).

23. Settersten, T. B., Patterson, B. D. & Gray, J. A. Temperature- and species-dependent quenching of NO $A^2\Sigma^+ (v' = 0)$ probed by two-photon laser induced fluorescence using a picosecond laser. *The J. chemical physics* **124**, 234308 (2006).

24. Gilmore, F. R., Laher, R. R. & Espy, P. J. Franck–condon factors, r-centroids, electronic transition moments, and einstein coefficients for many nitrogen and oxygen band systems. *J. physical chemical reference data* **21**, 1005–1107 (1992).

25. Konthasinghe, K. *et al.* Laser-induced fluorescence from N_2^+ ions generated by a corona discharge in ambient air. *Appl. spectroscopy* **69**, 1042–1046 (2015).

26. Danielak, J., Domin, U., Ke, R., Rytel, M. & Zachwieja, M. Reinvestigation of the emission γ band system ($A^2\Sigma^+ \rightarrow X^2\Pi$) of the NO molecule. *J. Mol. Spectrosc.* **181**, 394–402 (1997).

27. Piper, L. G., Cowles, L. M. & Rawlins, W. T. State-to-state excitation of NO ($A^2\Sigma^+ (v' = 0, 1, 2)$) by N_2 ($A^3\Sigma_u^+ (v' = 0, 1, 2)$). *The J. chemical physics* **85**, 3369–3378 (1986).

28. Kerst, T. & Toivonen, J. Intense radioluminescence of NO/N_2-mixture in solar blind spectral region. *Opt. express* **26**, 33764–33771 (2018).

29. Weschler, C. J. & Shields, H. C. Potential reactions among indoor pollutants. *Atmospheric environment* **31**, 3487–3495 (1997).

30. Fontijn, A., Sabadell, A. J. & Ronco, R. J. Homogeneous chemiluminescent measurement of nitric oxide with ozone. implications for continuous selective monitoring of gaseous air pollutants. *Anal. chemistry* **42**, 575–579 (1970).

31. Edmund Optics. *239nm CWL, 10nm FWHM, 25mm Mounted Diameter* (2019).

32. Marshall, S. J., Bayne, S. C., Baier, R., Tomsia, A. P. & Marshall, G. W. A review of adhesion science. *dental materials* **26**, e11–e16 (2010).

33. Semrock. *2016/16 Brightline single-band bandpass filter* (2019).

34. Brzozowski, J., Elander, N. & Erman, P. Direct measurements of lifetimes of low-lying excited electronic states in nitric oxide. *Phys. Scripta* **9**, 99 (1974).

35. Munson, B. R., Okiishi, T. H., Huebsch, W. W. & Rothmayer, A. P. *Fluid mechanics* (Wiley Singapore, 2013).

36. Fung, Y.-c. *Biomechanics: motion, flow, stress, and growth* (Springer Science & Business Media, 2013).

37. Python scipy integrate ode solver. https://docs.scipy.org/doc/scipy-0.14.0/reference/generated/scipy.integrate.ode.html. Accessed: 2019-04-25.

38. Albugues, F. *et al.* Destruction of the levels $C^3\Pi_u (v' = 0, v' = 1)$ of nitrogen by O_2, CO_2, CH_4, and H_2O. *The J. Chem. Phys.* **61**, 2695–2699 (1974).

39. Python scipy optimizer curve fit. https://docs.scipy.org/doc/scipy/reference/generated/scipy.optimize.curve_fit.html. Accessed: 2019-04-25.

40. Beligni, M. V. & Lamattina, L. Is nitric oxide toxic or protective? *Trends plant science* **4**, 299–300 (1999).

Acknowledgements

This work was supported by Business Finland, Finland Distinguished Professors (FiDiPro, Project: Novel Instrumentation for Nuclear Safety, Security and Safeguard NINS3) and EMPIR (Project 16ENV09, MetroDecom II). The work is part of the Academy of Finland Flagship Programme, Photonics Research and Innovation (PREIN), decision 320165.

Author contributions statement

Thomas Kerst and Juha Toivonen conceived of and designed the experiments. Thomas Kerst carried out the experiments, analysed the data and wrote the manuscript.